

Copyright is owned by the Author of the thesis. Permission is given for a copy to be downloaded by an individual for the purpose of research and private study only. The thesis may not be reproduced elsewhere without the permission of the Author.

Self-assembled Optical Diffraction Sensor for Water Quality Monitoring



Swapna Ashwin Jaywant

A thesis submitted in total fulfillment for the
degree of Doctor of Philosophy

in the
School of Food and Advanced Technology
Massey University

January 2020

I would like to dedicate this thesis to my loving husband and wonderful kids...

Declaration of Authorship

I hereby declare that except where specific reference is made to the work of others, the contents of this thesis are original and have not been submitted in whole or in part for consideration for any other degree or qualification in this, or any other university. This thesis is my own work and contains nothing which is the outcome of work done in collaboration with others, except as specified in the text and Acknowledgments. This thesis contains around 39,500 words including appendices, bibliography, footnotes, tables, and equations and has fewer than 221 figures.

Swapna Ashwin Jaywant

Acknowledgements

Firstly, I would like to express my sincere gratitude to my supervisor Dr. Khalid Mahmood Arif, and co-supervisor(s) Prof. Johan Potgieter, and Dr. Ebubekir Avcı for the continuous support of my PhD study and related research, for their patience, motivation, and immense knowledge. Their guidance has helped me at all times of my research and writing of this thesis. I could not have imagined having better advisors and mentors for my PhD study.

My sincere thanks to the technical and administrative staff at Massey University who gave access to the laboratory and research facilities. Without their support, it would not be possible to conduct this research.

I thank my fellow lab mates for the stimulating discussions while we were working together before deadlines, and for all the fun we have had in the last three years. Also, I thank my friends at Massey University. In particular, I am grateful to Muhammad Harris, Muhammad Asif Ali Rehmani, Pinky Mal, and Ayesha Shaukat for invaluable support during my PhD studies.

I would like to thank my family: my parents and in-laws, my sisters for supporting me throughout this journey and my life in general.

Last but not least, I also thank God for providing this opportunity.

Abstract

Water contamination is one of the current global issues; the freshwater sources being extremely restricted are causing a drinking water crisis in many countries. An increase in water contamination continuously decreases water quality. Generally, water pollution includes pathogenic, nutrients, and chemical (organic & inorganic) contaminants. Inorganic contamination involves metallic particles such as arsenic, lead, etc. Of these contaminants, arsenic (As) is a major concern due to its mutagenic and carcinogenic effects on human health. The World Health Organisation has recommended the maximum contamination limit (MCL) for As in drinking water to be 10 $\mu\text{g/L}$. Countries like Bangladesh, China, Vietnam, India, Chile, USA, and Canada are contaminated with As. Arsenic species are also found in New Zealand in 28 geothermal features from the Taupo Volcanic Zone and the Waikato region. Thus, a rising level of As in drinking water creates the need to periodically monitor its levels in potable water.

Commercially available methods are either laboratory-based or kit based techniques. The most common laboratory-based As detection methods are reliable. However, these are expensive due to the requirement for specific instrumentation. Hence, they are not considered to be field-effective for As detection. On the other hand, commercially available kit-based methods are portable but are not considered to be safe and reliable due to the production of toxic by-products. The development of a portable and sensitive As sensor with high throughput could be an asset.

In this research, we present a novel sensor with a unique surface modification technique to detect arsenite (As(III)) contamination of water. Here, the approach involves the potential usage of self-assembled optical diffraction patterns of a thiol compound (dithiothreitol or glutathione) on the gold-coated glass. The self-assembled patterns are obtained through a microcontact printing (μCP) procedure. Gold binds with the thiol compound through an Au-S linkage. In addition to this, As(III) has an affinity towards amino acids, amines, peptides, and organic micro molecules due to As-O or As-S linkages. The research indicates that the total time taken by the μCP process to transfer the patterns successfully on to the gold-coated substrate is inversely proportional to the concentration of the thiol molecules and pH value of the solvent. Further, the signal enhancement of these thiol-based self-assembled patterns allows for detection of the As(III) contamination. Simultaneously, the automated fluidic system is designed to provide fluid handling. The system is developed with the help of off-the-shelf and/or in-house fabricated components. The characterisation of fluidic components proved that the low-cost fluidic components work reliably in the fluidic network and can be used in

sensing applications for pumping, mixing, and circulation purposes. We also explore the possibility of using fused deposition modelling and selective laser sintering technology for printing of the flow chamber through printing microchannels. These two technologies have been compared in terms of the minimum possible channel size, fluid flow-rate, and leakage.

Overall, we developed a sensing scheme of a portable self-assembled diffraction sensor for As(III) detection. The developed sensor can detect dissolved As(III) up to 20 $\mu\text{g/L}$. The μCP of a dithiothreitol pattern has not been found in the literature yet. Hence, this research also provides a guide towards μCP of dithiothreitol on a gold-coated substrate.

Contents

Declaration of Authorship	ii
Acknowledgements	iii
Abstract	iv
List of Figures	ix
List of Tables	xii
Abbreviations	xiii
1 Introduction	1
1.1 Consequence of Water Pollutant on Human Body	2
1.2 Arsenic Detection	8
1.3 Problem Statement	8
1.4 Proposed Solution	9
1.5 Thesis Layout	10
2 Literature Review	12
2.1 Microfluidic Water Quality Monitoring Sensors	13
2.1.1 Microfluidic with electrochemical detection	15
2.1.1.1 Heavy metal detection	16
2.1.1.2 Nutrients	23
2.1.1.3 Pathogens	25
2.1.2 Microfluidic with optical detection	28
2.1.2.1 Heavy metal	33
2.1.2.2 Nutrients	37
2.1.2.3 Pathogen	39
2.1.3 Discussion and Outlook	41
2.2 Use of Aptamer in Arsenic Detection	44
2.2.1 Colorimetric detection	45
2.2.2 Fluorimetric detection	46
2.2.3 Electrochemical detection	46
2.2.4 Other detection methods	47
2.2.4.1 Resonance Rayleigh Scattering (RRS) detection	47

2.2.4.2	Surface enhanced Raman scattering (SERS) detection . . .	48
2.2.4.3	Electrochemiluminescence detection	48
2.2.4.4	FET based detection	48
2.3	Summary	48
3	Sensor Design and Fabrication	50
3.1	Introduction	50
3.2	Microcontact Printing	51
3.2.1	Chemicals and instruments	52
3.2.2	Substrate fabrication	53
3.2.3	Stamp fabrication	54
3.2.4	Inking	55
3.2.5	Printing	56
3.3	Interaction of Thiol Compounds with Gold and Arsenic	56
3.4	Signal Enhancement of Patterns	58
	60
4	Fluidic System	61
4.1	Introduction	61
4.2	Instrumentation	63
4.3	Micro Pump	63
4.4	Pinch Valve	65
4.4.1	Design and assembly	66
4.5	Fluid Presence Detection	67
4.5.1	Design principle and calculations	67
4.6	Flow Chamber	68
4.6.1	Fabrication of microchannel	69
4.6.2	Fabrication of flow chamber	70
4.7	Overall System	70
4.8	System Automation	71
5	Characterisation and Testing	75
5.1	Pattern Characterisation	75
5.1.1	BSA pattern	77
5.1.2	DTT pattern	80
5.1.3	GSH pattern	84
5.1.4	Effect of molecular weight on thiol microcontact printing	85
5.1.5	Pattern confirmation	86
5.2	Fluidic System Characterisation	87
5.2.1	Dosing peristaltic pump characterisation	87
5.2.2	Valve characterisation	89
5.2.3	Flow sensor characterisation	90
5.2.4	Flow chamber characterisation	91
5.3	Testing and Results	94
5.3.1	Arsenic detection	94
5.3.2	As(III) confirmation with signal enhancement	94
5.3.3	Results	99

6 Conclusion and Future Work	100
6.1 Conclusion	100
6.2 Future Work	102
A List of Publications	104
B Design and Data Files	114
C DRC 16 V-3 Forms	119
References	125

List of Figures

1.1	Of the total water, 96.5% is saline water, and just 3.5 percent is freshwater. Glaciers contain almost 68.7% of the total freshwater on the earth. Groundwater is 30%. Ground ice covers 0.86%. Just 0.3% of fresh water is available in rivers, lakes, and reservoirs. The remaining 1% is contributed by others (atmospheric humidity, soil dampness, etc.).	2
1.2	Schematic description of the sensor.	9
1.3	Schematic description of system layout.	10
2.1	Illustration of a microfluidic system.	14
2.2	Different orientation of electrodes in electrochemical detection methods (a) Schematic of Au-Ag-Au electrode integrated with microfluidic channel to detect Hg^{+2} [1]; (b) Illustration of reusable polymer chip for detection of Pb^{+2} [2]; (c) Electrodes printed on plastic substrate to detect As(III) [3]; (d) SWCNTs electrodes for As(III) detection [4].	16
2.3	Schematic of paper-based method including integrated commercial screen-printed carbon electrodes with filter paper strips for detection of Pb^{+2} and Cd^{+2} [5].	18
2.4	Pictorial presentation of the working scheme of As(III) bioreporter [6]. . .	18
2.5	(a) Nitrate sensor chip with wireless communication interface [7]; (b) Experimental set up of LTCC-based continuous flow potentiometric microanalyzer to determine potassium and nitrate [8]; (c) A mobile sensing platform with a plug-n-play microelectronic ionic sensor to detect nitrate [9];(d) nTiO ₂ modified GF based nitrate sensor [10].	23
2.6	(a) Electrochemical DNA-based sensor for E. coli determination [11]; (b) Custom made automatic biosensor for pathogenic detection [12].	26
2.7	(a) Wax printed μ PADs for colorimetric detection of Fe, Cu, Ni [13]; (b) 3D paper microfluidics for metal ion detection [14]; (c) Working principle of As(III) detector based on modified AuNP [15]; (d) T-shaped μ PAD with functionalised AuNp for As(III) detection [16]; (e) Rapid detection of Pb^{2+} with MUA modified AuNP [17].	33
2.8	(a) 3D paper-based fluorescence detection of Cu^{2+} and Hg^{2+} [18]; (b) E. coli based fluorescence detection of As(III) [19]; (c) Fluorescence detection of As(III) using portable bioreporter [20].	36
2.9	(a) Quantification of nitrite and nitrate using disposable μ PAD [21]; (b) Schematic of the flow system and detection cell of LED-based nitrate sensor [22]; (c) Schematic of FOCS method for nitrite measurement [23]. .	37
2.10	Scheme indicating a mobile-based multichannel paper chip for rapid E. coli detection [24].	40
2.11	Schematic of SPR-based pathogenic detection [25].	41

2.12	Summary of microfluidic sensors	42
3.1	Diagram showing the steps involved in microcontact printing of thiol ink on a gold substrate. 1. Take a PDMS stamp. 2. Immerse the PDMS stamp into the ink. 3. Blow away the ink with the help of the nitrogen stream. 4. Place the PDMS stamp on the substrate and apply gentle pressure. 5. Observe the pattern under the microscope.	51
3.2	Diagram illustrating the covalent binding of sulphur atom to the surface of the metallic substrate forming SAM with a terminal functional group.	52
3.3	Illustration of the process of developing PDMS stamps.	55
3.4	Printing methods: (a) liquid inking, (b) inking through PDMS reservoir, (c) direct inking, and (d) inking by immersing the PDMS stamp in the ink.	55
3.5	Molecule structure: (a) DTT and (b) GSH.	57
3.6	Interaction of DTT and GSH molecule with gold surface and As molecule.	57
3.7	Ars-3 structure [26].	59
3.8	Signal enhancement using biotinylated Ars-3 and streptavidin-coated magnetic particle.	60
4.1	Schematic layout of a typical fluidic system showing major components and fluid circulation path.	62
4.2	Schematic of (a) typical gear pump, (b) classical peristaltic pump, and (c) magnetically driven screw pump [27].	64
4.3	Dosing peristaltic pump	65
4.4	Schematic of the pinch type valve	66
4.5	Schematic of the pinch type valve	66
4.6	Schematic of Flow sensor	68
4.7	(a) CAD image of microchannel; (b) Cross sectional view of microchannel; (c) Pictorial view showing the internal measurements of microchannel.	69
4.8	CAD image of flow chamber	70
4.9	Automated fluidic system	71
4.10	Schematic diagram of the fluidic system	71
4.11	Block diagram of the fluidic system	72
4.12	Schematic of the graphical user interface	73
4.13	Flow instruction on button pressed	74
5.1	(a) The patterned side of the stamp is placed opposite the microscope lens.(b) The patterned side of the stamp is placed towards the microscope lens. Scale bar: 10 μm	76
5.2	PDMS stamp (a) Before cleaning, (b) After cleaning with DI water, (c) After cleaning with ethanol, (d) After cleaning with ethanol, followed by acetone. Scale bar: 10 μm	76
5.3	Main effects plot.	78
5.4	Two-way interaction plot.	79
5.5	DTT patterns obtained during experimental runs described in Table 5.4.	81
5.6	DTT patterns obtained during experimental runs described in Table 5.5.	82
5.7	Optical patterns obtained with DTT	83
5.8	Effect of concentration and pH value on inking period.	84
5.9	Optical patterns obtained with GSH	85
5.10	Effect of concentration and pH value on inking period.	86

5.11	Confirmation of pattern using fluorescent dye.	87
5.12	Dosing peristaltic pump.	88
5.13	Measured flow rate vs. pulse width modulation of pump driver.	88
5.14	Measured volumes vs. time duration.	89
5.15	Characterisation of valve operation	90
5.16	(a) Experimental set-up, (b) Microchannel printed with FDM method.	91
5.17	Change in flow rate vs developed pressure at the input port.	93
5.18	Design (a) and (b) at inflow velocities of 0.01 m/s & 0.1m/s.	93
5.19	Optical micro-graph of GSH patterns (a) Before arsenic exposure, (b) After As(III) (20 $\mu\text{g/L}$) exposure, (c) After As(III) (50 $\mu\text{g/L}$) exposure.	94
5.20	Illustration of signal enhancement procedure	98
5.21	(a) GSH pattern, (b) Pattern confirmation with fluorescent dye, (c) As(III) contaminated (1 mg/L) pattern after signal enhancement, (d) As(III) contaminated (50 $\mu\text{g/L}$) pattern after signal enhancement, (e) As(III) contaminated (20 $\mu\text{g/L}$) pattern after signal enhancement, (f) As(III) contaminated (10 $\mu\text{g/L}$) pattern after signal enhancement.	99
6.1	Illustration of optical signal detection strategy	102
A.1	A paper published in International Journal of Modern Physics B	106
A.2	A review paper published in Sensors	107
A.3	A paper published in ICST-2019 Conference proceedings	108
A.4	A paper published in M2VIP-2019 Conference proceedings	109
A.5	A paper published in APWC on CSE-2018 Conference proceedings	110
A.6	A poster presented at NZ Product Accelerator 2018	111
A.7	A poster presented at the 2nd International Symposium on Advanced Materials, Manufacturing Processes and Devices (MMPD) 2019	112
A.8	A poster presented at Manufacturing and Design (MaD) Conference 2019	113
B.1	Stamp layout on wafer.	114
B.2	PCB Layout	115

List of Tables

1.1	Contaminants and their potential health effects.	6
2.1	Comparison of electrochemical methods	19
2.2	Commercially available electrochemical sensors	22
2.3	Comparison of optical methods	29
2.4	Commercially available optical sensors	32
2.5	Advantages & disadvantages of detection methods.	44
2.6	Aptamer-based arsenic detection	49
4.1	3D printers and working parameters	69
5.1	Result of BSA pattern printing on the CD.	77
5.2	Variables used in experimental run.	77
5.3	Result of experimental run.	78
5.4	Result of experimental run using DTT with liquid inking method.	80
5.5	Result of experimental runs using DTT with inking by immersing PDMS stamp in the ink.	82
5.6	Sensor Output	90

Abbreviations

AKD	Alkylketene dimer
Ars-3	Arsenic specific aptamer
As	Arsenic
As(III)	Arsenite
AsH	Arsine
ASV	Anodic stripping voltammetry
AuNP	Gold nanoparticles
Au	Gold
BSA	Bovine serum albumin
BNC	Baby Neill Constant
CAD	Computer-aided design
CFU	Colony forming units
CL	Chemiluminescence
Cd	Cadmium
CD	Compact disk
Co	Cobalt
Cr	Chromium
Cu	Copper
CV	Cyclic voltametry
DTT	Dithiothreitol
DI water	De-ionized wat
DLS	Dynamic light scattering
DPASV	Differential pulse anodic stripping voltammetry
DPCSV	Differential pulse cathodic stripping voltammetry
DPV	Differential pulse voltammetry

E. coli	Escherichia coli
ELISA	Enzyme-linked immunosorbent assays
EPA	Environmental Protection Agency
EIP	Electrochemical impedance spectroscopy
EIS	Electrochemical impedance spectroscopy
f-MWCNT	Functionalised- multiwall carbon nanotube
FDM	Fused deposition modelling
Fe	Iron
FOCS	Fiber-optic chemical sensor
GCE	Gassey carbon electrode
GF	Graphene foam
GSH	Glutathione
H	Hydrogen
Hg	Mercury
HS	Hydrogen sulphide
HgBr	Mercury(II) bromide
ID	Inner diameter
LBW	Low birth weight
LCR	Inductance (L), capacitance (C), Resistance (R) meter
LEDs	Light-emitting diodes
LOC	Lab on a chip
LOD	Limit of detection
LSASV	Linear sweep anodic stripping voltammetry
LSCSV	Linear sweep cathodic stripping voltammetry
LSV	Linear sweep voltammetry
LTTC	Low-temperature co-fired ceramics
MB	Methylene blue
MCL	Maximum contamination limit
MLBs	Magnetically labelled bacteria
MSQ	Methylsilsesquioxane
MWCNTs	Multiwall carbon nanotubes
Mn	Manganese
NiR	Nitrate reductase

O	Oxygen
OCC	Occult cancer
OD	Outer diameter
P	Phosphate
Pb(OAc)	Lead
Pb(OAc)	Lead(IV) acetate or lead tetraacetate
PCR	Polymerase chain reaction
PDMS	Poly(dimethylsiloxane)
pDEP	Positive dielectrophoretic
PLA	Poly(lactic acid)
PMMA	Poly(methyl methacrylate)
POC	Point-of-care
QRE	Quasi reference electrode
RGO	Reduced graphene oxide
S	Sulphur
SAB	Spontaneous abortion
SAM	Self-assembled monolayers
SERS	Surface enhanced raman scattering
SLS	Selective laser sintering
SPR	Surface plasmon resonance
SWASV	Square wave anodic stripping voltammetry
SWCSV	Square wave cathodic stripping voltammetry
SWV	Square wave voltammetry
TEM	Transmission electron microscopy
Zn	Zinc
16-MHDA	16-mercaptohexadecanoic acid
μ PADs	Paper-based analytical devices
μ PED	Microfluidic paper-based electrochemical sensing device
μ CP	Microcontact printing

Chapter 1

Introduction

In this century, one of the major challenges that human beings are likely to face is water quality. Water helps us in living our life - it supports our farming, industries, tourism, and the welfare of communities. However, irrespective of its great significance to life on earth, water is knowingly ignored by this industrialised world. Occasionally it has been considered that there is plenty of freshwaters available. Still, only a tiny amount of freshwater exists on the earth in lakes, reservoirs, and river systems. Fig. 1.1 illustrates the overall water distribution on our planet. Water may turn out to be the most valuable commodity on the planet due to population growth and pollution. Water pollution occurs due to the addition of different contaminants to the water, which can cause great damage to human and environmental health. Hence, to counter its ill-effects, periodic water quality monitoring is necessary. This chapter gives information about the term “water quality” and discusses the reasons behind water impurities and their adverse effects on health. The significant As contamination problem has been discussed and a solution has been proposed.

Water pollution occurs due to many natural factors like precipitation, weather, basin physiography, soil erosion, etc. and anthropogenic factors like urbanization, industrial and agricultural activities, etc. [28]. The following factors are often used to provide a measure of water quality: concentration of dissolved oxygen (DO); levels of fecal coliform bacteria from human and animal wastes; concentrations of plant nutrients nitrogen and phosphorus; the amount of particulate matter suspended in the water (turbidity); and amount of salt (salinity). Quantities of pesticides, herbicides, heavy metals, and other

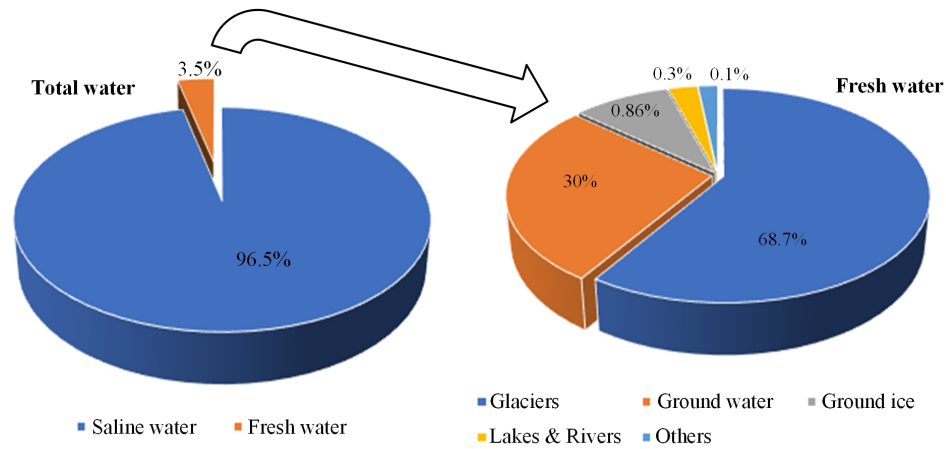


FIGURE 1.1: Of the total water, 96.5% is saline water, and just 3.5 percent is freshwater. Glaciers contain almost 68.7% of the total freshwater on the earth. Groundwater is 30%. Ground ice covers 0.86%. Just 0.3% of fresh water is available in rivers, lakes, and reservoirs. The remaining 1% is contributed by others (atmospheric humidity, soil dampness, etc.).

contaminants may also be measured to determine water quality [29]. Water Quality Standards are provisions for controlling the pollution entering the waters.

1.1 Consequence of Water Pollutant on Human Body

Water pollution is a widespread problem across the world. Diseases caused by contaminated drinking water result in the death of a million people every year - the majority are children [30]. Nutrients, toxic substances, and petroleum products enter the rivers, lakes, and other water bodies and cause water pollution. Water pollution or contamination occurs due to various sources. These sources can be categorized as point sources and non-point sources [28, 31]. Dumping of organic and inorganic wastes from industrial and domestic discards form the point sources of drinking water contaminants, whereas the non-point sources are land run-off, applying chemicals or leaks from buried solid waste landfills [32].

As mentioned above, there are many sources of contaminants in potable water. Considering the human body, these substances can be divided into essential trace elements, such as manganese (Mn), cobalt (Co), copper (Cu), chromium (Cr), zinc (Zn), and iron (Fe), and non-essential trace elements, such as arsenic (As), cadmium (Cd), mercury (Hg), and lead (Pb). Essential trace elements are required for life processes and sustainability, though they are only needed at trace level. However, excess intake of essential trace

elements may lead to adverse health effects. On the other hand, non-essential trace elements can induce some diseases such as various forms of cancer, reproductive disorders, cardiovascular disease, and neurological disease even at low concentrations. For example, human exposure to As can lead to skin lesions and induced skin cancer [33].

Environmental vulnerability resulting from heavy metals is gaining awareness worldwide due to extensive pollution in different parts of the world [34]. Heavy metals are commonly present in most surroundings. Their physiological and chemical characteristics make them extensively useful in various industrial fields. Industrial waste enhances the possibility of heavy metal exposure which leads to environmental pollution [35], such as for surface water, and soil contamination. Almost all heavy metals contain toxic substances. The presence of heavy metal ions like Cd, As, Cr, Pb, and Hg in water produces harmful long-term effects on human health [33, 36]. As exists in both the organic and inorganic form in nature and it has different types [37]. Among all the types, As(III) and As(V) are present abundantly in natural water and are highly toxic [38–40]. As exposure occurs through air, food, and water [41]. Long-term inorganic As toxicity can affect the cardiovascular, nervous, endocrine, and renal systems. It leads to skin lesions, pulmonary disease, hypertension, etc [42]. Furthermore, As toxicity causes different types of cancers [43–46]. Cd is a malleable silver-white toxic metal that appears in the earth's outer most layer. Its pollution naturally occurs due to volcanic eruptions, weathering, and river transport. Man-made activities like mining, smelting, tobacco smoking, disposal of sewage, etc. are equally responsible for the pollution [47]. The International Agency for Research on Cancer has classified Cd and its compounds as Group 1 carcinogens. Cd toxicity causes osteoporosis, renal dysfunction, preterm birth and low birth weights [48–50]. Cr is a steely-grey shiny metal that naturally is present in rocks, soil, animals, and plants. Industrial sources such as magnetic tapes, metal alloys, protective metal coatings, paint pigments, paper, rubber, and cement etc. release Cr in the environment [51]. Low-level Cr toxicity can cause types of ulcers and low blood sugar. Severe chromium toxicity can develop into lung cancer, gastrointestinal cancer, and DNA damage [48, 52, 53]. Pb is a shiny bluish-gray soft metal naturally present in the earth's crust. However, mostly it is accumulated in the environment due to activities like manufacturing, mining, and fossil fuel burning [54]. The Environmental Protection Agency (EPA) has considered Pb to be a carcinogen. Acute or short-term exposure to Pb may result in appetite loss, loss of hunger, headache, elevated blood

pressure, stomach ache, kidney dysfunction, exhaustion, insomnia, painful inflammation and stiffness of the joints, and vertigo. Chronic or long-term exposure to Pb can cause mental abnormality, congenital disorder, allergies, weight loss, paralysis, weak muscles, dementia, renal damage, and may even be fatal [48, 55]. Mercury (Hg) is a silvery liquid form of metal. Its contamination occurs in its surroundings due to industrial activities like paper and pulp preservatives, pharmaceuticals, cement production, and agriculture industry, etc.[56]. Increased levels of metallic, organic and inorganic mercury can lead to impairment of the brain, kidneys, muscles, and the fetus. It causes hypertension, cardiovascular consequences (coronary heart disease, myocardial infarction, cardiac arrhythmia, etc.), and sudden death [57]. EPA has reported methyl mercury and mercuric chloride as extremely carcinogenic compounds [48, 58].

Nutrients like nitrogen and phosphorous are significant contributors to water body pollution. Abundant nitrogen occurs naturally in our surroundings as approximately 80% of the air is comprised of nitrogen. When this atmospheric nitrogen encounters rainwater it produces nitrate and ammonium [59, 60]. Further, a reduction of nitrate results in nitrite ions [61, 62]. These ions can enter into the soil or surface water. The excessive use of fertilisers in agriculture is the principal non-point source of nitrogen and phosphorus. Another source of agricultural pollution is animal dung. In addition to this, the disposal of industrial waste and sewage are significant anthropogenic sources of nitrate pollution [30, 63]. The excessive presence of nitrite and nitrate ions causes an adverse health effect [64–67].

Nitrate is an essential ion for the human body to decrease blood pressure and improve blood flow. Still, its unnecessary intake can affect the human body. It can develop diseases like gastric cancer and Parkinsons disease. Newborns can be afflicted with blue baby syndrome [61]. It also provides a risk of thyroid cancer [68]. In rivers or lakes, the presence of excessive nitrate produces unnecessary algae and phytoplankton which causes eutrophication. This unwanted growth of algae and phytoplankton absorbs more marine oxygen through the decomposition process and badly affects aquatic life [59].

Domestic waste-water handling and disposal methods provoke the pathogenic contamination of water bodies. Pathogenic contamination results in developing viruses, bacteria, and protozoa in water [69]. Bacteria like *Escherichia coli*, *Enterococci*, *Bacteroides*, etc., are present in the intestines of warm-blooded animals. These are recognized as indicators

of faecal pollution [70, 71]. These bacteria can enter into the groundwater due to sewage leakage from septic tanks [72] and are responsible for waterborne diseases such as severe cholera, diarrhea, legionellosis, and typhoid fever [73]. Additionally, in the contaminated water supply rotaviruses, hepatitis A and E viruses, and the parasitic protozoa *Giardia lamblia* are frequently observed [74]. Monitoring of pathogenic pollution is also equally important as many outbreaks of *E. coli* have been reported worldwide that result in infections and deaths [75, 76].

Thus, it has become necessary to monitor the levels of contaminants in the drinking water to avoid an adverse health effect on human as well as aquatic life. Table 1.1 summarizes some effects among populations exposed to the impurities [52, 77] and also includes the maximum permissible limit of the contaminant along with contamination sources [78–82]. The table also indicates that As, Pb, and mercury can be considered as major harmful contaminants, but As should be considered as the most dangerous pollutant among all others due to its mutagenic and carcinogenic effects on human health.

TABLE 1.1: Contaminants and their potential health effects.

Contaminant MCL (mg/L)	Cancer	Developmental /Reproductive	Neurological	Other	Sources	Ref.
Arsenic (0.01)	Skin, internal	SAB	Peripheral	Cardiovascular, Immunologic, Dermatological	Geothermal activity, Agricultural application, Mining & smelting, Industrial applications	[42-46, 48]
Lead (0.01)	Internal (OCC)	Birth defects	Autism,Dyslexia, Hyperactivity	Haemoprotein, Weight loss, Muscular weakness, Paralysis, Kidney damage	Industrial & Electronics wastes Natural deposits, Mining, Manufacturing process, & Fossil fuel burning	[48, 55] ,[54]
Mercury (0.002)	Internal	Damage to fetus	Neurobehavioral disorders	Cardiovascular, Thyroid, Asthma, Nausea & Vomiting, Diarrhea, Skin rashes, Cardiovascular	Natural deposits, Land run-off Agricultural & Industrial applications, Paper & pulp preservatives	[48] [56-58]
Cadmium (0.004)	Pancreatic Ovarian Breast	Premature birth, LBW	Neuron cell death	leading to kidney disease, Oxidative stress, Osteoporosis, DNA damage DNA damage	Natural deposits, Mining, smelting, Tobacco smoking, disposal of sewage	[47, 48] [49, 50]
Chromium (0.05)	Lung and gastrointestinal	NA	NA	Nausea & , vomiting, Low blood sugar, Damage liver & kidney, Dermatological	Natural deposits in soil & rocks, Volcano irruption, Coal & Oil combustion, Sewage sludge, Cement production	[51, 52] [48, 53]
Nickel (0.02)	Lung & Nasal	NA	NA	Lung Disease, skin diseases, liver toxicity	Volcanic irruption, Forest fires Industrial & Domestic waste-water, Sewage sludge	[83, 84]

Table 1.1 continues..

Contaminant MCL (mg/L)	Cancer	Developmental /Reproductive	Neurological	Other	Sources	Ref.
Aluminum (0.05 to 0.2)	NA	NA	NA	Nausea & vomiting, Mouth ulcers, Diarrhea, Skin rashes, Arthritic pain,	Industrial applications	[48, 85, 86]
Iron (0.3)	Lung	NA	NA	Gastrointestinal bleeding, Vomiting & Diarrhea	Natural deposits Corroded iron pipes	[48]
Nitrate (50)	Internal	SAB Blue baby syndrome	NA	Gastric problems Parkinsons diseases	Natural deposits, Agricultural usage, Animal waste, Septic tanks, Sewage sludge	[61, 68]
Nitrite (0.2)		Blue baby syndrome		Gastric problems	Natural deposits, Agricultural usage, Animal waste, Septic tanks, Agricultural applications	[64–67]
Pesticide - 1,3-dichloropropene (0.02)	Carcinogenic	LBW	NA Tumors	Skin irritations		[61]
E. coli (less than 1/100 mL)	NA	NA	NA	Diarrhea, renal failure, anemia and other serious health problem	Sewage leakage, Animal waste	[72, 73]
Rotavirus Zero	NA	NA	NA	Vomiting, Dehydration Severe fatigue	Disposal of untreated waste-water	[74]
Protozoa (Less than 1(oo) cyst/100L)	NA	NA	NA	Diarrhea, Fatigue, Nausea, Abdominal cramps	Fecal contamination	[69]

NA : Not Applicable; LBW : Low birth weight; SAB : Spontaneous abortion

1.2 Arsenic Detection

Arsenic is one of the most toxic metallic elements. The majority of the researched As detection methods use optical techniques, electrochemical techniques, surface plasmon resonance, and surface-enhanced Raman spectroscopy. These current detection methods are divided into two main classifications, i.e. accuracy-based and availability-based methods.

Accuracy-based methods include the laboratory-based methods such as surface-enhanced Raman spectroscopy, surface plasmon resonance sensors or more expensive lab-based transmission electron microscopy (TEM). These techniques involve specialised equipment and complex calculations, which correspond to a negative impact limiting the use of the overall system. On the other hand, availability-based systems are usually based on colorimetric approaches. These methods tend to be less reliable and measure small samples of water which limits their accuracy.

1.3 Problem Statement

Higher concentrations of contaminants in water are responsible for fatalities across the world. The harmful outcomes are increasing due to two main reasons: first, the level of contaminants in the water is naturally rising with no current practical method to keep track of the natural changes, and the second is human growth, which leads to the need for expansion to new water sources with unknown quality. Without the presence of reliable methods to keep track of the rising concentrations of contaminants in the water, we cant treat the water sufficiently well to remove the excessive impurities.

This study is focused on the development of a novel sensor that is used to detect the presence of water contaminants. The major emphasis is given to the detection of dissolved heavy metal like As(III). Current methods for As detection either require expensive equipment or produce toxic by-products. It is very important to have a selective, sensitive, and portable detection method that can be used for water quality monitoring.

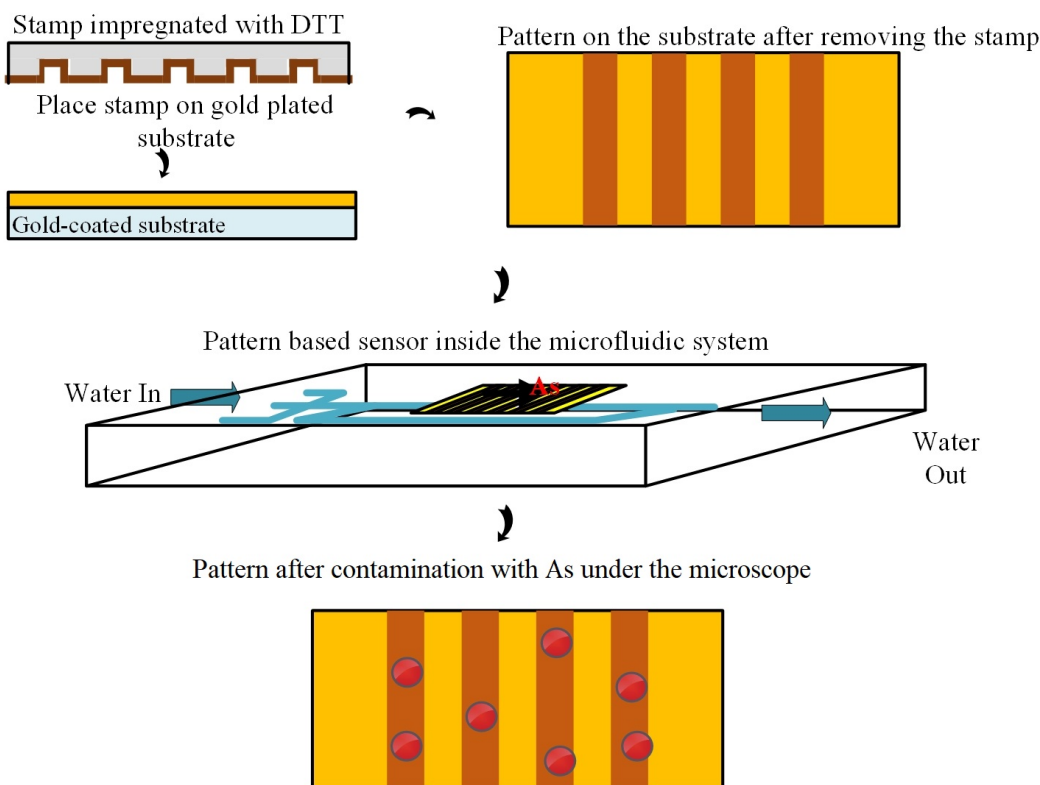


FIGURE 1.2: Schematic description of the sensor.

1.4 Proposed Solution

This research aims to limit human exposure to high As(III) levels by providing a simple method to measure its levels in the water. This work investigates the viability of using a printed pattern of thiolated ligand on a gold-coated glass substrate to indicate As(III) presence. To achieve this, the water sample flows over the thiol patterned gold-coated glass. Then the pattern attracts As creating a layer of As(III) on top of the thiolated ligand which is detected at a later stage in the form of a change in light scattering angle and intensity with the help of signal enhancement as depicted in Fig. 1.2 and 1.3.

An ambition of the research is to plug the research gap on the methods available to accurately measure As levels outside the laboratory with ease. The research is considered to be a novel method as it involves microcontact printing (μ CP) of self-assembled thiol (either DTT or GSH) patterns on the gold-coated substrate – a method that has not been reported as yet. A sensor usually works in conjunction with a suitable fluidic system. The fluidic components decide the size of any detection assay. Here, we present a

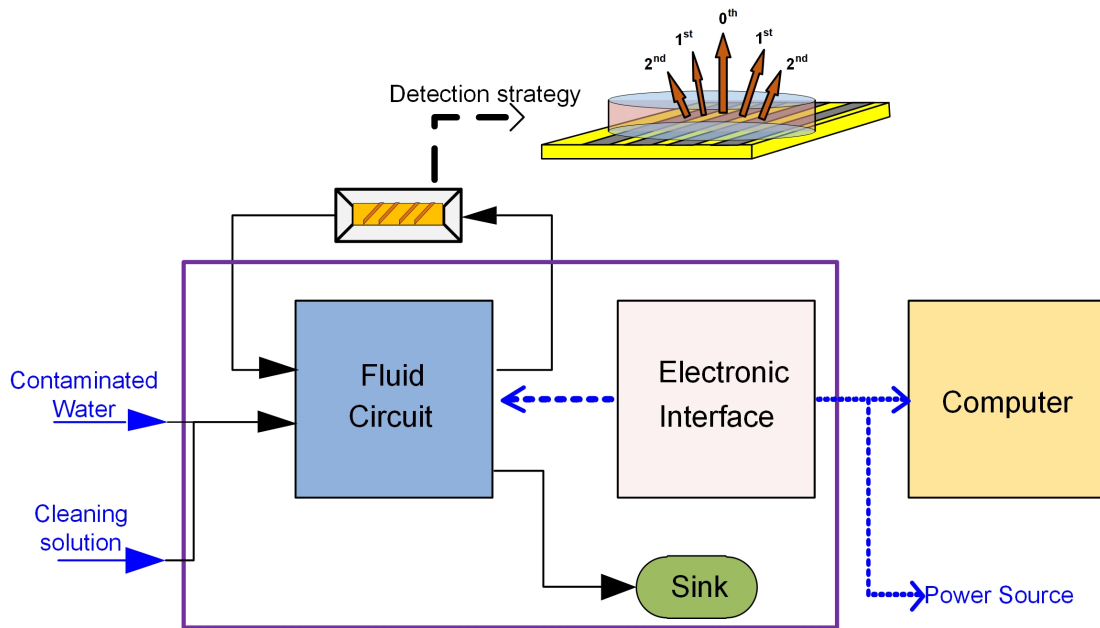


FIGURE 1.3: Schematic description of system layout.

microfluidic-based sensor to accomplish a portable detection method which also provides high throughput.

1.5 Thesis Layout

The remaining part of this report focuses on the following:

- Literature review
- Sensor design and fabrication
- Fluidic system
- Characterization and testing
- Conclusion

The next chapter, Chapter 2, presents a comprehensive literature review of this research work. Emphasis is given to heavy metal, nutrients, and pathogenic contamination. The chapter describes the current developments in microfluidic sensors for overall water quality monitoring. Also, various aptamer-based As sensors are discussed in the chapter.

Thereafter, in Chapter 3, sensor design and the fabrication process is discussed in depth. It includes patterning of thiol compounds on the gold-coated substrate using the μ CP method. Hence the μ CP technique is explained in detail. It includes substrate fabrication, stamp fabrication, the inking process, and the printing process. Further, it describes the interaction of thiol compounds (DTT and GSH) with gold and As along with the chemical structure of thiol compounds. Lastly, the chapter explains the necessity of a signal enhancement step to detect As(III) contamination.

Chapter 4 explains the details of the automated fluidic system that is developed using off-the-shelf and/or in-house fabricated components. The rationale behind the selection of these fluidic components is presented, followed by an explanation about the designing and fabrication process of the components. Lastly, details about the automated process are provided, including PCB design and software development.

In Chapter 5, characterisation of the thiol patterns and the fluidic system is described. Thiol pattern characterisation includes the various parameters which are considered such as the cleanliness of the PDMS stamp, surface property, the concentration of the thiol compound, and the inking and stamping period of the stamp, etc. ANOVA analysis of the thiol concentration, inking, and stamping is provided to explain the effect of these parameters on the μ CP process. Then the effect of the concentration of the compound and pH value on the inking period is provided. The fluidic system characterisation includes a pump, valve, and flow sensor characterisation. Finally, test results of the As(III)-contaminated pattern are provided.

Chapter 6 discusses the conclusion and future work.

Chapter 2

Literature Review

The literature review is broadly classified into the following sections:

- Microfluidic detection for water quality that provides a comprehensive review of microfluidic water quality monitoring sensors
- Aptamer-based arsenic detection

The chapter describes the current developments in microfluidic sensors for overall water quality monitoring that includes heavy metals, nutrients, and pathogenic detection. Specific emphasis is given on the role of microstructure in sensors. Methods outlined here are categorized based on the transduction system including electrochemical and optical detection. Electrochemical detection covers techniques like electrochemical impedance spectroscopy (EIS), cyclic voltammetry (CV), and square-wave anodic stripping voltammetry (SWASV), etc. On the other hand, optical detection covers colorimetric, fluorescent, chemiluminescence (CL), surface-enhanced Raman scattering (SERS), and surface plasmon resonance (SPR) sensors. The advantages and limitations of each method along with their challenges while implementing field-effective sensors are also discussed in the review. In the final section, aptamer-based detection of As is discussed.

2.1 Microfluidic Water Quality Monitoring Sensors

During the past 50 years, heavy metals have significantly invaded our biosphere. Heavy metals (e.g. As, Pb, Hg, etc.) naturally exist in the surroundings, and various anthropogenic actions are also responsible for adding heavy metals to the environment [87]. Most of these heavy metals may cause fatal effects on public health due to their potentially mutagenic or carcinogenic effects on the human body [30, 33, 34, 88]. Nutrient contamination is also a concern for water pollution. A key source of nutrients (mostly phosphorus and nitrogen) is land run-off since the nitrate and phosphorus ions are not held by soil particles. Pathogen contamination is another cause for concern [89]. Water polluted with organic waste, human and animal excrement is a potent source of pathogenic bacteria, protozoa, viruses, and parasitic worms. It results in gastrointestinal illness and can be a potential risk to human health. *Escherichia coli* (*E. coli*) is generally considered as faecal indicator bacteria (FIB). Bacterial counts are typically used to evaluate the influence of sewage pollution [90–92]. Higher concentrations of contaminants in water are responsible for fatalities across the world.

The harmful outcomes of water pollution are increasing due to two main reasons: first, the level of contaminants in the water is continuously rising and there are no current practical methods to keep track of the natural changes, and the second is human growth, which leads to the need of expansion to new water sources of unknown quality. For this purpose, periodic water quality monitoring becomes very essential [93]. The traditional methods used for water monitoring are sensitive and reliable. However, mostly they are expensive as they rely on specific instrumentation (laboratory-based and non-portable). Also, the samples used in these methods require transportation from the site to the laboratory, which is time-consuming and, most importantly, is not field-effective. Hence, there is an increasing need to develop prompt, portable and inexpensive sensors with high sensitivity and reliability. An ideal sensor should have a low cost, high sensitivity and selectivity, a high throughput, be user-friendly, and should provide in-field operation ability. It should also meet the WHO guidelines for portable sensor requirements [94]. From these perspectives, microfluidic devices are significantly appealing technologies to achieve the Lab-on-a-chip (LoC)-based point-of-care applications [95].

Microfluidics is the technology that precisely manipulates a small volume of fluids, using channels with dimensions of tens to hundreds of micrometers [96–99]. This technology

has advantages such as faster reaction times, better process control, reduced waste generation, system compactness and parallelization, and reduced cost and disposability [96, 100–103]. Most of the microfluidic devices are disposable and are used for one-time measurements. Earlier, microfluidics mainly focused on the integration of microsensors with fluidic components (actuators, pumps, valves etc.) and on the miniaturization of analytical assays. Thereafter, Micro Total Analysis Systems (μ TAS) evolved using micro-fabricated structures. The miniaturization with microfluidics flourished in many life sciences fields such as genetic analysis, cell biology and protein analysis [104]. Currently, these devices are widely applied in all branches of science such as chemistry, biology, engineering, and bio-medical sciences, etc. In earlier days, silicon was used to fabricate the microfluidic devices [105–107]. Then glass and polydimethylsiloxane (PDMS) were used for fabrication purpose. Nowadays, even thermoplastic and paper are accepted as fabrication materials [95, 108, 109]. Several manufacturing techniques are available for microfluidic sensors such as injection moulding, softlithography, and mass-production technologies like etching. Among these methods, softlithography technique using polydimethylsiloxane (PDMS) is a highly popular method [110, 111]. However, this process requires special equipment, and in many cases access to a clean room [112]. Currently, researchers are also making use of commercial 3D printers to fabricate microfluidic sensors as it is possible to fabricate the micro-structures in one step from a computer based design. The frequently used approaches are inkjet printing, stereolithography (SLA), extrusion printing, etc. [113, 114]. Microfluidic sensors can be

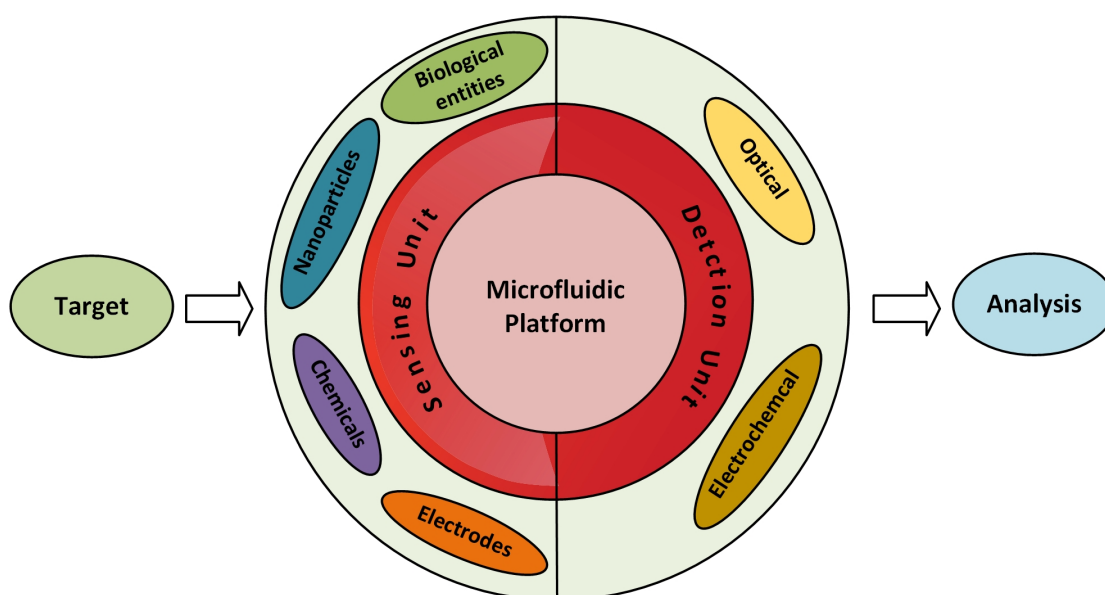


FIGURE 2.1: Illustration of a microfluidic system.

categorised in two types: one in which the microfluidic system measures the parameters inside it, the other in which the measurement of parameters takes place with the help of external integrated equipment [115–117]. Figure 2.1 represents the microfluidic system in two main parts - the sensing unit and the detection unit. The sensing unit involves elements such as biological entities, functionalised nanoparticles, and metal electrodes, etc., whereas the most commonly used detection systems with microfluidics are optical- and electrochemical-based systems [117, 118]. It is possible to perform multiple analyses on the microfluidic platform by just modifying its microchannel patterns. Micromixers have a pivotal point in enhancing the sensitivity of the microfluidic-based sensors [119–121]. Any extensive pre-analysis is not necessary while detecting the pollutants using microfluidic sensors. Hence, microfluidic LoC devices have been broadly studied as a substitute for conventional lab-based methods. Recent reviews presented contamination related to heavy metal [122], nutrients [123], and pathogens [124, 125] individually.

2.1.1 Microfluidic with electrochemical detection

Generally, the conventional electrochemical methods include a three-electrode system containing a reference electrode, a working electrode, and a counter electrode. An interaction between the analyte and electrode surface produces an electrical signal. According to this working principle, the detection method can be classified as amperometric, voltammetric, and potentiometric [126]. Measuring micro-volumes of the sample was difficult with the silver (Ag) electrode-based methods though it has a high sensitivity towards heavy metal detection [2]. The majority of these methods needed equipment like a rotator, stirrer, etc. Such limitations have been eliminated with the help of microfabrication technologies by incorporating them on the microfluidic platform. The reference, measuring, and the working electrode can be included in a microfluidic channel [127]. This miniaturization provides many advantages such as higher processing speed, mass production, portability, reduced cost, multiple analysis and simplicity [122]. These microfluidic electrochemical sensors can be used in point-of-care (POC) applications for water quality monitoring. For the last decade, microfluidic-based electrochemical sensors have been the subject of considerable study. Several research based sensors are discussed and listed in Table 2.1 and commercially available sensors are listed in Table 2.2.

2.1.1.1 Heavy metal detection

Voltammetric detection

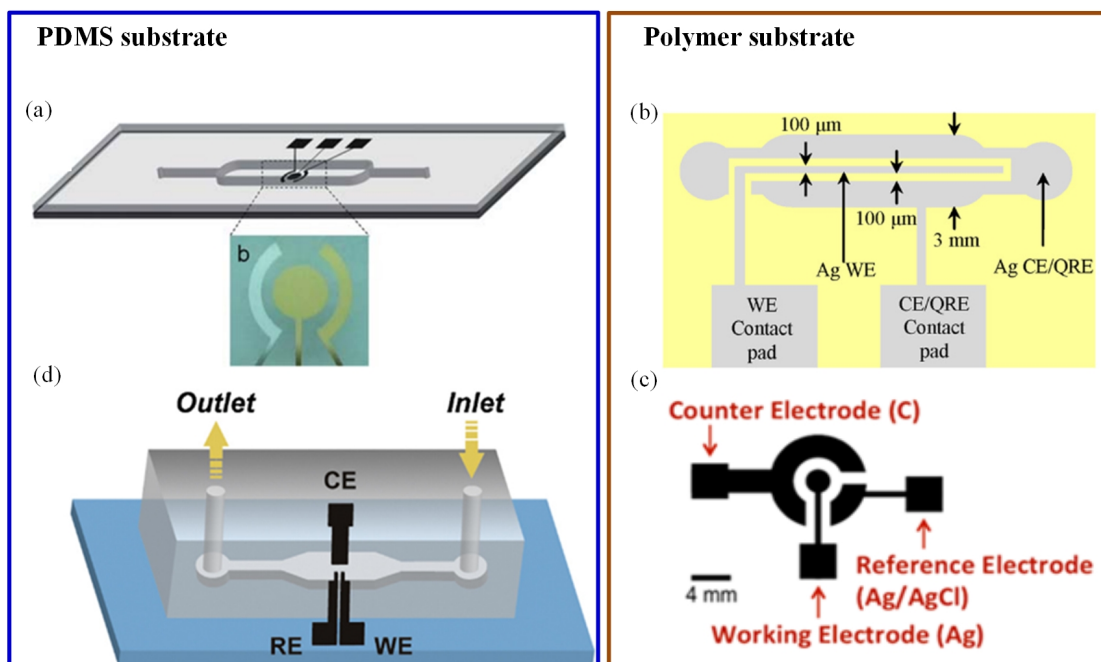


FIGURE 2.2: Different orientation of electrodes in electrochemical detection methods (a) Schematic of Au-Ag-Au electrode integrated with microfluidic channel to detect Hg^{+2} [1]; (b) Illustration of reusable polymer chip for detection of Pb^{+2} [2]; (c) Electrodes printed on plastic substrate to detect As(III) [3]; (d) SWCNTs electrodes for As(III) detection [4].

Chen et al. [1] developed a Hg^{+2} detector with high sensitivity and reproducibility. A three-electrode system (Au-Ag-Au) was integrated with a microfluidic channel as illustrated in Fig. 2.2a. A novel microfabrication technology (two-step photolithography) was used to develop the sensor. It turned out to be a disposable sensor due to reduced cost and less reactant consumption. Anodic stripping voltametry and differential pulse voltametry electrochemical analysis were used for detecting the Hg^{+2} ions. The low detection limit (3 ppb) was achieved by this sensor [1]. A similar three-electrode-based reusable polymer lab chip sensor was developed by Jung et al. [2] for Pb^{+2} detection as shown in Fig. 2.2b. A SWASV was used to perform Pb^{+2} analysis, the sensor was highly sensitive and environmentally friendly. The achieved limit of detection (LOD) was 0.55 ppb with 300 seconds deposition time. Another three-electrode system was used in As detection as shown in Fig. 2.2c. In this system, a disposable plastic substrate was used to print the electrodes (carbon, silver, and silver/silver chloride ink). When a water drop was introduced at the electrodes, the induced current was measured with the help of CV. The method could detect As with LOD of 1 ppb [3]. One more unique method

was reported in which the integration of gold nanoparticles with a microfluidic channel was performed using electrochemical deposition. It consisted of three electrodes, gold nanoparticles, and a microfluidic channel. Electrodes were constructed with single-walled carbon nanotubes (SWCNTs) and placed into a microfluidic device as shown in Fig. 2.2d. Gold nanoparticles were used as an electrolyte material for glucose and As detection. SWASV measurements were done for ultratrace As(III) analysis. The device provided rapid and sensitive results; it could detect up to 4.5 ppb within 60 seconds [4]. In 2016, an electrochemical sensor was screen-printed on flexible polyethylene terephthalate material. It was demonstrated for selective monitoring of Pb^{+2} and Hg^{+2} metal ions where electrodes were metalized by carbon- and silver-based inks. The results were reported using CV. The average peak current's shift was noticed at 50 μM of Hg^{+2} and Pb^{+2} . However, the system was not portable as it did not consist of a read out circuit [128].

In the last few years, paper-based microfluidics has become popular due to the following benefits first, no need of components like pumps and tubes as it works on capillary forces and, secondly, its cost-effectiveness [129–134]. As an example, an economical and simple microfluidic paper-based electrochemical sensing device (μPED) has been fabricated by Shi et al. [5] for detecting Pb^{+2} and Cd^{+2} in aqueous samples. They have integrated commercial screen-printed carbon electrodes with filter paper strips as shown in Fig. 2.3. The electrochemical technique was also linked with biological engineering. In such a combined system, the signal produced by biosensor is analyzed through a three-electrode system. The detection was carried out with the help of SWASV and found a very good limit of detection (2.0 ppb for Pb^{+2} and 2.3 ppb for Cd^{+2}). The device also exhibited high sensitivity and stability with real samples without pretreatment of the water sample. Some researchers have also recommended the use of bioreporters for heavy metal detection. For example, Corts-Salazar et al. [6] utilized the natural *E. coli* defence system against toxic As(III).

In this method, they used a commercially available disposable microchip. It contained 16 independent electrochemical cells. The *E. coli* reporter strain was filled in the microchip. When bioreporter encountered As, β -Gal activity was produced within 25 min- 50 min. The reported LOD for the method was 0.8 ppb. The principle of bioreporter is illustrated

Voltammetric detection on paper substrate

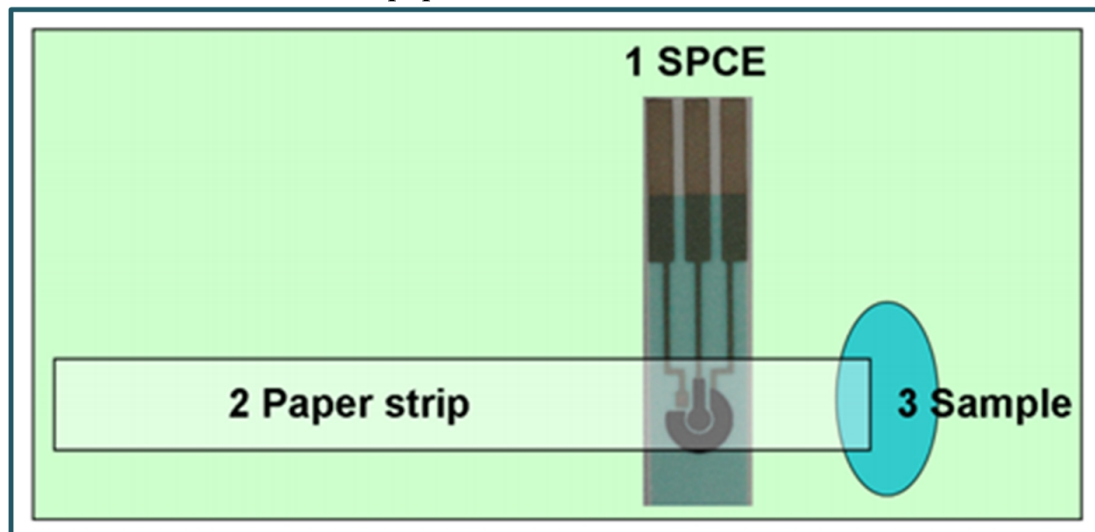


FIGURE 2.3: Schematic of paper-based method including integrated commercial screen-printed carbon electrodes with filter paper strips for detection of Pb^{+2} and Cd^{+2} [5].

in Fig. 2.4. Thus this microfluidic biosensor has the potential to detect As with high sensitivity.

Amperometric detection on plastic substrate

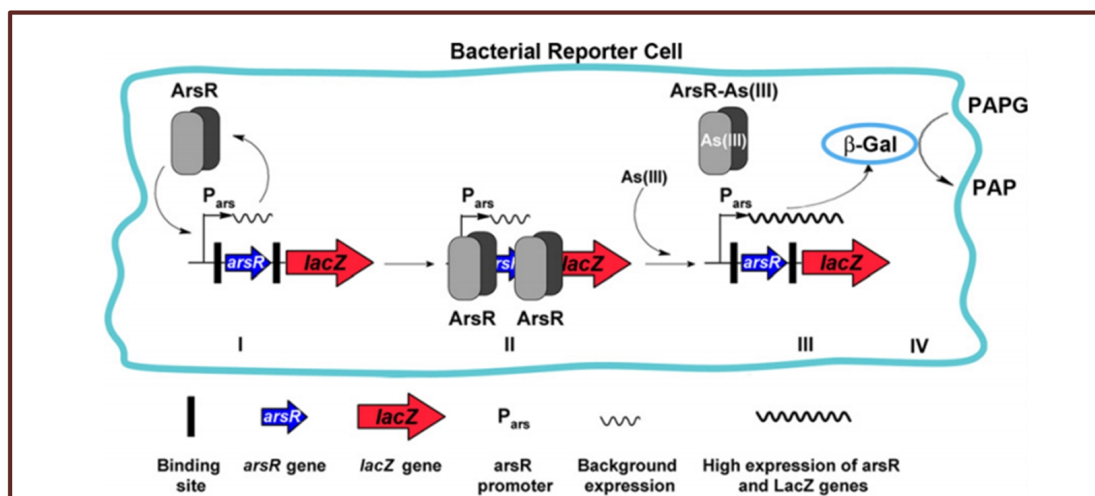


FIGURE 2.4: Pictorial presentation of the working scheme of As(III) bioreporter [6].

TABLE 2.1: Comparison of electrochemical methods

Electrochemical methods						
Target Analyte	Detection Principle	Sensing Element	Sensing Material	Substrate	LOD	Real Sample Ref
Hg ⁺²	ASV	Electrode system	WE: Au CE: Au	PDMS	3 ppb	No [1]
Pb ⁺² & Hg ⁺²	CV	Electrode system	RE: Ag WE: carbon CE: Ag RE: Ag/Cl	Polyethylene terephthalate	50 μ M each	No [128]
Pb ⁺²	SWASV	Electrode system	WE: Ag CE/QRE: Ag	Polymer	0.55 ppb	No [2]
Pb ⁺² & Hg ⁺²	SWASV	Electrode system	WE: carbon CE: carbon RE: Ag pseudo	Paper	2.0 & 2.3 ppb, resp. water	Soda water & dirty ground [5]
As	CV	Electrode system &	WE: Ag CE: Carbon	Plastic	1 ppb	No [3]
As	SWASV	Electrode system	RE: Ag/AgCl WE: Au/SWCNT CE&RE: SWCNT	PDMS	4.5 ppb	No [4]
As(III)	Amperometry	Bioreporter with Electrode system	WE:Au CE & RE:Ag and E. coli	Plastic	0.8 ppb	Tap & ground - water [6]
Nitrate	CV	Electrode system	WE & RE: Ag CE: Au	Glass	25 ppb	[7]

Electrochemical methods continues..

Target Analyte	Detection Principle	Sensing Element	Sensing Material	Substrate	LOD	Real Sample	Ref
Nitrate	CV	Electrode system	WE: Ag CE: Au RE: Ag	Glass	0.2 ppm	Field & Environmental water	[9]
Nitrate & Potassium	Potentiometric	Electrode system	WE: Polymeric membrane RE: Ag/AgCl	Green tapes	9.56 & 0.81 mg/L, respectively	water from Recycling unit	[8]
Nitrate	Potentiometric	Electrode system with modified working electrode	WE:f-MWCNTs RE:Ag/AgCl	Lipophilic carbon nanotubes	5×10^{-7} M	Desalinated seawater	[135]
Nitrate	ELS	Electrode system with modified working electrode	WE: NiR/nTiO ₂ -GF CE: Au	PDMS	1 μ M	No	[10]
Nitrate & Nitrite	SWV	Electrode system with modified working electrode	WE: Ag/AgCl RE: Cu/MWCNT/RGO/GCE	GCE	20 & 30 nM, resp.	Tap & mineral water	[65]
E. coli	Voltammetry	Electrode system with modified working electrode	WE: immobilised DNA probe on Au CE & RE:Pt	Glass	100 nM	No	[11]
Hepatitis B	ASV	Electrode system	WE: GCE CE: Pt wire RE: Ag/AgCl and DNA modified AgNP	Paper	85 pM	No	[136]

Electrochemical methods continues..						
Target Analyte	Detection Principle	Sensing Element	Sensing Material	Substrate	LOD	Real Sample Ref
E.coli	Positive dielectrophoresis	Sensing & focusing electrode	Not specified	PDMS	300 CFU/mL	No [137]
E. coli	EIS	Interdigitated electrodes	Modified silicon sensor chip	Silicon & PDMS	10 cells/mL	No [138]
E. coli & S. aureus	EIS	Coplanar electrode	Au electrode	Silicon	522 cells/mL	No [139]
E. coli & Enterococci	Coulter principle	Microfluidic sensing chip	Resistance detection circuit	PDMS	Individual cell	Ballast water sample [140]
Salmonella typhimurium	Impedance analyzer	Interdigitated electrodes	Au electrode with immobilised antibodies	PDMS	3×10^3 CFU/mL	No [141]

WE: Working electrode; CE: Counter electrode; RE: Reference electrode

TABLE 2.2: Commercially available electrochemical sensors

Target Analyte	Measurement Principle	Measuring Range	Features	Company	Ref
Arsenic	Paper based electrochemistry test strips	Not specified	Easy-to-use, Quantitative, Fast, Low cost, Non-toxic, disposable	Bio Nano Consulting	[142]
Copper, Lead, and Cadmium	Stripping Square Wave Voltammetry with carbon-carbon-silver electrodes	Not specified	Easy-to-use, Quantitative, Simple, easy to use, cost effective	PalmSense	[143]
Heavy metals	Potentiometric cell with carbon-bismuth electrodes	Not specified	Simultaneous analysis, Portable systems,	GTQ (Chemical Transducers research Group)	[144]
Nitrate	Potentiometric cell with liquid membrane ion selective electrodes	0.6 to 200.0 ppm	In-situ results, Low cost detection of nitrate-nitrogen in freshwater samples	MEDIRAY	[145]
Nitrate	Potentiometric cell with ion selective electrodes	0.5 to 450.0 mg/L	Simple to use	Xylem	[146]
Nitrate	Potentiometric cell with ion selective electrodes	1 to 14,000 mg/L	Calibration free operation	Vernier	[147]
Nitrate	Potentiometric cell with ion selective electrodes	0.62 to 6,200 ppm	Replaceable sensing modules durable polyetherimide (PEI) body BNC Connection	HANNA instruments	[148]

2.1.1.2 Nutrients

Gartia et al. [7] fabricated an economical, sensitive, and portable electrochemical-based measurement system for quantitative detection of nitrate in a groundwater sample (Fig. 2.5a). The sensor chip was fabricated on a glass substrate. The working and reference electrodes were made up of a thin layer of silver. The counter electrode was a gold deposited thin layer. The uniformity of current distribution between electrodes was enhanced using a concentric layout for the counter and working electrodes. They fabricated a miniaturized potentiostat circuit with wireless interface to make the sensor field-deployable. When the performances of a microsensor and a macroelectrode-based electrochemical system were compared, the precise examination proved that the convention macroelectrodes had far less sensitivity than the microsensor. The CV determination of nitrate ions in numerous water specimens was performed using the sensor. The LOD for the microsensor was approximately 25 ppb.

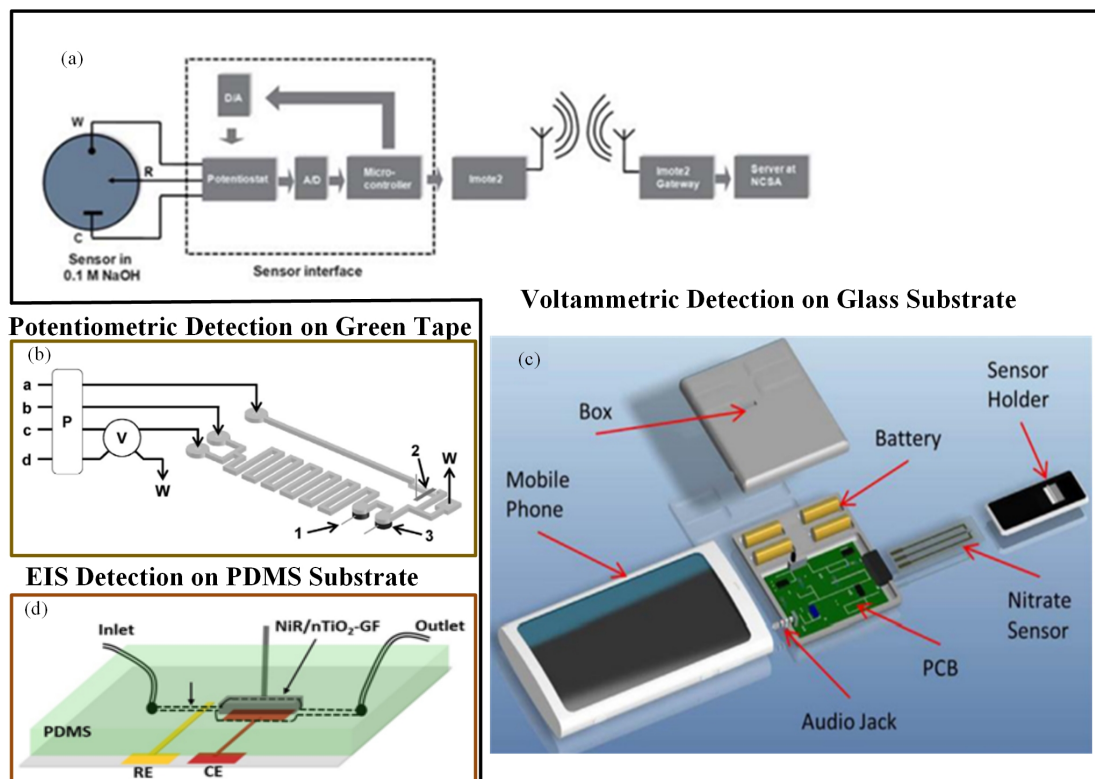


FIGURE 2.5: (a) Nitrate sensor chip with wireless communication interface [7]; (b) Experimental set up of LTCC-based continuous flow potentiometric microanalyzer to determine potassium and nitrate [8]; (c) A mobile sensing platform with a plug-n-play microelectronic ionic sensor to detect nitrate [9];(d) nTiO₂ modified GF based nitrate sensor [10].

In a similar manner, Wang et al. [9] developed a mobile phone electrochemical sensing platform for nitrate quantification as shown in Fig. 2.5c. A mobile phone sensing platform included a plug-n-play microelectronic ionic sensor which performed electrochemical computation utilizing the smartphone audio jack. A LOC sensing system incorporated a microelectrochemical sensor, a mobile app and a controlling unit to control the microfluidics along with the sensor and also manage the liquid specimens. On the glass substrate, reference and working electrodes were constructed from a silver layer and gold layer was used to create the counter electrode. The assay utilized an audio jack to interface the sensor instead of a camera. A user-friendly mobile application interface made a testing procedure very simple to use. This compact smartphone-based application could determine nitrate concentration with a LOD of 0.2 ppm in 60 seconds. Additionally, the mobile app could save the data on cloud servers.

Calvo-Lpez et al. [8] developed a compact low-temperature co-fired ceramics (LTCC)-based continuous flow potentiometric microanalyzer prototype to concurrently detect the occurrence of nitrate and potassium ions in the specimens of a water recycling process (Fig. 2.5b). The microsystem combined microfluidics with the sensing mechanism within the same substrate. The detection system comprised of two ion-selective electrodes that were constructed using a screen-printed Ag/AgCl reference electrode and ion-selective membranes. A detection limit was 0.81 mg/L and 9.56 mg/L for potassium and nitrate ions respectively.

Generally, voltammetric procedures are easy, quick, inexpensive, and not requiring specimen pretreatment before the investigation of the ions in the real specimens. Still, the production of electrodes that are modified chemically is the main obstruction in such sensors. Enhancing the ability to transfer electrons between the electrode surfaces and the electroactive analytes is the principal objective of modified electrodes. Many carbon nano-structured materials like multiwall carbon nanotubes (MWCNTs), graphene, included with metal nanoparticles have been adopted extensively currently, for accomplishing this purpose [149]. Cuartero et al. [135] reported use of such carbon nanotubes in their method. They developed a technique to determine nitrate in seawater using the direct potentiometric method by in-line coupling to an electrochemical desalination module. Generally, the presence of highly concentrated sodium chloride in seawater causes difficulties in determining the nutrients nitrite, dihydrogen phosphate, and nitrate at the low micromolar level. In traditional analytical procedures like colorimetry,

UV absorption, fluorescence, chemiluminescence, and ion chromatography applied for estimating nitrate levels in seawater, very complex pretreatment is necessary. In this method, a different strategy was accomplished for the reduction of chloride concentration with a simple electrochemical transformation. A custom-made microfluidic-based flat desalination cell was combined with the potentiometric sensor (flow cell). The flow cell included ion-to-electron transducer and a miniaturized reference electrode where the transducer was made of lipophilic carbon nanotubes (f-MWCNTs) based nitrate selective electrode. The LOD of this assay was 5×10^{-7} M. Bagheri et al. [65] fabricated a novel method in which they deposited CuNPs upon MECNTs-reduced graphene oxide nanosheets (Cu/MWCNT/RGO) and detected nitrite and nitrate ions individually and simultaneously. The sensitivity and selectivity of GCE were improved due to the nanoparticles deposition on MWCNT-RGO nanocomposite. The output recorded the concentrations of both ions within a span of 0.1 to 75 μ M while determining the analyte simultaneously. The LOD for nitrite ion was 30 nM and for nitrate ion was 20 nM.

Ali et al. [10] described a microfluidic sensor in which nitrate monitoring was performed with the help of the EIS technique. An electrochemical electrode used in the method was a porous graphene foam (GF) scaffold. The electrochemical response was improved by modifying the GF scaffold with electrospun nTiO₂ and nitrate selectivity was increased by modifying the scaffold with nitrate reductase (NiR) enzyme molecules. Nitrate solutions passed over the nTiO₂ activated porous GF and very good interaction with distinct receptor NiR bound at the scaffold surfaces occurred for nitrate detection (Fig. 2.5d). The sensor had high sensitivity, selectivity, and rapid detection time in nitrate ions quantification.

2.1.1.3 Pathogens

Pathogen detection can be performed with a DNA/protein/cell-based probe. Nucleic acid detection has been recognized as a highly sensitive and selective technology. DNA based pathogen analysis can be obtained either by direct target probing or after target amplification. Kim et al. [11] designed a compact, low-cost, electrochemical DNA-based sensor to provide real-time, continuous monitoring of pathogens. A mobile interface was coupled with the sensor that provided the analysis in terms of safe or unsafe water. The electrochemical sensor consisted of two working electrodes with platinum-based

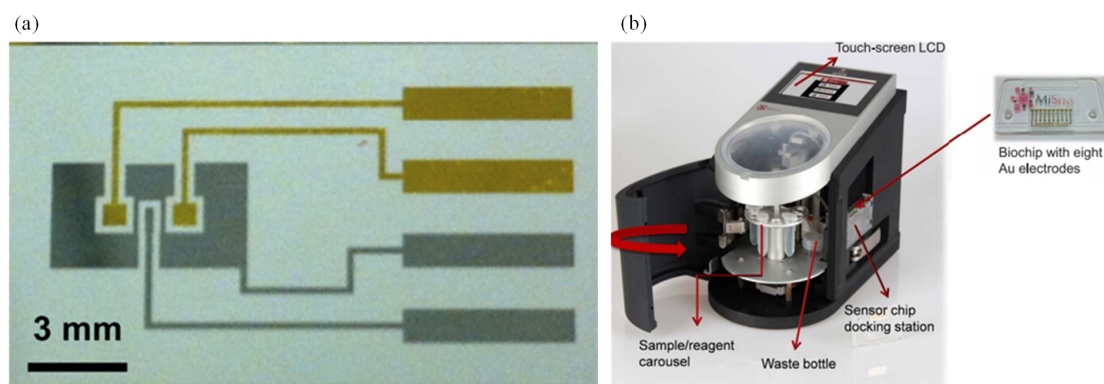


FIGURE 2.6: (a) Electrochemical DNA-based sensor for *E. coli* determination [11]; (b) Custom made automatic biosensor for pathogenic detection [12].

reference and counter electrode (Fig. 2.6a). Immobilization of the working electrode was done with a DNA probe in the stem-loop structure. The MB provided the electron transfer which resulted in the current peak. When *E. coli* was introduced into the chamber, hybridization of the DNA probe took place. This resulted in the opening of the stem-loop structure which further resulted in a reduction of the current peak. This method provided qualitative results and was suitable for POC use. Li et al. [136] fabricated another electrochemical DNA-based sensor to detect hepatitis B virus (HBV). It was a simple paper-based biosensor designed with an origami paper structure and was functionalised with a DNA-modified AgNP. The use of DNA increased the speed, stability, and robustness of the biosensor. Its LOD was 85 pM.

Altintas et al. [12] fabricated a custom-made fully automatic biosensor for pathogen quantification. This device involved a novel biochip design integrated with the microfluidic system along with real-time amperometric measurements. The microfluidic system consisted of a plug and play type biochip docking station that also served as a flow cell for the electrode array along with the electronic connections (Fig. 2.6b). The sensor surface was modified with the self-assembled monolayer (SAM) of mercaptoundecanoic acid and placed. SAM coated electrode arrays were then activated with polyclonal rabbit anti-*E. Coli* antibody. Then an *E. coli* sample was introduced on the electrode surface. Subsequently, a horse radish peroxidase coupled detector antibody was injected. Thus the sandwich immunoassay was used for determination of *E. coli*. This work reported a rapid, sensitive, and specific detection of a waterborne pathogen *E. coli*. The sensor output was enhanced through the use of gold nanoparticles when compared with the standard sandwich method. The detection limit was 50 colony forming units (CFU)/mL.

The EIS method can illustrate various characteristics of electrochemical technique such as adsorption, capacitance, diffusion coefficients, electron transfer rate constants, and charge transfer resistances. Its cost-effectiveness, simplicity, and sensitivity have allowed researchers in the recent past to use it in a bio-sensing platform with many label-free transduction methods including impedance flow cytometers and Coulter counters [150–152]. A sample of particles scattered in a liquid is guided in the direction of electrodes through a microfluidic channel when an alternating electric field is applied in EIS. The size and configuration of the particles are responsible for alterations in the electric field to particle displacements. The electrical current analysis is used to measure these alterations [152]. Several such examples of EIS based detection methods are reviewed in the following paragraph.

Kim et al. [137] reported a label-free *E. coli* detection method that utilized positive dielectrophoretic (pDEP) focusing, capturing, and impedance measurement. This (pDEP)-based system consisted of an *E. coli*-focusing and sensing electrode. Inclusion of the passivation layer avoided the adhesion of *E. coli* to the electrode. The change in impedance occurred due to trapping of the *E. coli* cell on the sensor electrode. The assay evaluated 300 CFU/mL within 1 min. Jiang et al. [138] designed a portable microfluidic smartphone-based EIS sensor with Bluetooth connectivity. The microfluidic sensor consisted of a microhole array silicon substrate with interdigitated sensing electrodes on it and a sensing microfluidic chamber aligned with a nano-porous filter paper. This filter paper allowed bacteria to pass through while blocking big dirt particles in water samples. The unit also included an impedance network analyzer chip with a microcontroller to perform EIS measurement and analysis. The developed android-based software app was able to remotely control the microcontroller through Bluetooth. The app could perform functions like a commercially available LCR meter. The LOD for the bacteria sensing was 10 *E. coli* cells per milliliter. Clausen et al. [139] developed another impedance-based real-time microfluidic sensor to measure the bacteria levels in water samples with the water samples flowing continuously through the sensor. This method could discriminate *E. coli* from solid particles with the help of electrical response in the high-frequency phase. Additionally, the method was able to recognize different bacteria cells - *Staphylococcus aureus* (*S. aureus*) and *E. Coli*. It provided LOD of 522 cells/mL with real-time continuous monitoring of bacteria in an aqueous sample utilizing impedance flow Cytometry. Maw et al. [140] utilized a submicron resistive pulse sensor

based on the Coulter principle for *E. coli* monitoring. The sensitivity of this method was improved due to sample handling in a microfluidic chip and the phenomena of microscale hydrodynamic flow. The unit was made up of a supply section, base unit, detection system, data acquisition system, signal processing unit, and display unit. The base unit comprised of a PDMS microfluidic chip and four electrodes and detection occurred at the microfluidic platform. This label-free and automatic method provided a rapid result and appeared to be a user-friendly device.

Ghosh et al. [141] presented an economical and easy microfluidic biosensor for quick and accurate measurement of *Salmonella typhimurium*. The microfluidic chip involved the interdigitated electrode array. The electrode array surface was immobilised with anti-*Salmonella* antibodies. The biosensor provided qualitative as well as quantitative impedance analysis within 3 hours. Its LOD was 3×10^3 CFU/mL. The authors also compared the performance of the microfluidic biosensor with the non-microfluidic biosensor. They found two to three times higher impedance response for the microfluidic biosensor with lower LOD compared to the non-microfluidic biosensor.

2.1.2 Microfluidic with optical detection

Many electrochemical methods have been presented for water quality monitoring in this review paper. The optical strategies due to their simplicity and cost-effectiveness, are equally popular too. In optical-based microfluidic devices, the optical changes happen due to the chelation between the recognition element and the target constituents. These optical-based microfluidic devices are based on various techniques such as colorimetry, CL, fluorescence, SERS, and SPR. The colorimetric devices include measurement of the colour change associated with the reaction between the analyte and the sensing element. The colour variation can be observed by the bare eye or with the help of an optical detection method [153]. In the fluorescence detection method, the analyte-induced changes are responsible for variations in characteristics of fluorochromes including fluorescence intensity, fluorescence polarization, and lifetime [122]. Several research-based examples of such detection methods are considered in the following paragraphs and are described in Table 2.3. Some commercially available sensors are listed in Table 2.4.

TABLE 2.3: Comparison of optical methods

Optical methods							
Target Analyte	Detection Principle	Sensing Element	Sensing Material	Substrate	LOD	Real Sample	Ref
Cu(II)	Colorimetric	Chemical	Sodium diethyldithio-	Paper	0.29 ppm	Distilled water	[14]
Ni(II)		Compound	carbamate		0.33 ppm	Reservoir water	
Cd(II)			Dimethylglyoxime Cation		0.19 ppm	Beach water	
Cr(VI)			Diphenylcarbazide		0.35 ppm		
Hg ²⁺	Colorimetric	Nanoparticles	Platinum nanoparticles & 3,3',5,5'-tetramethylbenzidine	Paper	0.01uM	Pond & tap water	[154]
Pb ²⁺	Colorimetric	functionalised nanoparticles	AuNP functionalised with 11-mercaptopoundecanoic acid	PDMS	10 μ M	No	[17]
As(III)	Colorimetric	functionalised nanoparticles	AuNP functionalised with α -lipoic acid & thioguanine	Paper	1.0 ppb	No	[15]
As	Colorimetric	functionalised nanoparticles	AuNP functionalised with α -lipoic acid	Paper	Quality analysis	Bangladesh groundwater	[16]
As(III)	Colorimetric	HachEZ Arsenic Test Kit	Standard Gutzeit reaction reagents	Plastic	3 μ g/L	No	[155]
Cu ²⁺ & Hg ²⁺	Fluorescence	Quantum dots	CdTe quantum dots	Paper	0.035 μ g/L	Lake & sea water	[18]
As(III)	Fluorescence	Bioreporter cell	E. coli	PDMS	0.056 μ g/L	Tap water	[20]
As(III)	Fluorescence	Bioreporter cell	E. coli	PDMS	10 μ g/L	No	[19]
As(III)	SERS	functionalised nanoparticles	AgNP functionalised with glutathione/4-mercaptopyridine	PDMS	50 μ g/L	Tap water	[156]
			glutathione/4-mercaptopyridine		0.67 ppb	Mineral water	
As(IV)	CL	Chemical Compound	Luminol & Vanadomolybdoarsenate heteropoly acid	PDMS	8.9 $\times 10^{-8}$ M	Tap water	[157]

Optical methods Continues..							
Target Analyte	Detection Principle	Sensing Element	Sensing Material	Substrate	LOD	Real Sample	Ref
Nitrate	Colorimetric	Chromogenic agent	Chromotropic acid & Sulphuric acid & Sulphuric acid	PDMS	0.70 mg/L	Drinking water, freshwater, Wastewater, & Seawater	[22]
Nitrate	Colorimetric	Chromogenic agent	Griess reagent	Fiber	7 $\mu\text{g/L}$	Lake water	[23]
Nitrate	Colorimetric	Chromogenic agent	Griess reagent	PMMA	0.0782 ppm	Tap water	[158]
Nitrite & Nitrate	Colorimetric	Chromogenic agent	Griess Reagent	Paper	1.0 μM	Bottled drinking water	[21]
Nitrite & Nitrate	Colorimetric	Chromogenic agent	Zinc microparticles	PMMA	19 μM	Tap water & Synthetic water	[159]
Nitrite & Nitrate	Colorimetric	Chromogenic agent	Griess Reagent	PMMA	0.02 μM	River water &	[160]
Nitrite & Nitrate	Colorimetric	Chromogenic agent	Imidazole buffer	PMMA	0.025 μM	Sea water &	[160]
E. coli	PCR	Biological elements	Copper activated cadmium column	PMMA	20 nM	Recreational lake water	[161]
E. coli	Fluorescence	Biological elements	Polyclonal antibodies	PMMA	6 CFU	Waste water	[162]
Roravirus	Fluorescence	Biological elements	Magnetic beads conjugated with antibodies	PDMS	-	Drinking water	[162]
Antimicrobial-Resistant Bacteria	Colorimetric	Chromogenic agent	Graphene oxide Nitrocefin	Glass	10 ⁵ PFU/mL	No	[163]
				Paper	10 mU/mL	Sewage water, River water	[164]

Optical methods Continues..

Target Analyte	Detection Principle	Sensing Element	Sensing Material	Substrate	LOD	Real Sample	Ref
E. coli	Fluorescence	Biological elements	Streptavidin coated magnetic markers	PDMS	-		[165]
E. coli	Light scattering	Biological elements	Antibody-conjugated beads	Paper	10 CFU/mL	Field water	[24]
E. coli	SPR elements	Biological	Au surface modified with MUA, EDC/NHS, Protein G, & anti-LPS antibody	PMMA	-	No	[25]
Roravirus	Fluorescence		Graphene oxide	Glass	10 ⁵ PFU/mL	No	[163]
Antimicrobial-Resistant Bacteria	Colorimetric	Chromogenic agent	Nitrocefin	Paper	10 mU/mL	Sewage water, River water	[164]

TABLE 2.4: Commercially available optical sensors

Target Analyte	Measurement Principle	Measuring Range	Features	Company	Ref
Arsenic	Kit based colorimetric	0 to 500 ppb	Easy-to-use, Effective way	Hach	[166]
Arsenic	Kit based colorimetric	0 to 500 ppb	Result in 12 minutes, 100 tests per kit	FilterWater.com	[167]
Arsenic	Kit based digital colorimetric	2 to 100 ppb	Reaction time 20 minutes	Palintest Water analysis technology	[168]
Arsenic	Atomic fluorescence spectrometry	10 ppt	easy-to-learn and, easy-to-use system, Can be automated	P S Analytical	[169]
Lead, thallium, mercury, cadmium iron, nickel & zinc	Color-based visual detection	Not specified	Simple to use, Results in 15 to 60 Seconds	ChemSee	[170]
Nitrate	Portable photometer	0.0 to 30.0 ppm	Low-Cost Analysis	HANNA instruments	[171]
Nitrate	UV absorbance with	0 to 50 mg/L	Easy to use Not suitable for seawater	HydroMetrics	[172]
Nitrate	UV absorbance with	0.05 to 200 mg/L	Modern communication systems allow data to be accessed in real-time in real-time	OTT ecoN	[173]
C. jejuni, C. coli, C. upsaliensis & C. lari	PCR-Campylobacter detection Kit	Not specified	Optional anti-fouling wiper Flexible sensor options specific, rapid, & reliable detection, Amplification limit of one copy per reaction Ready-to-use Kit	BioVision	[174]

free from ambient light interference [175]. Mentele et al. [13] reported a paper-based colorimetric device (μ PADs) for metal ion (Fe, Cu, Ni) detection (Fig. 2.7a). This method provides a rapid and an inexpensive way of metal ion detection. The possibility of utilizing paper microfluidics as a 3D device was proved by Wang et al. (Fig. 2.7b) [14]. They developed a 3D paper-based microfluidic device for multiplex heavy metal (Cu (II), Ni (II), Cd (II), and Cr (VI)) detection through a simple combination of patterned paper by wax printing, tape, and stacking. The colorimetric determination was performed in association with a smart-phone camera. The developed technique was rapid, low-cost, and user-friendly.

To avoid toxic chemical reactions in As analysis, researchers have investigated and found gold nanoparticles (AuNPs) to be promising sensor materials in the colorimetric probe. Nath et al. [15] determined As(III) with the help of simple paper-based microfluidics along with a gold nano-sensor (AuTATG). The steady flow rate of the paper substrate pores allowed a very low concentration of As to remain in a microchannel for a long enough period so that it interacted with the nano-sensor. A rapid reaction of AuTATG with As ions resulted in a visible dark bluish-black precipitate at the interfacial zone. The working principle is illustrated in Fig. 2.7c. However, these μ PADs were not tested against groundwater samples. When similar implementation was tested with groundwater samples, the interference from several naturally occurring metals was observed [16]. To eliminate this limitation, Chowdury et al. [16] developed a T-shaped μ PAD using the same functionalised gold nanoparticles (Au-TA-Au) as illustrated in Fig. 2.7d. Additionally, they adjusted the pH value of the water sample to avoid the other metal interference. However, this assay provided just a qualitative result. Chen et al. [154] reported one more user-friendly and a rapid μ PAD for mercury(II) ion (Hg^{2+}) measurement in water, for which, they made use of oxidization of tetramethylbenzidine due to platinum nanoparticles and suppression of the reaction due to the presence of (Hg^{2+}) ion. The whole interaction resulted in a visible colour change that was provided as a digital readout through the fiber optic module (Fig. 2.7e). The sensor was capable of measuring (Hg^{2+}) concentrations till $0.01\mu\text{M}$.

Fan et al. [17] designed a portable, power-free microfluidic device to detect lead (Pb^{2+}). They detected Pb^{2+} with MUA modified AuNPs (MUA-AuNPs). The chemical reaction between Pb^{2+} and MUA caused the aggregation of the modified nanoparticles which in

turn produced the solution colour change from red to purple. The output could be observed with the bare eye with the help of water drop. It was a rapid and inexpensive method with a LOD of 10 μM . In 2017, Bonyar et al. [155] developed a custom-tailored colorimetric semi-automated portable device for As(III) detection in drinking water. They integrated a commercially available As test kit into a disposable microfluidic cartridge as shown in Fig. 2.8a. The Gutzeit reaction was carried out in the cartridge with automatic camera-based colour evaluation. The entire operation was easy to perform due to its user-friendly semi-automatic action and required approximately 1 hour to obtain a result.

Miniaturization of fluorescence detection was possible due to the use of the light-emitting diodes (LEDs) in the optical detection system. LEDs can emit at various wavelengths and they can easily fit into typical chip features [116]. Fluorescence detection is an extremely sensitive technique. However, according to Li et al. [116], its major limitation is that it can be used with the analytes that have native fluorescence or that can easily be fluorescently labelled. Still, many researchers have employed fluorescence detection to determine water pollutants. Qi et al. [18] developed a 3D paper-based fluorescence sensor to determine Cu^{2+} and Hg^{2+} ions. It was based on a combination of quantum dots (QDs) and an ion imprinting technique on 3D origami paper. CdTe QDs were implanted on the exterior of the glass fiber paper (Fig. 2.8a). The change in fluorescence was produced due to the transfer of the photoluminescent energy of the QDs to its ion imprinting-QDs complex. Bacterial bioassays have shown better performance in As detection compared to a chemical field kit [176]. Theytaz et al. [19] created a microfluidic chip containing immobilised *E. coli* biosensor bacteria (Fig. 2.8b). The *E. coli* generated green fluorescent protein in response to As(III). The major drawbacks of the developed method were its low LOD (50 $\mu\text{g/L}$) and the use of an epifluorescence microscope that made it a lab-based method. Similarly, Buffi et al. [177] demonstrated fluorescence detection of As(III) with the help of a bacteria-based bioassay. The natural defence system of *E. coli* against As(III) was used to produce a fluorescence signal. The *E. coli* was embedded in small agarose beads. These beads were stored on a microfluidic chip; the fluorescence microscope was then used for signal detection. Hence the bioassay cannot be considered as a portable device. Further, in 2014, this assay was enhanced by Truffer et al. [20]. They incorporated an electronic device with a small optical setup to measure fluorescence from bacterial reporter cells (Fig. 2.8c). As a result, the device

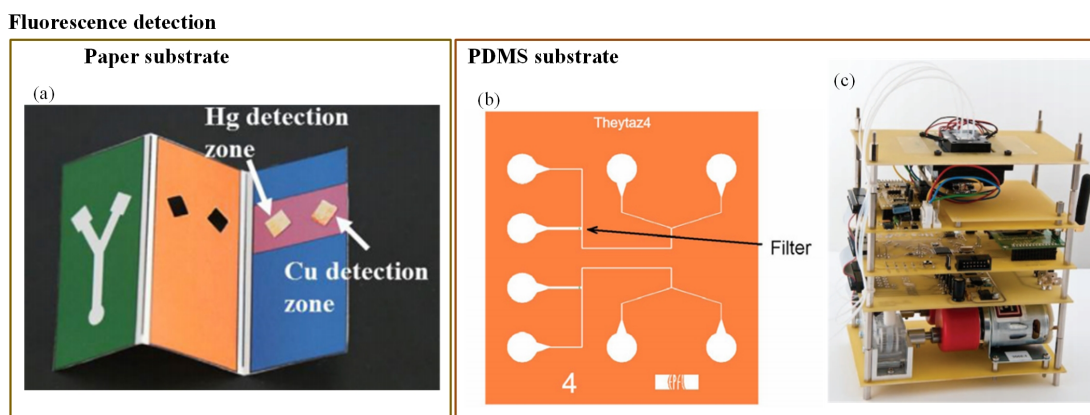


FIGURE 2.8: (a) 3D paper-based fluorescence detection of Cu^{2+} and Hg^{2+} [18]; (b) *E. coli* based fluorescence detection of As(III) [19]; (c) Fluorescence detection of As(III) using portable bioreporter [20].

displayed significant potential for field measurements.

Currently, SERS integration with LoC devices is rapidly being adopted in biological and environmental analysis. Qi et al. [156] displayed prominent potential in integrating SERS technology with microfluidics in the field of water quality monitoring. They implemented a continuous flow detection of As(III) ions rapidly. Silver nanoparticles were modified with glutathione/4-mercaptopyridine (GSH/4-MPY). As(III) has a high affinity towards GSH. Hence, as As(III) came in contact with GSH/4-MPY, aggregation of nanoparticles occurred that produced a Raman signal. The developed assay was highly sensitive and reproducible with the LOD of 0.67 ppb.

Som-Aum et al. [157] developed a highly sensitive microfluidic sensor based on the CL method that could detect As(III) in water. In this method, sorption of a As(V) pre-concentration in the form of vanadomolybdoarsenate heteropoly acid (VMoAs-HPA) ion-paired with hexadecyltrimethylammonium bromide on the surface of polystyrene beads packed in the microfluidic tool was observed. The matrix effect was removed by adding 1×10^{-8} M ethylenediaminetetraacetic acid to all work solutions. Additionally, the interference from phosphate and chromate was eliminated by the synthesis of sorption pre-concentration. That also helped to enhance the sensitivity. The method obtained LOD of 8.9×10^{-8} M within 5 min.

Colorimetric detection with chromogenic agent

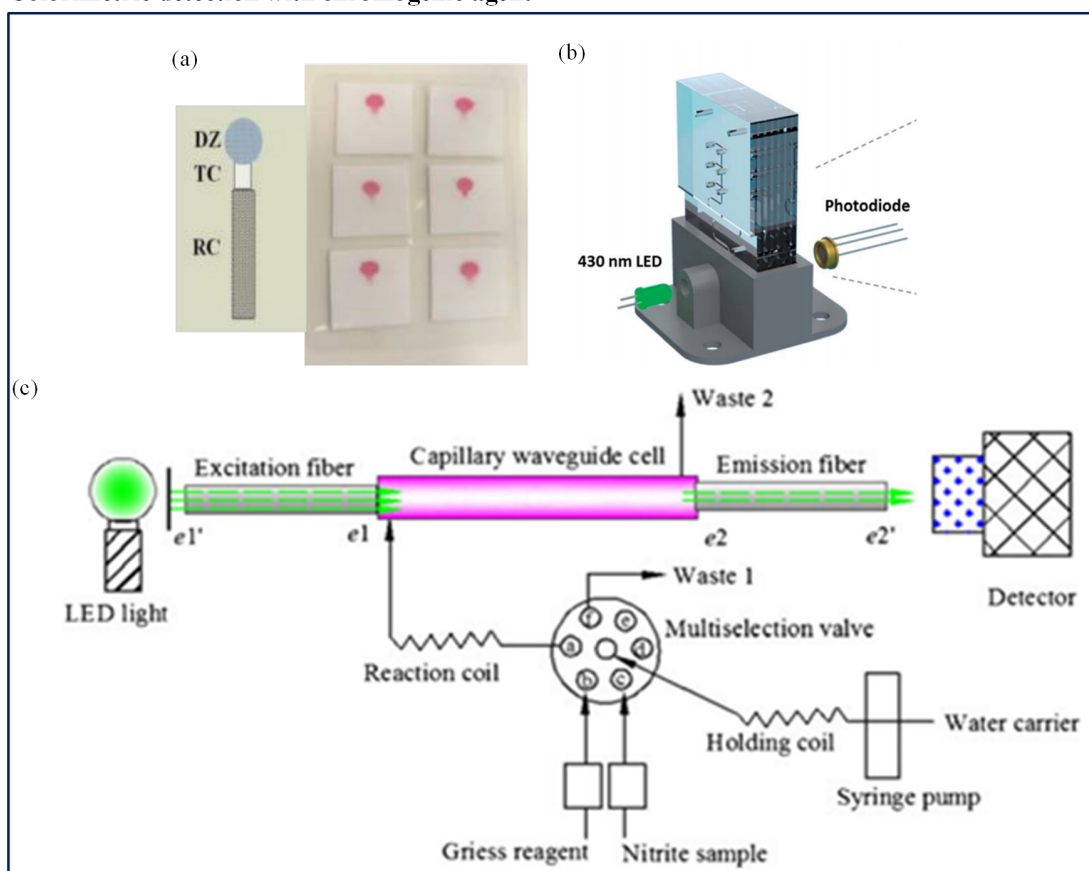


FIGURE 2.9: (a) Quantification of nitrite and nitrate using disposable μ PAD [21]; (b) Schematic of the flow system and detection cell of LED-based nitrate sensor [22]; (c) Schematic of FOCUS method for nitrite measurement [23].

2.1.2.2 Nutrients

Most of the available spectrophotometric methods for nitrate measurement in natural waters need conversion to the more reactive nitrite before detection. Different types of nitrate reduction methods have been presented, using a variety of reduction materials like hydrazine, copperized cadmium, zinc, nitrate reductase, and irradiation by ultra-violet light. Among all the methods available, the Griess assay is the most established method of colorimetric nitrite analysis [178]. Beaton et al. [159] first reported such microfluidic-based colorimetric nitrate analysis using the Griess method. It was an in situ stand-alone systems which was compact and consumed low power (1.5 W). Use of colored polymethylmethacrylate (PMMA) helped to reduce background light interference which made it a high-sensitivity system. The system displayed the detection with

high-resolution and produced a better output with a detection limit of $0.02 \mu\text{M}$ for nitrite and $0.025 \mu\text{M}$ for nitrate. Another microfluidic method was developed by Khanfar et al. [158] to detect nitrate ions in water in an inexpensive and portable way. It was based on the Griess procedure. The microfluidic chip had a long-coated PMMA channel constructed with layers of different thicknesses. The detection system included a LED and photodiode. However, its LOD was low (0.0782 ppm). Jayawardane et al. [21] developed a cost-effective disposable μPAD to determine nitrite and nitrate (Fig. 2.9a). This method also used a Griess reaction for nitrite determination. However, for nitrate detection, nitrate was reduced to nitrite using zinc microparticles inside the μPAD channel. The μPAD was fabricated by an inkjet printing method. The hydrophilic μPAD channel was integrated with zinc microparticles and worked as a virtual flow-through solid-phase reactor which was a unique concept. The LOD of this method was $1.0 \mu\text{M}$ and $19 \mu\text{M}$ for nitrite and nitrate respectively. This user-friendly method was suitable for a field measurement. Recently, Vincent et al. [160] deployed a sensor within the Seaglider. The sensor employed colorimetric detection, using the Griess assay to determine nitrate and nitrite. The sensor was comprised of a three-layer PMMA chip. The chip included microchannels, mixers, photodiodes and LED. The chip was installed with electronics, valves, and syringe pump. Eventually, the chip was covered in a housing that was filled with mineral oil and consisted of the internally fitted pressure-compensating bladder. The LOD of the system was 20 nM . Cogan et al. [22] constructed a low-cost, robust microfluidic sensing platform and LED-based optical detection system to determine nitrate in natural waters and wastewater. It was a complete system consisting of the colorimetric measurement unit, a power unit, wireless communication, storage for sampling, reagent, and waste in a small unit. The chromotropic method for nitrate analysis was applied. The colorimetric measurement unit included a LED and a photodiode (Fig. 2.9b). The author claimed advantages such as ease of operation, inexpensive, low consumption of power, high throughput, limited waste generation, and compactness in design. Xiong et al. [23] designed a novel miniaturized cost-effective colorimetric fiber-optic chemical sensor (FOCS) system for nitrite detection through interfacing with a microfluidic capillary waveguide. It was based on the Griess-Ilosvay reaction. When the reaction occurred between nitrite and Griess reagents, it generated colorimetric azo dye. The light intensity was changed when the light interacted with the azo dye. The method achieved LOD of $7 \mu\text{g/L}$. The sensor comprised three sections: a capillary waveguide flow cell, a light source connected with an excitation fiber and a detector connected with

a detection fiber as shown in Fig. 2.9c. The microfluidic capillary waveguide also acted like a disposable sampling vessel, a reagent flow-through cell, and a light transmission element.

2.1.2.3 Pathogen

A colorimetric method is commonly used in optical detection of various pathogens due to its simplicity and easy readouts. Many times, imaging devices (cell phone camera, portable scanner, and digital camera) are incorporated with the colorimetric methods to provide the analysis interpretation. Wang et al. [179] demonstrated a paper-based *E. coli* detection method. They used methylsilsequioxane (MSQ) barriers to lyse the bacterial cells before the analysis. They also compared MSQ with other barrier materials, wax and alkylketene dimer (AKD). For this purpose, they printed circular barriers of MSQ, AKD, and wax. They found MSQ barriers better than the other materials. The change in colour was recorded with the help of the iPhone 4S camera. Although the assay was affordable and rapid, it was just a qualitative indicator. Boehle et al. [164] developed a cost-effective paper-based colorimetric method to detect antimicrobial-resistant bacteria. This method could identify the presence of b-lactamase mediated resistance. An array of paper-wells was used to optimize the reaction between b-lactamase and nitrocefin. The time required for the analysis was approximately 1 hour with LOD of 10 mU/mL. San et al. [24] developed another paper-based method to detect *E. coli* from field water samples in association with a smartphone. The multichannel paper chip was preloaded with antibody-conjugated beads. The water sample was applied to the inlet of the paper chip which allowed passing of the bacterial antigens. The smartphone was used to capture the digital images at some angle and to measure the light scatter intensity coming from microbead immunoagglutination (Fig. 2.10). The entire analysis time was just 90 seconds. The assay was simple to use and did not require any external hardware. The only necessary device was a smartphone with a built-in gyro-sensor and an installed software application.

Fluorescence detection is another common method in optical pathogen detection. Goldberg et al. [162] reported specific capture and detection of bacterial contamination in water. They developed a unit which consisted of *E. coli* seizing along with droplet

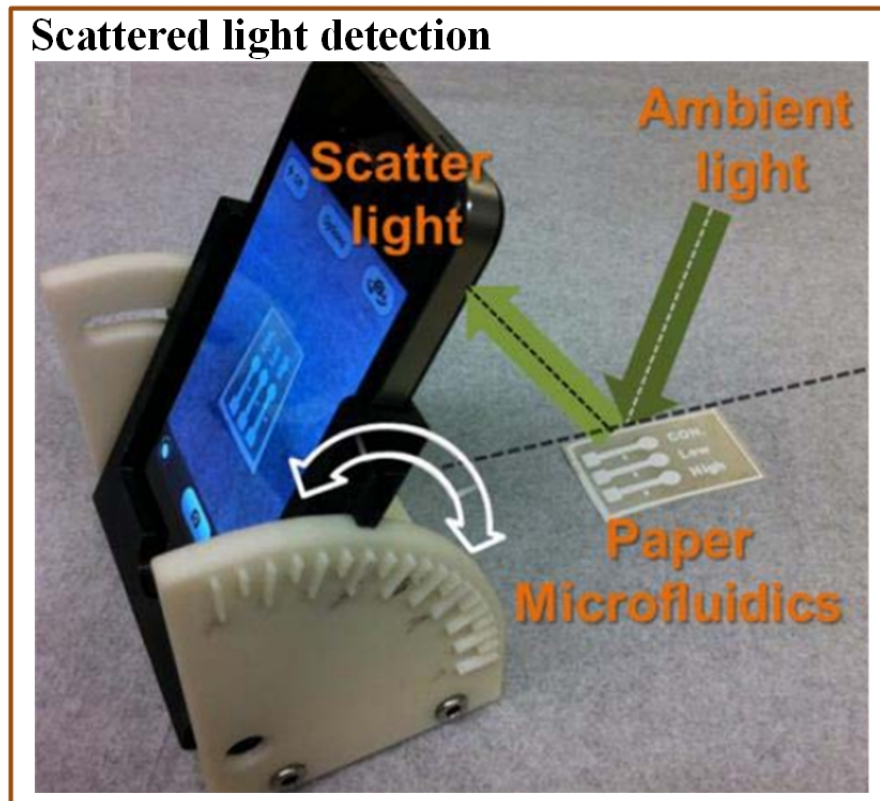


FIGURE 2.10: Scheme indicating a mobile-based multichannel paper chip for rapid *E. coli* detection [24].

microfluidics, portable proprietary fluorescence microscopy, and cloud-based data management and sharing. In this scheme, they used magnetic beads coupled with specific antibodies to capture *E. coli*. Further, the seized *E. coli* were conjugated fluorescently labeled antibodies. Subsequently, automated optical fluorescence microscopy was used for the purpose of detection. The entire water quality analysis took place in eight hours from sample collection to online result display. Malec et al. [165] proposed a labelled base biosensor where the *E. coli* was labelled with streptavidin-coated magnetic markers developing compounds. Video microscopy along with particle tracking software was utilised for quantitative measurement. The developed microfluidic platform was integrated with microconductors that generated a magnetic field gradient. When the fluid with the MLBs was brought into the microfluidic platform, a magnetic field gradient accelerated the MLBs towards the outlet. The method was able to provide a real-time approach for the detection of pathogens from a small volume liquid sample.

Many researchers implemented the integration of a polymerase chain reaction (PCR) test on a microfluidic platform. For example, Dharmasiri et al. [161] developed a PMMA microfluidic chip with eight parallel inputs covalently bonded with polyclonal antibodies.

The chip was used for the isolation and detection of *E. coli*. The quantification was performed after isolation by an off-chip real-time quantitative PCR test. Fluorescent

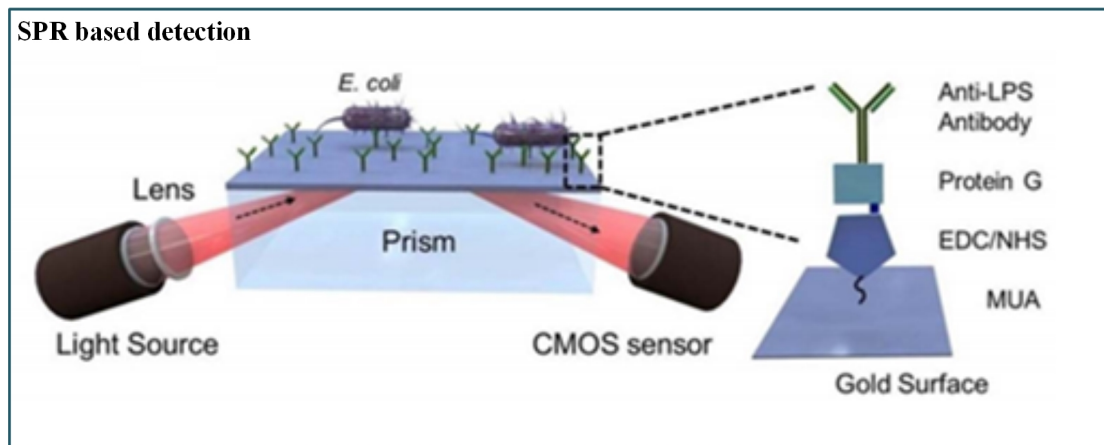


FIGURE 2.11: Schematic of SPR-based pathogenic detection [25].

microscopy was used to examine the fluorescently labelled cells in the microfluidic chip's channels. This entire process took just under five hours. The LOD was approximately 6 CFU. Li et al. [163] developed an integrated microfluidic device for rapid detection of pathogenic rotavirus. The device integrated reverse transcription (RT) and PCR with an online fluorescence detection technique. The microfluidic section incorporated the grooved copper heating block for RT and a heated cylinder for amplification. The RT-PCR technique with fluorescence microscopy was able to amplify and measure rotavirus RNA within one-hour. Tokel et al. [25] presented a portable, multiplex, inexpensive microfluidic-integrated SPR platform for rapid detection of bacteria such as *E. coli* and *S. aureus*. It was a label-free pathogen detection platform consisting of microfluidic and SPR technologies. This method utilized a Protein G-based surface chemistry for *E. coli* determination that allowed immobilization of antibodies in a favourable orientation. However, the result was presented as a graph, whereas a direct readout could have been more appropriate (Fig. 2.11).

2.1.3 Discussion and Outlook

Regular water quality monitoring is a must due to the harmful effects of water contaminants on the various functional systems of a human body. A microfluidic-based sensor is the most suitable method for this purpose. The sensor comprises a sensing and detection unit on the microfluidic substrate. This review explores several sensors mainly with the

sensing unit mostly based on chemicals, biological elements, electrodes and nanomaterials. The materials used for the sensing unit and substrates are listed in Fig. 2.12. Furthermore, the review includes the sensors based on two signal transduction methods - electrochemical and optical detection.

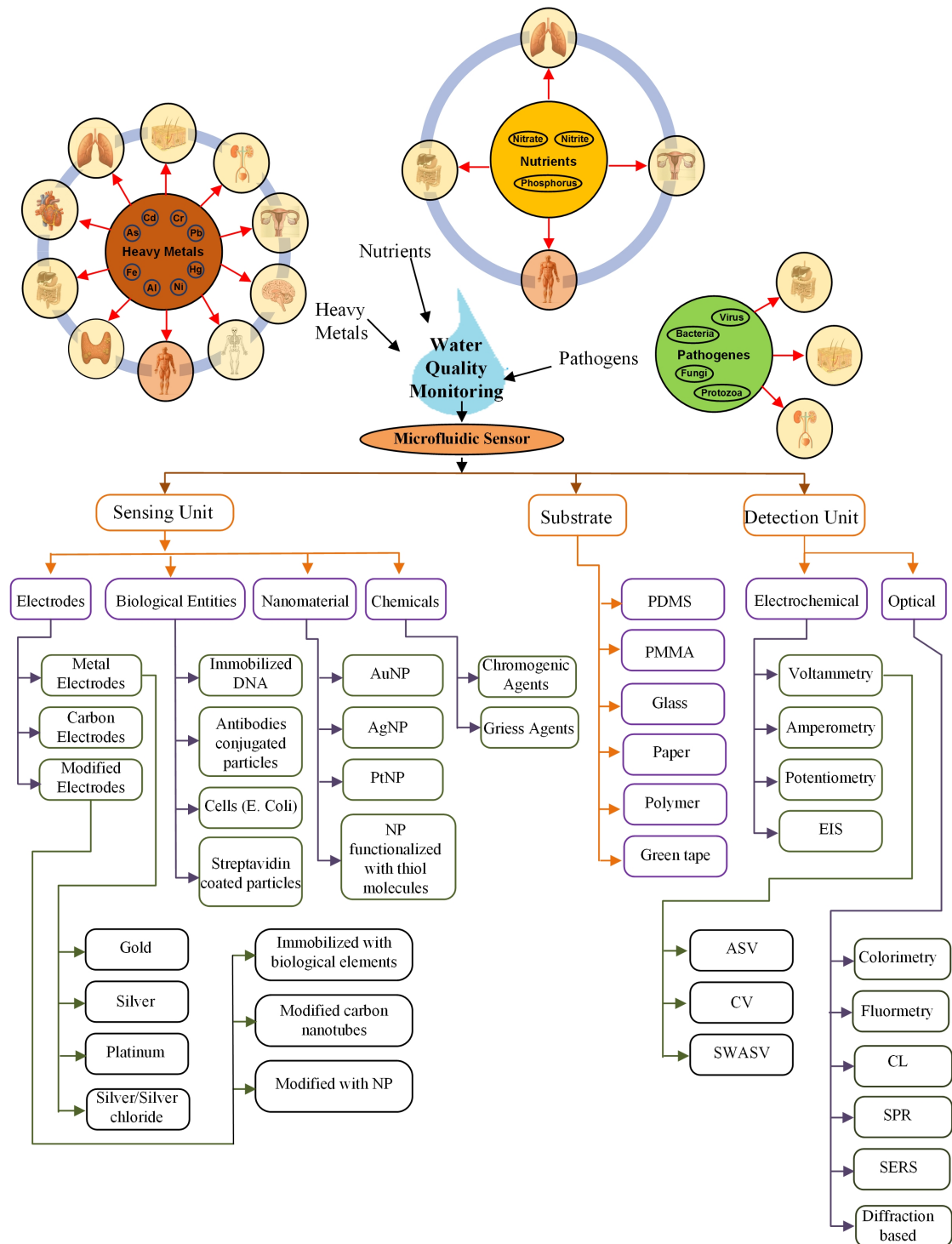


FIGURE 2.12: Summary of microfluidic sensors

Electrochemical detection is a big hope for microfluidic devices considering its high sensitivity, selectivity, miniaturization, and the possibility of mass production. Its adaptability with different microfabricated electronic parts leads to a portable device. To increase the sensitivity of electrochemical sensors, modification of electrodes with bioreporters or nanomaterials is advisable. However, a significant concern in regard to these sensors is the fabrication of chemically modified electrodes since it involves a very complicated process. Various optical sensing methods are successfully used in association with microfluidics including colorimetry, chemiluminescence, fluorescence, SPR, etc. The colorimetric analysis provides simple qualitative results in terms of a colour change. The colorimetric methods give relative results, they cannot yield exact quantitative results. These methods also require washing or rinsing step before the next measurement can be taken in the microfluidic chip. Compared to colorimetric methods, chemiluminescence techniques have higher sensitivity. Also, the elimination of an external light source makes the instrumentation simple. However, the availability of a limited number of chemiluminescence reagents is the main disadvantage of this technique. The fluorescence detection is another highly sensitive method. Still, it is limited to analytes that possess inherent fluorescence or that can be labelled fluorescently. SPR and SERS are highly sensitive and selective optical detection methods. However, integration of these methods with a microfluidic platform can be an issue due to non-portable instrumentation. An optical diffraction method is yet another sensitive detection method, though it still remains unaddressed in water quality monitoring. This method can produce highly sensitive results and can be incorporated with microfluidic technology. Table 2.5 summarises the advantages and disadvantages of electrochemical and optical methods individually. Field implementation is also an important aspect of discussion while discussing sensitivity and selectivity. Though there are a few challenges while implementing these sensors in the real world, the major hurdle associated with these sensors is field deployability. Many sensors discussed here represent the possibility of in situ and real-time measurement. However, those remain lab-based methods due to interfacing of lab-based measuring devices. Another challenge is in real sample measurement due to interference of the matrix effect. Usually, insoluble particles are suspended in the natural samples, which can influence the detection methods. In the case of optical detection, such particles can change the analyte concentration due to the stimulation of light scattering, while in electrochemical detection such particles can modify the chemical electrodes. These challenges can be addressed by incorporating suitable measuring as well as filtering devices

TABLE 2.5: Advantages & disadvantages of detection methods.

Method	Advantages	Disadvantages
Electrochemical	High sensitivity High selectivity Miniaturized electrodes makes the system portable Possibility of mass production	Tedious fabrication process of electrode
Colorimetric	Simple analysis Provides qualitative results Quick Response	Provides relative output
CL	High sensitivity Do not require external light source Portable	Limited number of CL reagents available
Fluorescence	High sensitivity High selectivity Portable	Limited to analytes that possess inherent fluorescence External light source necessary
SPR	High sensitivity High selectivity Label free detection	Portability may be an issue
SERS	High sensitivity High selectivity	Highly sensitive to environmental changes
Optical diffraction	High sensitivity High selectivity Portable	Occasionally signal enhancement by sequential amplification is necessary

along with the sensing mechanism using microfluidics.

Microfluidic technology plays an important role in making the water quality sensors field effective, as size reduction and automation are highly possible through this technology. However, the technology has its own challenges such as improper mixing in microchannels caused by laminar flows through it, which can potentially be addressed by implementing passive mixing microfluidic structures. Another challenge is the fabrication of microchannels with random geometries. Additionally, fabrication of the microfluidic sensor may sometimes remain a laboratory prototype that needs access to cleanroom equipment and trained staff to operate. It is possible to overcome these challenges with the help of rapidly emerging 3D printing technology.

2.2 Use of Aptamer in Arsenic Detection

Aptamers are short DNA or RNA oligomers that have an affinity to specific molecules. These oligomers are formed from the randomised nucleic acid library. Due to the real-time in-field detection of heavy metals, aptamers are considered as a promising platform

for environmental monitoring [180]. Many aptamer-based sensing of various metal ions with high sensitivity and selectivity have been reported [181, 182]. Kim et. al. [26] selected the As-binding single-stranded DNA aptamer Ars-3 using affinity column-based on the SELEX technique (systematic evolution of ligands by exponential enrichment). They used Ars-3 for the removal of As(III) from the groundwater. Many researchers have developed biosensors with such aptamer for As(III) detection. A few such examples are discussed below.

2.2.1 Colorimetric detection

Aptamers are used with colorimetric devices by many research groups where AuNPs were functionalised with aptamers, polymers, and surfactants to detect As(III) in aqueous solution. Wu et. al. [183] developed a sensitive, rapid, and cost-effective colorimetric biosensor for As(III) detection. The detection was based on the aggregation of AuNPs, which is controlled by a cationic polymer poly(diallyldimethylammonium) (PDDA) and an Ars-3 aptamer. In the absence of As(III), aptamers hybridise with PDDA and inhibited the PDDA-induced aggregation of AuNPs. In the presence of As(III), aptamers formed a complex with As(III) that resulted in the aggregation of AuNPs. The LOD was 5.3 ppb. To improve the LOD (0.6 ppb), another colorimetric based biosensor was developed in which aggregation of AuNPs was controlled by a cationic surfactant (Hexadecyltrimethylammonium bromide i.e. CTAB) and an Ars-3 aptamer [112]. Wu et. al. [184] reported one more Ars-3 based colorimetric biosensor for As(III) detection with LOD of 6 ppb. In this biosensor, they inhibited the catalytic activity of hemin by Ars-3 which was recovered in the presence of As(III). Nguyen reported the selective and sensitive colorimetric detection of As(III) using a synergistic molecular assembly of an aptamer (Ars-3) and cetyltrimethylammonium bromide (CTAB) on gold nanoparticles (AuNPs). The As(III) ions interacted with Ars-3 aptamerAuNPs resulted in aggregation due to presence of CTAB, which developed a red-shift in the surface plasmon resonance (SPR) band and a visual colour change. The LOD of the sensor was 16.9 ppb [84]. A simple colorimetric technique was developed to determine As(III) in groundwater with the help of Ars-3 and AuNPs [85]. In the absence of As(III), the AuNPs were covered with a negatively charged Ars-3 such that even a high NaCl concentration could not induce their aggregation. When As(III) was added, it formed a complex with Ars-3 resulted uncovering of the AuNPs. This resulted in NaCl induced aggregation. However,

the detection limit of the sensor was 161 $\mu\text{g/L}$ which was much higher than the MCL of the As.

Yang et. al. [83] obtained another unique As(III)-binding peptide with a sequence of T-Q-S-Y-K-H-G. They used the phage display technique for the screening of the peptide. This peptide caused the aggregation of AuNPs in the absence of As(III). Upon addition of As(III), it interacted with the peptide and prevented the aggregation of AuNPs. This biosensor achieved the LOD of 4 $\mu\text{g/L}$.

2.2.2 Fluorimetric detection

Ensafi et. al. [86] developed a fluorimetric aptasensor with high sensitivity and selectivity where aggregation of cationic cysteamine-stabilized CdTe/ZnS core/shell quantum dots was controlled through aptamer. The aggregation of quantum dots resulted in fluorescence quenching. In the presence of As(III), the aptamer-As(III) complex prohibited aggregation of the quantum dots. This de-aggregation improved the fluorescence intensity of the quantum dots. The aptasensor reported a very low detection limit of 1.3 pmol/L. Similarly, highly selective As detection platform was constructed using a blend of G-quadruplex DNA, a label-free aptamer, and a phosphorescent transition metal complex. The detection limit was of ca. 0.57 $\mu\text{g/L}$ [185]. Another group created a novel fluorogenic sensing probe to detect As(III) with remarkable LOD of 0.9 ppb in which they used mesoporous silica nanoparticles with aptamers. Pores of silica nanoparticles (MCM-41) were loaded with rhodamine B and then the external surface was functionalised with Ars-3. Upon addition of As(III), rhodamine B was released which resulted in fluorescence [186]. Similarly, Pan et. al. [187] developed an ultrasensitive aptamer biosensor for As(III) detection with LOD of 5 ng/L where the change in fluorescence was recorded due to the presence of As(III).

2.2.3 Electrochemical detection

Vega-Figueroa et. al. [188] developed a label-free impedimetric aptasensor using As-specific (ArsSApt) aptamer. ArsSApt was immobilised on the gold substrate and further exposed to As(III). The resistance through the aptamer layer was decreased with the increased As concentration due to the ArsSAptAs(III) interaction. The detection limit

was 0.05 ppm. Similar aptasensor was developed by Cui et. al. [189] with differential pulse voltammetry technique. An innovative, highly sensitive and selective aptasensor was presented by Baghbaderani et. al. [190] where they introduced a chitosan-Nafion (Chit-Naf) interface to detect As using impedance spectroscopy (EIS) technique. They applied a unique amplification approach based on CNTCOOH-BSA conjugate through which impedimetric response of the aptasensor towards As increased significantly. They achieved a detection limit of 74 pM. Mushiana et. al. [191] reported an electrochemical aptasensor for As(III) detection in water making use of carbon nanoparticle (CNPs) and gold nanoparticles (AuNPs) immobilisation platform. The immobilisation was performed through drop coating CNPs on a glassy carbon electrode (GCE) followed by electrodeposition of AuNPs on the CNPs modified electrode using cyclic voltammetry. This nano-platform modified GCE was further immobilised with thiolated aptamer. The LOD of this method was 0.092 ppb.

2.2.4 Other detection methods

2.2.4.1 Resonance Rayleigh Scattering (RRS) detection

Wu et. al. [192] developed As aptasensor. The sensing unit contained Ars-3 aptamers and crystal violet (CV) molecules. The size of large nanoparticles was decreased due to the presence of As(III), which in turn a decline of RRS intensity at 310 nm; while the diameter of small nanoparticles was increased and caused an increase in RRS intensity. The change in RRS intensity was dependent on the size variation of nanoparticles that was changed directly by As(III) concentrations. LOD of the method was 0.2 ppb. A simple and selective method reported by Tang et. Al. [193] was based on aptamer (ssDNA) modified nanogold probe (AussDNA) to trace As(III) from water samples. In the presence of As(III), AussDNA forms a stable complex which induced aggregation of nanogold. This reaction was responsible for increased RRS intensity at 278 nm. There was a linear relationship between RRS intensity and As(III) concentration. The method was able to detect up to 1.9 ng/mL with high selectivity.

2.2.4.2 Surface enhanced Raman scattering (SERS) detection

Song et. al. [167] Proposed a SERS based strategy where they combined As-specific aptamer with Raman labelled Au@Ag core-shell nanoparticles. In this scheme, 4-mercaptobenzoic acid (4-MBA) and As(III) specific-aptamer (Ars-3) were absorbed on Au@Ag. The addition of As(III) resulted in the complex of As(III) and aptamer which induced the aggregation of Au@Ag. This, in turn, produced a proportional SERS signal. The detection limit of this assay was 0.1 ppb.

2.2.4.3 Electrochemiluminescence detection

Liang et. al. [194] constructed a ratiometric electrochemiluminescence (ECL) indicator for As(III) detection. As(III) was detected based on synergistic quenching of ECL emission of $Au-g-C_3N_4$ NSs using As(III) and $Ru(bpy)_3^{2+}$ and simultaneously generating the second ECL signal of $Ru(bpy)_3^{2+}$ with an increased intensity. The selectivity and sensitivity was intensified due to coupling of dual quenching effect of As(III) and $Ru(bpy)_3^{2+}$ with the second signal of $Ru(bpy)_3^{2+}$

2.2.4.4 FET based detection

JH An et. al. [195] fabricated highly selective and sensitive field-effect transistor (FET)-type aptasensors for As(III) detection where As-specific aptamer combined with CFMNSs and further integrated into a liquid-ion gated FET system. The interaction between the aptamer and As(III) resulted in field-induced current variations. The detection limit of the aptasensor was ca. 1 pM.

2.3 Summary

In the first part of this present review, microfluidic-based sensors for water quality monitoring have been extensively discussed in detail. This includes a comparison of microfluidic-based electrochemical and optical methods with advantages and disadvantages for the detection of contaminants such as heavy metals, nutrients, and pathogens in

TABLE 2.6: Aptamer-based arsenic detection

Method	Material	LOD	Ref.
Colorimetric	PDDA, and AuNP	5.3 ppb	[183]
	CTAB and AuNP	0.6 ppb	[112]
	Hemin	6 ppb	[184]
	peptide T-Q-S-Y-K-H-G-C and AuNP	4 $\mu\text{g/L}$	[83]
	CTAB and AuNP	16.90 ppb	[84]
Fluorescence	AuNPs	161 $\mu\text{g/L}$	[85]
	CdTe/ZnS quantum dots	1.3 pmol L	[86]
	G- quadruplex DNA and a phosphorescent transition metal complex	ca. 0.57 $\mu\text{g/L}$	[185]
Electrochemical	Silica nanoparticles [MCM-41] loaded with rhodamine B	0.9 ppb	[186]
	Gold substrate	0.05 ppm	[188]
	Carbon nanotubes & Modified glass electrodes	74 pM	[190]
RRS	Carbon nanoparticles & AuNPs	0.092 ppb	[191]
	CV molecules	0.2 ppb	[192]
SERs	Nanogold	1.9 ng/mL	[193]
	Au@Ag core-shell nanoparticles & 4-MBA	0.1 ppb	[167]
ECL	$Au - g - C_3 N_4$ & $Ru(bpy)_3^{2+}$ NSs	0.0007 ppt	[194]
FET based	CFMNSs	ca. 1 pm	[195]

water that have been published in the last decade. Water quality analysis with microfluidics is a flourishing technology as it contributes to rapid, economical, and user-friendly detection methods. It is especially suitable for in-situ testing, particularly in limited-resource circumstances. The current challenges with in-situ testing and real samples are also discussed in the review. Such challenges can be addressed by including 3D printing technology along with the microfluidic platform.

In the second part, aptamer-based As sensors have been explored. However, the As-specific aptamer Ars-3 seems to be highly popular as the majority of the aptasensors are making use of Ars-3 for As detection. The aptamer provided highly selective and sensitive results. These aptasensors have used different detection strategies such as colorimetric, fluorescence, electrochemical, RRS, SERs, ECL and FET based methods. Table 2.6 summarises the materials used in and the detection limit of these methods. All of them are based on the change in the output signal (visual colour, fluorescence, light intensities or electrical parameters) due to aggregation of nanoparticles.

Chapter 3

Sensor Design and Fabrication

3.1 Introduction

Immobilisation of thiol compounds on solid surfaces is becoming popular in the field of research due to chemical stability, physical robustness, and terminal functionality. Specifically, the patterns of ligands in analytical assays are essential to obtain a miniaturised sensor system. The miniaturisation offers advantages like cost-effectiveness and integration for simultaneous detection. Several micro-patterning methods like photolithography, micro-spotting, and μ CP are available that are being used in developing the sensing element of the sensors. However, of all the above-mentioned methods, the μ CP technique is the most effective method. Several advantages of μ CP have been reported in the literature, e.g. (i) it is not as expensive as photo-lithography technique, (ii) it can create multifunctional nano/micro-structures on various surfaces, and (iii) usage of the clean-room is not mandatory [196, 197]. Hence, μ CP technique was used for obtaining the patterns while developing the sensor.

Despite all the advantages of this method, there are a few limitations of the method too, such as stamp deformation [198, 199], the volatility of ink, and diffusion of the ink molecules due to longer contact time. Furthermore, water-soluble ink does not permeate due to hydrophobic surface properties of PDMS which affects the printed SAM quality [199, 200]. Hence, we experimented to find out the other additional factors such as molecular weight and pH value of the ink which affect μ CP process.

This chapter represents the study of two different thiol compounds for obtaining patterns. One of the thiols is dithiothreitol (DTT). Till now, researchers have used self-assembled monolayers (SAM) of DTT on the gold substrate, however, no one has attempted to print DTT pattern on the gold substrate. The other thiol is the glutathione (GSH). The chapter explains the hypothesis of the sensor and fabrication details. In the first section, the μ CP technique is discussed which includes the procedure of substrate fabrication and stamp fabrication along with the inking and the printing details. The next section explains the interaction of thiol compounds with gold and As molecule. In the last section, the necessity for signal enhancement of the thiol patterns is discussed.

3.2 Microcontact Printing

The μ CP is being used in the research areas such as BioMEMS, LOC (Lab on a Chip) devices or cell biology for surface passivation using patterned monolayers with sub-micron resolution [201–203]. This technique is introduced by Whitesides and his colleagues in 1993 [204]. It is comparable to the conventional stamping method as it comprises of the ink, a stamp, and a substrate. The major difference between these methods is patterns are formed on micro or nanoscale structures. A polymeric stamp with respite pattern is generally used in μ CP to produce the patterns. The stamp is “inked” by either putting a drop of ink (proteins, etc.) on the stamp or immersing the stamp in the ink.

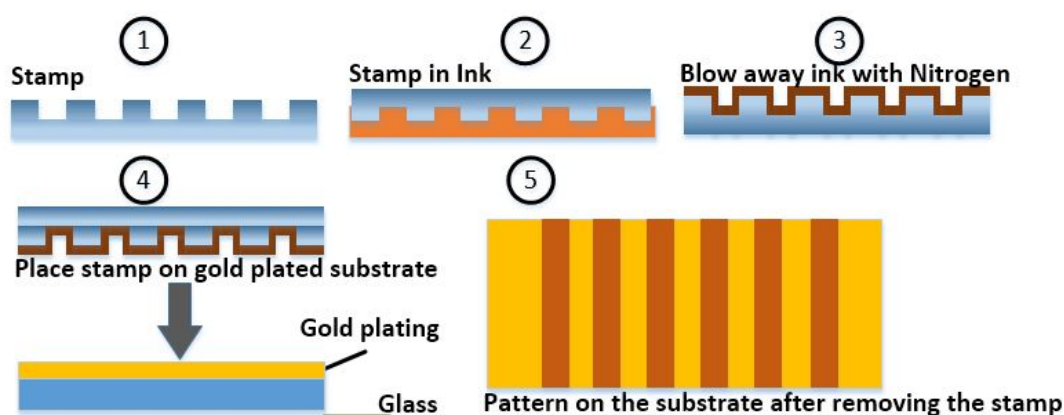


FIGURE 3.1: Diagram showing the steps involved in microcontact printing of thiol ink on a gold substrate. 1. Take a PDMS stamp. 2. Immerse the PDMS stamp into the ink. 3. Blow away the ink with the help of the nitrogen stream. 4. Place the PDMS stamp on the substrate and apply gentle pressure. 5. Observe the pattern under the microscope.

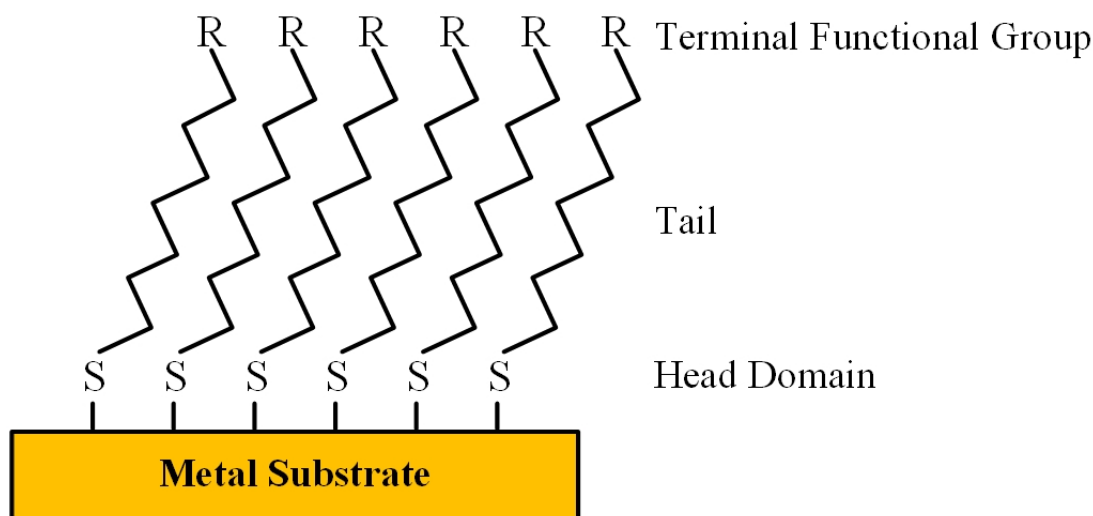


FIGURE 3.2: Diagram illustrating the covalent binding of sulphur atom to the surface of the metallic substrate forming SAM with a terminal functional group.

Thereafter, the stamp is brought into contact with the substrate surface. PDMS is a widely used material to make the stamps for μ CP [199]. Fig. 3.1 outlines the major steps involved in the μ CP process.

The application of this method is primarily dependent on the type of ink used. Variety of inks is used for this purpose like thiol compounds, synthetic polymers, dendrimers, proteins, DNA etc. Hence, different applications of μ CP are available such as micromachining, patterning proteins, cells or DNA in biosensors on various surfaces such as gold, silver, copper, glass, polymer etc. [205]. Patterning self-assembled monolayer (SAM) of alkane thiolates or thiols using μ CP is currently considered as a valuable application due to its superior control over the surface chemistry and parallel processing [206]. SAMs consists of the head domain that binds with the substrate surface, a tail which forms ordered structures away from the substrate surface. Generally, tails have a functional end group. Majority of the times thiol molecules are used to form the SAMs. Thiol is an organic compound that comprises a carbon-bonded sulfhydryl ($-\text{SH}$) group. In the case of thiols, sulphur atom covalently bounds with the surface of the substrate, and terminal functional group changes the surface chemistry of the substrates (Fig. 3.2).

3.2.1 Chemicals and instruments

Analytical reagent grade chemicals were used. All chemicals were purchased from Sigma Aldrich, New Zealand. GSH ($\text{C}_{10}\text{H}_{17}\text{N}_3\text{O}_6\text{S}$), DTT ($\text{C}_4\text{H}_{10}\text{O}_2\text{S}_2$), phosphate buffer saline

(PBS pH 7.4), pH 10 buffer solution, and ethanol were used as received without modification. Deionized (DI) water was used for all experiments. SYLGARD[®] 184 silicone elastomer kit was also purchased from Sigma Aldrich, NZ. The Ars-3 (/5'Biosg/GGTAAT-ACGACTCACTATAGGGAGATACCAGCTTATTCAATTTTACAGAACAACCAACGT-CGCTCCGGGTACTTCTTCATCGAGATAGTAAGTGCAATCT-3) and TE-buffer (10 nM Tris, 0.1 mM EDTA, pH 8.0) were purchased from Integrated DNA Technologies, Singapore. BioMag[®] Streptavidin (Nuclease-free with a mean diameter of 1.5 μm) was purchased from Bang Laboratories, NZ. Initially, the gold-coated slides glass slides were purchased from Thermo Scientific, NZ. Subsequently, Desk Sputter Coater (DSR1) was used to prepare the gold-coated glass substrate. Advanced vortex mixer (VELP Scientifica) was used for mixing the thiol solutions thoroughly and, an optical microscope (Nikon-H600L) was used to observe the self-assembled patterns.

3.2.2 Substrate fabrication

The “substrate” has been well-defined by Love and co-workers [207]. According to them, its a surface that firmly supports the SAM. For obtaining SAMs, choice of substrates is available from planer surfaces (glass or silicon slides with layers of thin metallic films, metal foils, single crystals) to highly curved nanostructures (colloids, nanocrystals, nanorods) [207]. However, the most widely used substrates for μCP of thiol SAMs are thin metallic films (gold, silver, copper, aluminium, and nickel) on the silicon wafer, glass, mica or plastic slides. Such substrates can be simply produced by methods like physical vapour deposition, electrodeposition, sputtering, or electrodeless deposition.

In the sensor, gold-coated glass is used as a substrate. There are many reasons to make it as a substrate in the experimentation. The primary reason is that gold is a rationally inert material. It does not react with most of the chemicals and does not have the property of corrosion at room temperature. Hence samples can be easily handled under atmospheric conditions. Secondly, gold has a very high affinity towards the thiols without undergoing any uncommon reaction [207–209]. Furthermore, a thin film of gold can be easily obtained by physical vapour deposition, sputtering, or electro-deposition.

The gold-coated glass substrate was prepared in the laboratory. Here, the glass slides were cut into the pieces of size 0.8 cm x 0.8 cm. Next, these pieces were cleaned with ethanol followed by rinsing in DI water and drying with ultra-high purity nitrogen (BOC,

NZ) stream before sputtering. The layer of gold (50 nm thickness) was sputtered on these glass slides using the sputtering machine DSR1. These gold-coated substrates were cleaned with DI water and dried with nitrogen gas before use. A new set of gold-coated substrates was prepared separately for each experiment.

3.2.3 Stamp fabrication

The stamp is a fundamental element in the μ CP process. The stamps used in the experimentation were made of a silicone elastomer PDMS (Sylgard[®] 184, silicone elastomer kit). It is the most commonly used material for stamps [197]. PDMS was used for stamp fabrication during the μ CP process due to the following reasons :

- PDMS is a liquid prepolymer at room temperature because of its low melting point (about -50°C) and glass transition temperature (about -120°C) [210]. Patterns with micro size features can be reproduced faithfully using PDMS stamps.
- Also, the effective transfer of the ink to the substrate is highly possible. It is likely to lift the stamp off the substrate without spreading the patterned ink due to its elastomeric property.
- Furthermore, PDMS can be easily separated from the master mould during fabrication because of the low surface energy.
- Finally, PDMS is relatively inert and does not react with many chemicals [207].

To fabricate the stamps a master mould having 10 μm alternating patterns was used. The stamp master was obtained from BW Foundry, The University of Sydney. During fabrication of the stamps, the silicone elastomer base was mixed with a curing agent in a 10:1 ratio, degassed for 1hr and then poured onto the master mould [197, 210]. Later, at 60°C , curing was carried out for 3 hrs which was followed by cooling at room temperature. The cured stamp was gradually peeled off the mould and carefully stored in a cleaned petri dish. Figure 3.3 pictorially depicts the stamp fabrication process.

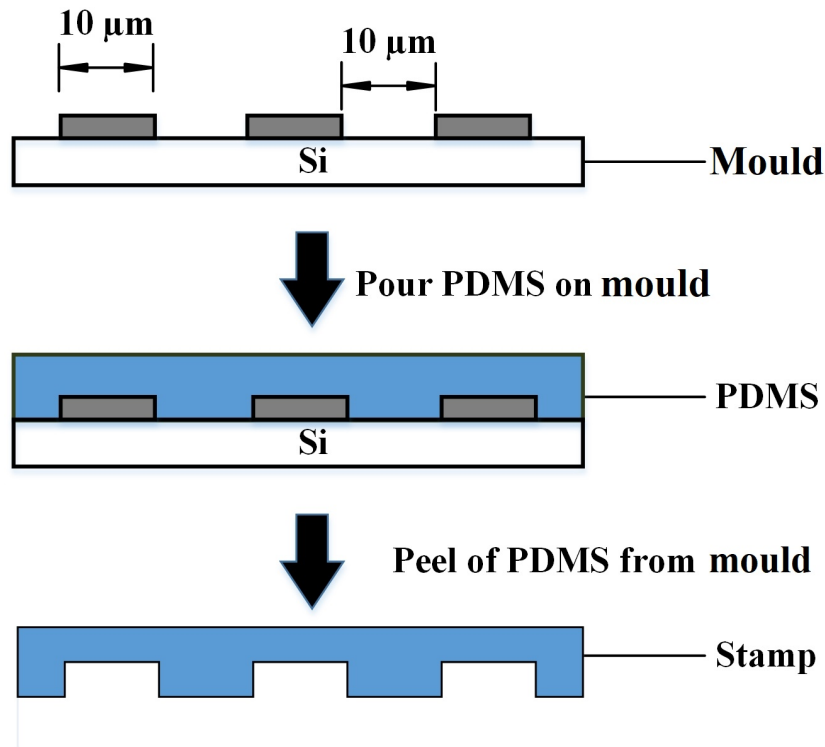


FIGURE 3.3: Illustration of the process of developing PDMS stamps.

3.2.4 Inking

Inking of the PDMS stamp is an important step during the μCP process. This stage ensures the deposition of the ink layer on the stamp. There are various well-known inking methods: liquid inking, inking through PDMS reservoir, direct inking, and inking by immersing the PDMS stamp in the ink [197, 205] as illustrated in Fig. 3.4. Method(a)-liquid inking and method(d)-inking by immersing PDMS stamp in the ink were explored and found method(d) was more suitable for μCP of DTT and GSH. The PDMS stamp

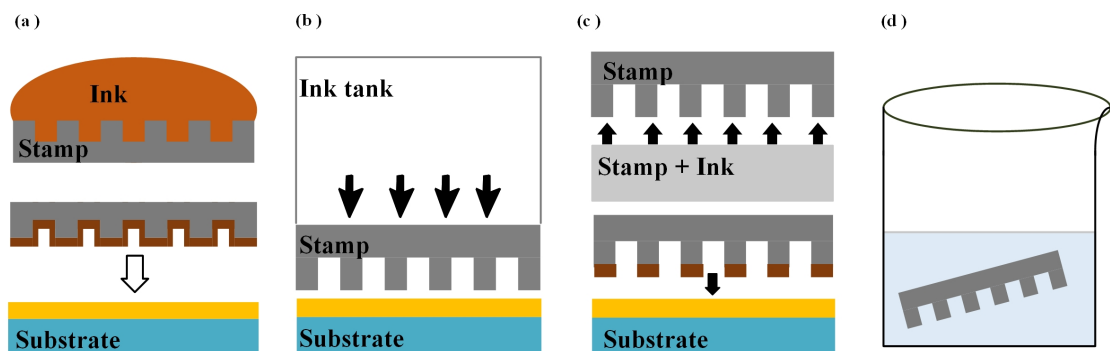


FIGURE 3.4: Printing methods: (a) liquid inking, (b) inking through PDMS reservoir, (c) direct inking, and (d) inking by immersing the PDMS stamp in the ink.

was cut into smaller pieces (0.5 cm x 0.5 cm) before stamping. The smaller stamps were cleaned using an ultrasonic cleaner with ethanol for half an hour at 30°C before use. Different concentrations of the ink were prepared using DI water as well as two buffers (PBS and buffer solution with pH 10). The thiol solution mixed rigorously using vortex mixer at speed of 1600 rpm. The stamp was inked with the prepared solution.

3.2.5 Printing

To transfer the ink on the substrate printing was performed. For this purpose, any excess thiol solution was removed from the stamp using a moderate stream of nitrogen gas. Next, the stamp was brought into contact with the gold-coated substrate. Gentle pressure was applied on the stamp to ensure the precise contact between the gold coating and stamp. The stamp was removed from the substrate, which was followed by rinsing of the substrate using DI water to remove any unbounded thiol molecules.

The printing task went through many phases and to obtain accurate μ CP patterns. Great efforts were taken into practising μ CP. To achieve expertise in the technique, initially, it was performed with the help of BSA and then DTT and GSH were used for printing purpose.

3.3 Interaction of Thiol Compounds with Gold and Arsenic

Interaction of gold with thiol compound is well known. Gold binds with thiol through Au–S linkage [211–215]. In addition to this, As(III) has an affinity towards amino acids, amines, peptides and organic micro molecules due to As–O or As–S linkages [216, 217]. Two thiol compounds (DTT and GSH) with different molecular weight were used to observe the effect of molecular weight on μ CP. DTT is a dithiol compound with two thiol functional groups in it. GSH is a monothiol compound having one thiol functional group in it. The molecular weight of DTT is lower compared with GSH. Figure 3.5 explains the chemical structure of DTT and GSH.

Figure 3.6 illustrates the interaction of DTT and GSH with gold and As. The molecules of DTT and GSH were first stabilised on the gold-coated substrate through Au–S linkages

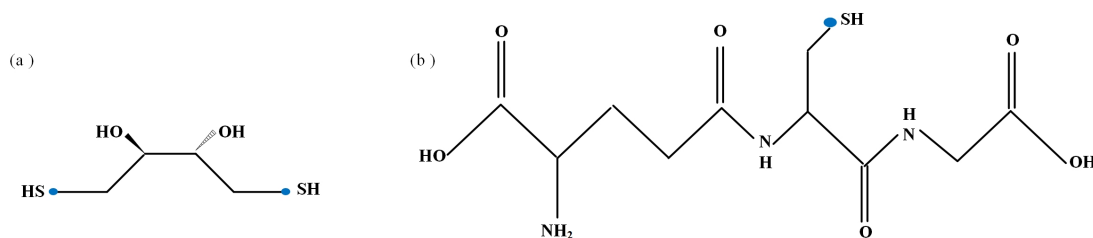


FIGURE 3.5: Molecule structure: (a) DTT and (b) GSH.

[211, 217] to produce a stable pattern. Since DTT has two thiol groups, one group can form Au-S bond with the gold surface and the other can form As-S bond with the arsenic present in the aqueous sample [214, 218, 219]. In case of GSH, the molecules first stabilized on the gold surface using Au-S bond and then As bound through As-O link. The adsorption of thiol onto the gold surface starts with physisorption, during which Au-SH coordination bonds form. After this chemisorption takes place in which disassociation of S-H bond and the formation of Au-S bond occurs. The strength of the Au-S interaction formed on the gold surface depends upon various conditions such as:

- Different surface properties (oxidized or reduced)
- A pH value of the solution and a type of solvent
- The time duration of the interaction [215].

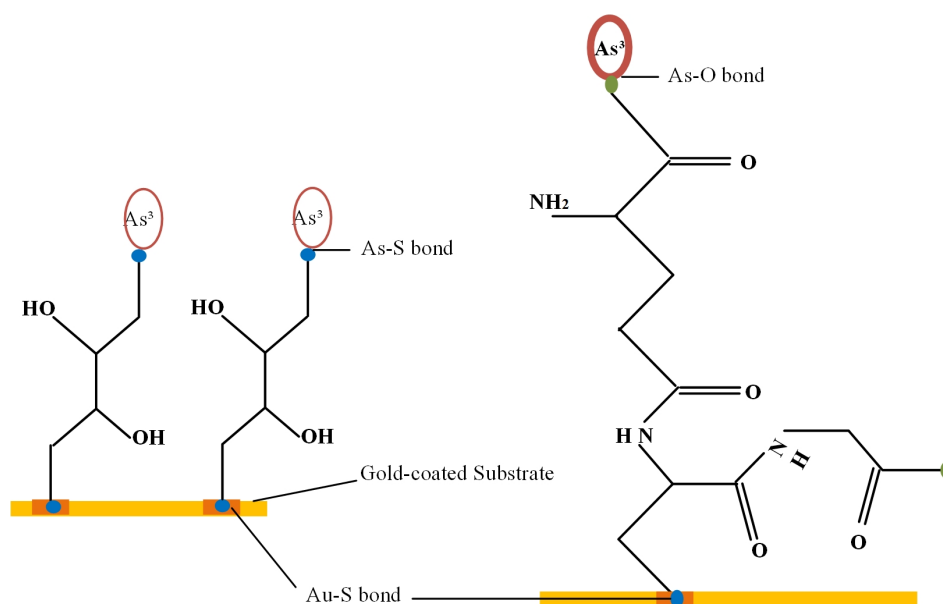


FIGURE 3.6: Interaction of DTT and GSH molecule with gold surface and As molecule.

A pH value is very important in the formation of Au–S bond. At lower pH, disassociation of S–H is prohibited, hence more Au–SH co-ordination bond formations take place. On the other hand, higher pH favours the disassociation of S–H which in turns increases Au–S covalent bond. The ethanolic solution reduces gold surface and aqueous solution oxidizes gold surface. Hence aqueous solvent enhances the stability of covalent bond [215].

In addition to this, the time duration of the interaction also plays an important role in covalent bond enhancement. A minimum 3 second is required to dissociation of S–H bond and formation of Au–S bond. However, this time may vary according to the thiol molecules [215].

3.4 Signal Enhancement of Patterns

As described in the above section, As can form a layer on the thiol pattern. However, the thickness of the layer can be in a few nanometers, which is very difficult to identify by any detection method. Hence, a signal enhancement of the patterns is necessary for As detection. For this purpose, immobilisation of magnetic particles can be performed using As-specific aptamer (Ars-3) and streptavidin onto As-contaminated thiol patterns.

Aptamers are artificially developed chemical antibodies from the randomised nucleic acid library through binding, separation, and amplification process. It can specifically bind with a target molecule with high affinity. Aptamers are preferred over antibodies due to their advantages such as easy to prepare, simplicity of detection, higher sensitivity, easy to modify, and non-immunogenic property. In 2009, Kim et. al [26] developed a single-stranded DNA aptamer Ars-3 to remove As from Vietnamese groundwater. The sequence of the aptamer is: (5' GGTAATACGACTCACTATAGGGAGATACCAG CT-TATTCAATTTTACAGAACAACCAACGT CGCTCCGGGTACTTCTTCATCGAGATAGTAAGTGCAATCT-3') and structure is as shown in Fig. 3.7. Ars-3 has a very high affinity towards As(III) and As(IV). Additionally, we modified Ars-3 at the 5th terminal with biotin. Hence the modified sequence of Ars-3 is: (/5Biosg/GGTAATACGACTCAC TATAGGGAGATACCAGCTTATTCAATTTTACAGAACAACCAACGTCGCTCCGG GTACTTCTTCATCGAGATAGTAAGTGCAATCT-3'). Streptavidin always has an affinity towards biotin. Thus, due to modification of Ars-3 it can bind with As molecule

as well as with streptavidin. In this work, magnetic particles of 1-micron size coated with streptavidin were used that can bind with biotinylated Ars-3. These magnetic particles can be observed under the microscope and it can be used in diffractometric detection. In this way, a signal enhancement is useful for detection purpose.

Figure 3.8 depicts the signal enhancement process in detail. Ars-3 binds to an As molecule present on the thiol pattern. As the 5' terminal of Ars-3 modified with biotin, BioMag[®] Streptavidin also binds to the Ars-3.

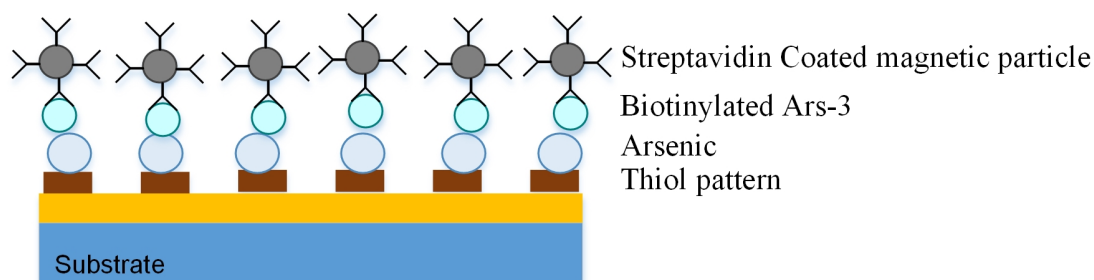


FIGURE 3.8: Signal enhancement using biotinylated Ars-3 and streptavidin-coated magnetic particle.

Chapter 4

Fluidic System

4.1 Introduction

Sensing applications or sensors determine the presence or concentration of molecules, biological structures, microorganisms, etc. The term sensor is used for a compact device that includes sensitive element like chemicals, biological entities (antibodies, aptamers, enzymes, etc.), nanoparticles, electrodes, etc. This element functions as a transducer to measure one or more analytes. Often, these analytes are human samples such as blood, urine, serum, etc. Hence, a microfluidic system is required for sample preparations, processing the throughput, mixing the reagents and controlling the flow conditions for detection purpose [220]. For example, in many diagnostic and therapeutic technologies, a microfluidic system is essential to perform cell separation and sorting steps [221]. Thus, the processing of fluid plays an important role in sensing applications and this processing includes pumping or mixing of sample liquids or circulation of reagents [222]. Components like a micropump, microvalve, and flow sensor are considered to be the functional components of any microfluidic system [223]. During the last decade varieties of micropumps and microvalves have been developed [224–232]. Generally, these components are either built-in fabricated or pre-fabricated. Built-in fabricated fluidic components are specifically developed for certain applications which cannot be considered as generic fluidic components. Some explored prefabricated fluidic components require pneumatic actuation [233, 234]. Pneumatically actuated fluidic components are not useful in portable applications. In addition to this, most of these microfluidic components possess low throughput [229].

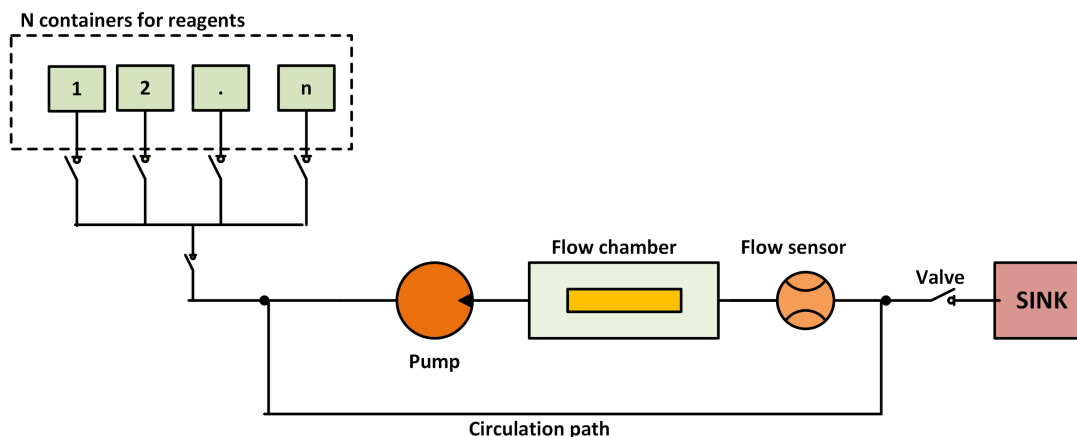


FIGURE 4.1: Schematic layout of a typical fluidic system showing major components and fluid circulation path.

The general schematic of the system is shown in Fig. 4.1. This automated system can be used in the sensing scheme where pumping, mixing, and circulation of reagents is necessary. It also provides high throughput. The major components that are used in the system are a pump, valves and flow sensor. To obtain the precise control of fluid in the system it is beneficial to operate such complex processes automatically. Hence, the fluidic components in the system are computer-interfaced to operate the assay sequences in an automated fashion. In the current system, fluidic connections between the automated dispensing system and the flow chamber were accomplished using silicone tubing. Silicone is used for the tubing as it is an inert material that does not react with any substance which flows through it. Another advantage of using silicone tubing is that it provides a quick and easy connection method.

In this chapter, an automated fluidic system is presented which is developed using off-the-shelf and/or in-house fabricated components. The chapter mainly describes the evaluation of the working of low-cost fluidic components such as pump, valve and flow sensor. Initially, the rationale behind the selection of these fluidic components is presented. Next, the evaluation process of components is explained. The chapter also discusses the possibility of using fused deposition modelling (FDM) and selective laser sintering (SLS) technology for the printing of the flow chamber through printing microchannels. In the last section, system automation is discussed in detail.

4.2 Instrumentation

The fluidic system involved solenoid type normally open and normally closed pinch valves along with the dosing peristaltic pump. The valves and tubing were purchased from Cole-Parmer, New Zealand. The dosing peristaltic pump was purchased locally. Automation of the fluidic system was done using Arduino atmega 2560 small and relay card along with the Labview software.

The FDM-based 3D-printer used was a Tiertime UP 02, equipped with a 0.2 mm nozzle and the printer was controlled through UPStudio software. And, a software – Inventor Professional 2020 (Autodesk) – was used to create the required 3D-objects. A coloured polylactic acid (PLA) having a diameter of 1.70 mm was used as a filament in this work. The SLS-based 3D-printer used was DTM Sinterstation 2500 Plus. The 3D-objects were printed with a nylon powder known as Precimid 1170. A Pico Plus Syringe Pump from HARVARD APPARATUS was used for injecting the water at different flow rates. Pressure measurements were performed with the help of a Pump PX3 Series pressure transducer.

4.3 Micro Pump

A pump is the most important component in the fluidic system; therefore, it was necessary to select an appropriate off-the-shelf pump before selection of any other components. Several types of pumps and their working mechanisms were explored. A brief overview of different types of pumps is as follows [223, 235, 236]:

Gear Pump: This is the straightforward type of rotary positive displacement pump. It involves two interlocked gears that rotate in a compact casing as shown in Fig. 4.2a. The fluid is trapped by the tooth spaces and forcefully thrown around the outer periphery. The fluid does not move back on the interlocked portion, because the teeth interconnect highly at the centre [235].

Peristaltic pump: A peristaltic pump is another type of positive displacement pump. In this pump, unidirectional fluid flow is caused by the peristaltic motion. Typical peristaltic pumps produce the wave-like motion by a roller along the circumference as shown in Fig. 4.2b. The flexible tube is fitted inside a circular pump casing that contains

the fluid. This flexible tube is compressed by several rollers, shoes, or wipers attached to a rotor. The portion of the tube under the compression closes due to rotation of the rotor which in turn forces the fluid through the tube [223].

Screw pump: A screw pump is a slightly complex type of rotary pump that utilizes one, two or three screws with opposing thread e.g., one screw turns clockwise and the other counter-clockwise. The schematic illustrated in Fig. 4.2c represents a magnetically driven screw pump. It consists of one screw. This single screw rotates inside a close-fitting container. Permanent magnets are attached to the screw and magnets are attached to the outside of the motor as shown in the figure. Due to magnetic coupling between the magnets, a screw is rotated. This rotation of the screw causes the flow of the fluid in the forward direction. The fluid enters from the feed port and exits from the discharge port. Like other types of rotary pumps, the gap between the moving parts and the pump's casing is nominal [27, 236]. After studying the working principles of the above pumps, it is observed that, in the gear pump and screw pump, fluid comes in direct contact with the pump. To avoid contamination, it is preferable to prevent fluid contact with an external object. The peristaltic pump has no actual contact with the fluid. It has an internal motor that rotates and pushes on the tube thus creating an area of low pressure behind it and an area of high pressure in front of it.

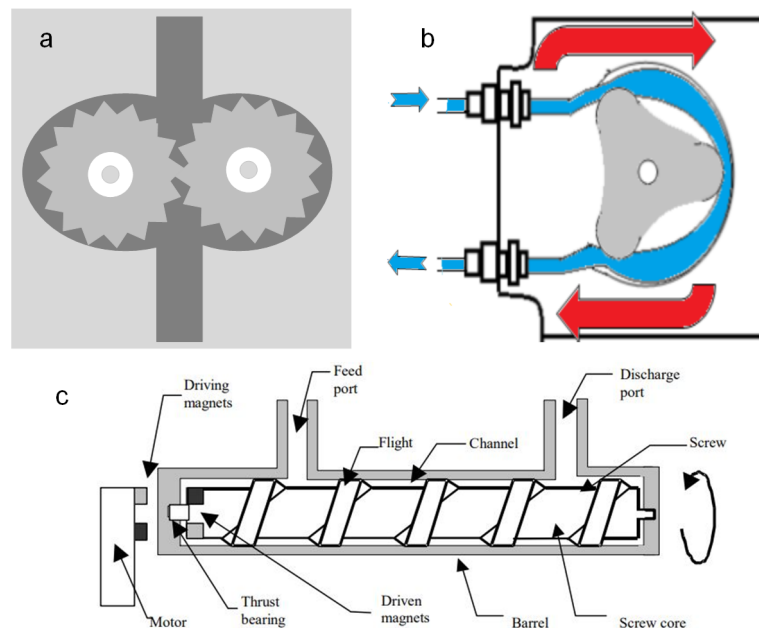


FIGURE 4.2: Schematic of (a) typical gear pump, (b) classical peristaltic pump, and (c) magnetically driven screw pump [27].



FIGURE 4.3: Dosing peristaltic pump

This creates a flow of fluid with no contamination occurring. For this reason, it has been decided to use the peristaltic pump in the fluidic system. Furthermore, to make the system cost-effective, a low-cost dosing pump has been used which is displayed in Fig. 4.3. This is a 12 volt dosing peristaltic pump.

The pump has dimensions of 64 mm length, 28.8 mm diameter, 31.4 mm pump head diameter with the tubing sizing of 5.0 mm OD and 2.8 mm ID. By changing the applied voltage polarities, the direction of the fluid flow can be changed. In the current system, this is achieved with the help of software programming.

4.4 Pinch Valve

Valves are necessary elements for most of the fluidic analysis assays as sample liquids and reagents must be properly retained until required. Essential characteristics of valves are: 1) easily removable, 2) quick action, 3) low power consumption, 4) wide operation range, 5) leakage-free, 6) zero dead volume and 7) contamination-free valving [229]. Different types of valves are available. Mainly they are classified as active and passive valves. Further, those are categorized such as check valves, ball-type valves, pinch-type valves, etc. [237]. Depending upon the application, valving can be the proportional type or on-off type. In the current system, on-off type valving was required.

After analyzing various types of valves the most suitable design for the current system would be pinch-type valves because of their characteristics such as leakage-free flow, quick response, zero dead volume and easy replacement of tubing [229].

4.4.1 Design and assembly

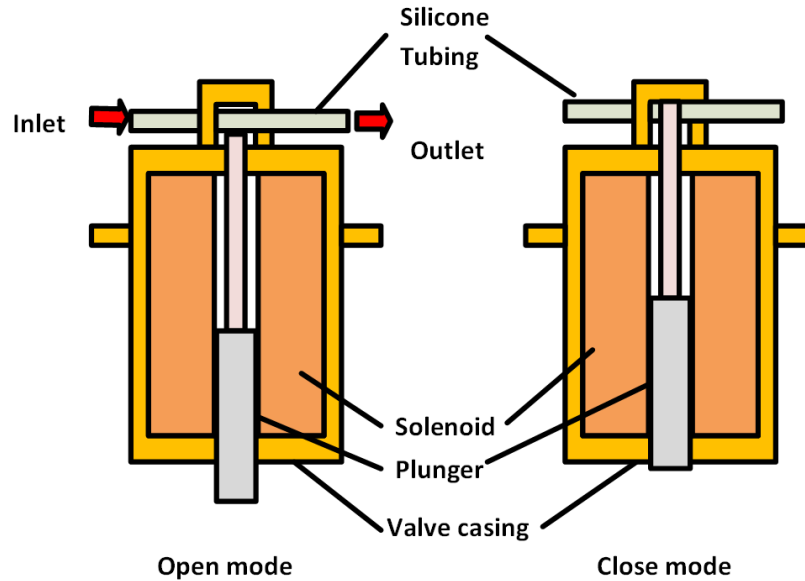


FIGURE 4.4: Schematic of the pinch type valve

The working principle of the solenoid-type pinch-valve is illustrated in Fig. 4.4. It includes conventional solenoid, plunger and silicone tube. In a normally open mode, the actuation of the solenoid lifts the plunger towards the tube, to close the valve. On the other hand, in the normally close mode type valve, the actuation of the solenoid pulls the plunger away from the tube which in turn causes the valve to open.

Figure 4.5 shows the pinch valves that have been used in the system. The valves used in the fluidic system are two-way normally closed and two-way normally open-type solenoid pinch valves. The diameter of each valve is 19.30 mm and the height is 48.23 mm with the tubing size of 1/16" ID x 1/8" OD.



FIGURE 4.5: Schematic of the pinch type valve

4.5 Fluid Presence Detection

Along with pumps and valves, a flow sensor is the key element of microfluidic systems [238]. The flow sensor is required to detect the presence of the fluid in the tubing. The fluid flow detection is essential for triggering the opening and closing of the valves so that liquid can be easily measured in the system. Many off-chip flow sensors are commercially available to deal with this problem. However, such flow sensors have a few disadvantages, like – large size; difficulties in interfacing; long response time; high-cost, etc. [238]. Hence, we have introduced an electro-optical-based flow sensor as shown in Fig. 4.6. The flow sensor has been constructed with the help of an LED and a photosensitive diode. The 3D printing technique has been used for the implementation of housing for the sensor. The dimensions of the flow sensor are: 38.2 mm in length and 20.2 mm in width and 18 mm in height.

4.5.1 Design principle and calculations

The design of the flow sensor is very simple as it is made up of a photodiode and an LED. A detailed version of this type of sensor has been reported for the colorimetric detection of different biomolecules in [239]. However, our design is based on light scattering by the fluid present in the tubing. As the fluid flows through the tube, it scatters light and thus causes a voltage drop in the photodiode output. This voltage drop is read by an analog-to-digital converter. Through experimentation, we have found that the drop in voltage is significant even for clear water and thus the sensor provides an effective means of fluid presence detection. We have used silicon photodiodes for measuring the scattered light. In the case of the light source, many options were available in terms of the colour. With the help of experimentation, it has been found that a white LED is more sensitive than red, blue, and yellow. Hence, we have finalised the white LED as a light source. While constructing the flow sensor we have kept the light source and light detector on either side of the tubing as illustrated in Fig. 4.6.

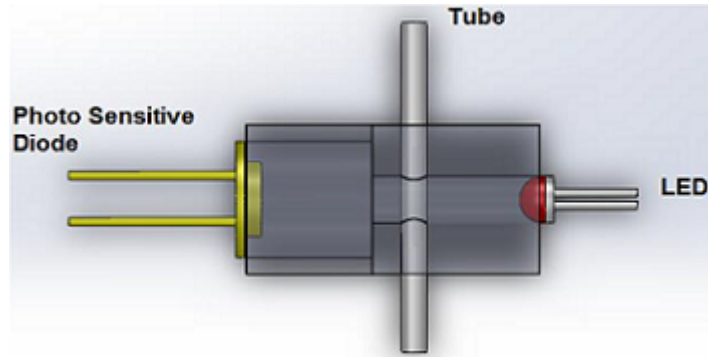


FIGURE 4.6: Schematic of Flow sensor

4.6 Flow Chamber

The flow chamber is an important part of the fluidic system that holds the self-assembled patterned base sensor in it. For fabrication of such a part, several methods are available such as injection moulding, soft-lithography, etc. Among many methods, a soft-lithography technique using PDMS micro moulding is a highly popular method [110, 111]. Microfluidics fabrication using PDMS can be easily prototyped with simple procedures [240]. However, this multi-step process requires special equipment and, in many cases access to a cleanroom. Furthermore, it generally manufactures the final product at the second step (casting). The process is manual and cannot be fully automated [110].

Due to advancements in modern additive manufacturing methods, 3DP has been shown as a promising platform for the fabrication of microfluidic devices. 3D printers convert a computer-aided design (CAD) into a physical 3D object by depositing the desired material in a layer-by-layer fashion [241]. The main advantages of 3DP are the automated fabrication process, cost-effectiveness, higher printing resolution, etc. Additionally, these machines make the process simpler and lower the size of the required infrastructure and can be used as desktop printers [242]. The major benefit of using 3DP is the elimination of the need for a mould to cast the final shape/product. This allows a significant reduction in the material cost, creates the possibility of mass manufacturing, and saves significant development time. The possibility of using FDM and SLS technology for manufacturing a flow chamber was explored by printing the microchannels with these technologies.

TABLE 4.1: 3D printers and working parameters

3D printer	Layer Thickness (mm)	Nozzle Diameter (mm)	Material used
FDM	0.1	0.2	PLA
SLS	0.1	NA	Precimid 1170

4.6.1 Fabrication of microchannel

The microchannels were fabricated with different diameter sizes. Each microchannel consisted of an inlet port and a main channel as shown in Fig 4.7. The input connector was connected at the inlet port. The inner diameter of the inlet port was kept constant at 0.5 mm. However, the main channel was fabricated with various diameter sizes (0.25 mm, 0.3 mm, 0.35 mm, 0.4 mm, 0.45mm, and 0.5 mm). Two different processes were explored during the fabrication of these microfluidic channels: FDM and SLS. Pressure measurements were performed on these channels at different flow rates. In the SLS printer, the inside power of the laser was set at 18 watts and the outline power was kept at 9 watts. The slicer fill spacing was kept at 0.15 mm. The FDM printer was optimised with nozzle temperature at 207°C and platform temperature at 68°C to achieve the best results during the printing process. Other process parameters used during manufacturing

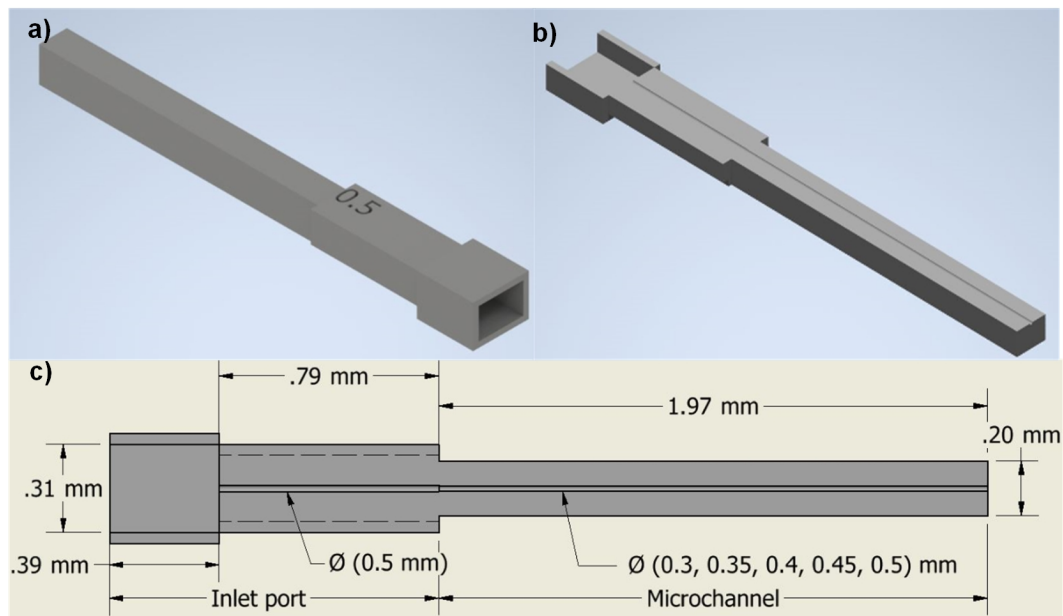


FIGURE 4.7: (a) CAD image of microchannel; (b) Cross sectional view of microchannel; (c) Pictorial view showing the internal measurements of microchannel.

are summarized in Table 4.1. 3D printed channels were cleaned, and the syringe was connected to each input port of the microchannels to provide the inlet connection.

4.6.2 Fabrication of flow chamber

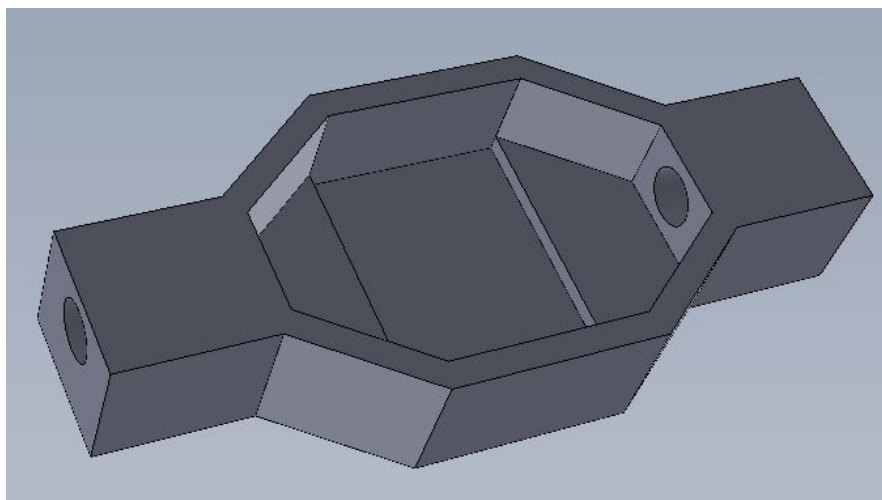


FIGURE 4.8: CAD image of flow chamber

Finally, the flow chamber has been fabricated using 3D printing techniques. It consists of an inlet port, a main body, and an outlet port as shown in Fig. 4.8. The input connector was connected at the inlet port. The inner diameter of the inlet and outlet port is kept at 3.2 mm. The size of the main body is 10 mm * 10 mm * 06mm.

4.7 Overall System

The overall layout of such an automated fluidic system is illustrated in Fig. 4.9. This system can be used for bead-based diffractometry sensing [200]. In this sensing method, microcontact printed patterns of thiols are exposed to target bound nanoparticles, and optical devices like gratings are formed for analysis purposes. This process requires a lot of fluid processing for washing and flowing the nanoparticles and buffer solution over the printed pattern. Overall, the system includes two containers, pump, six valves, chamber and flow sensor as shown in Fig. 4.10. The containers are used to hold the reagent and solution for cleaning purposes. The chamber provides a place to hold the microcontact printed chip. There are two possible fluid flow modes in the system i.e. continuous flow and circular flow. The continuous flow is used to fill the tubing and the chamber. Valves

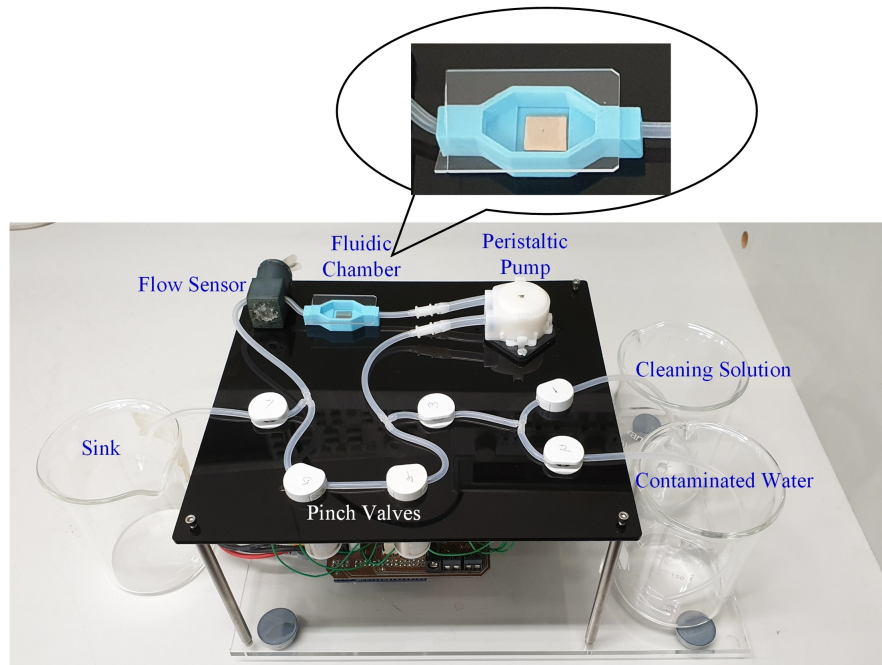


FIGURE 4.9: Automated fluidic system

are used to make the fluid flow circularly for analysis purposes. After completion of the analysis, the fluid can be disposed of in the sink.

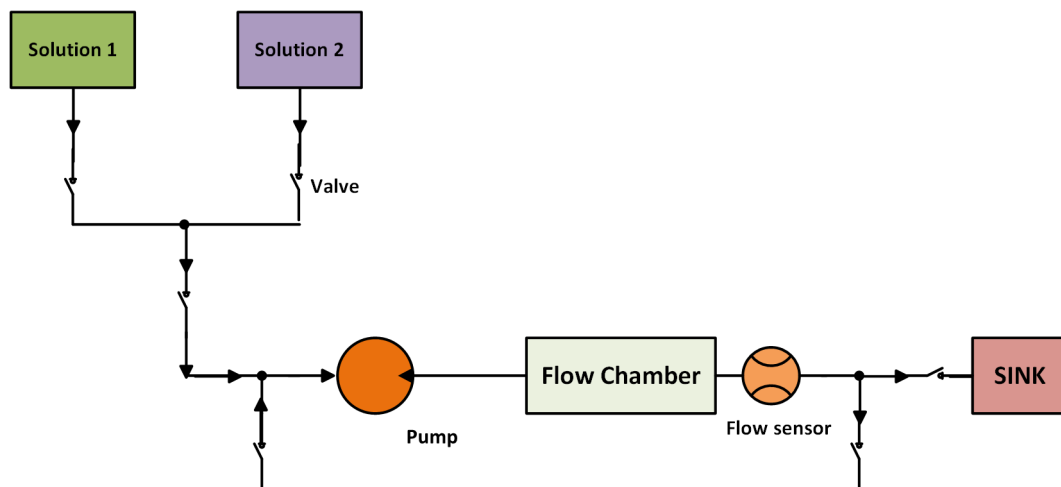


FIGURE 4.10: Schematic diagram of the fluidic system

4.8 System Automation

The PCB has been designed to interface the fluidic components with the controller. The layout of the PCB is attached in Appendix B. Figure 4.11 illustrates the block diagram of the system. The fluidic system consists of 7 pinch valves and a peristaltic pump

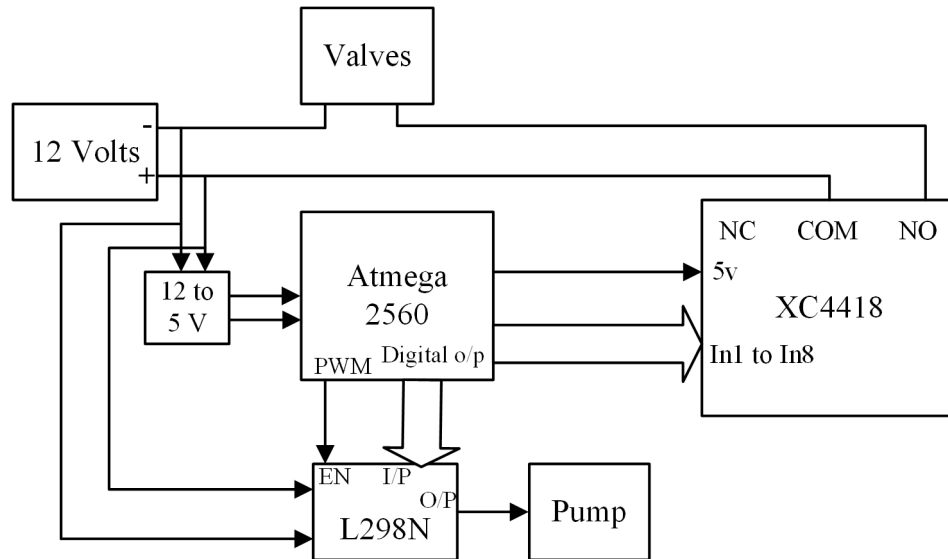


FIGURE 4.11: Block diagram of the fluidic system

to control the liquid flow. All the valves have been controlled using an eight-channel relay board (XC- 4418). A dual full-bridge driver (L298N) has been used to control the speed of the pump. The 12-volt power supply has been used for the valves and a pump whereas a 5-volt power supply has been used for an Arduino board and a relay card. An Arduino controller (Atmega 2560) has been controlling the entire operation of the system. A relay board has been interfaced with the Arduino through the digital I/O pins (from pin no. 16 to 30) of the Arduino. For this, the digital I/O pins are configured as output pins through the software program. The input pins of the dual full-bridge driver are connected to the digital I/O pins of the Arduino controller whereas enabled pins of the dual full-bridge driver are connected to PWM capable pins of the Arduino controller. The output pins of the dual full-bridge driver are connected to the pump.

The software has been developed in the Labview which in turn controls the pump and valves ON and OFF. The program is also capable of adjusting the direction of the pump (i.e. forward or reverse). Figure 4.12 displays the user interface that has been prepared to achieve the automation of the system. “Labview interface for arduino” has been downloaded for developing the software. As shown in Fig. 4.12, there are 6 boolean buttons (Valve 1 to Valve 6) through which the user can switch on/off the valves. “Pump On” and “Pump Off” boolean buttons are used for switching on and off the pump respectively, whereas the “Pump Reverse” button is used to rotate the pump in the reverse direction. These buttons have been interfaced with the arduino digital

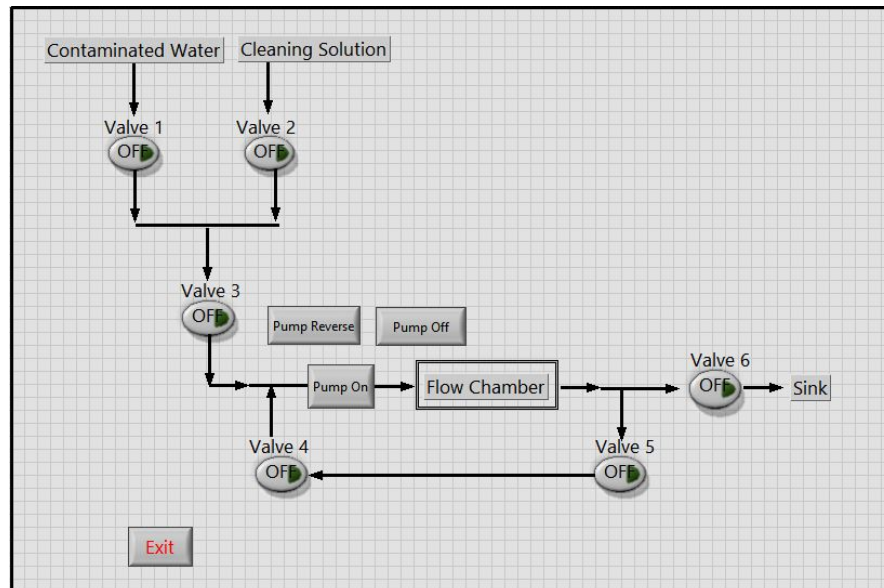


FIGURE 4.12: Schematic of the graphical user interface

pins with the help of “Labview interface for arduino”. All the arduino digital pins have been configured in output mode. “Exit” button is used to exit from the user interface.

User can operate the fluidic system in the following steps

- Step 1: Fill the “Flow chamber”. If water needs to be filled in the chamber then only valves 1 and 3 will be initialized. The path given below will fill the chamber with water. Water Container – Valve 1 – Valve 3 – Pump (Forward direction) – Flow chamber.
- Step 2: Circulate water in “Flow chamber”. If water needs to be circulated through the chamber, then only valves 4 and 5 will be initialized. The following path will help to circulate the water. Flow chamber – Valve 5 – Valve 4 – Pump (Forward direction) – Flow chamber.
- Step 3: Empty the “Flow chamber”. If flow chamber needs to be emptied then only valve 4, valve 5 and valve 6 will be initialized. The following path will empty the chamber. Flow chamber – Pump (Reverse direction) – Valve 4 – Valve 5 – Valve 6 – Sink

Figure 4.13 represents the flow of the instructions, when a user presses the button “Valve n” (n represents valve numbers from 1 to 6), “Pump on”, “Pump off” and “Pump reverse”.

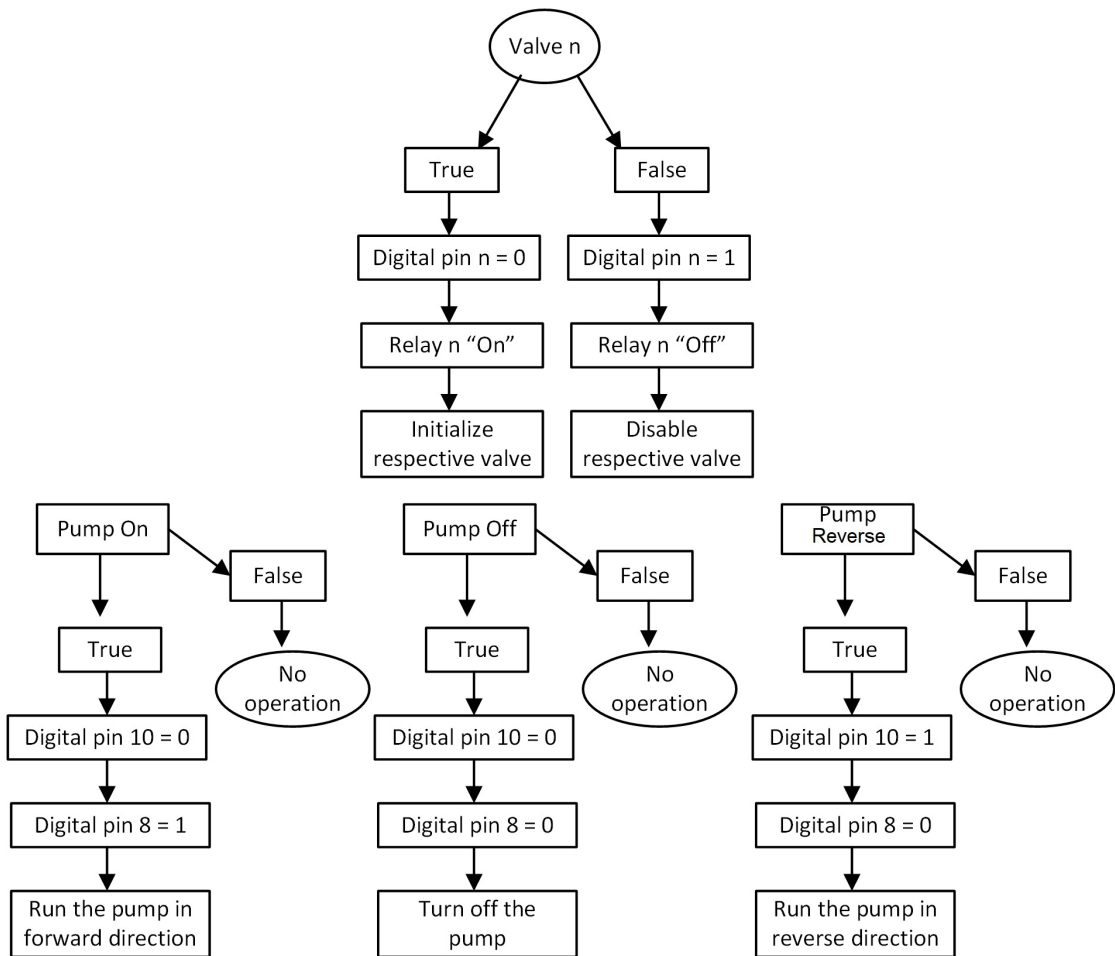


FIGURE 4.13: Flow instruction on button pressed

Chapter 5

Characterisation and Testing

In this chapter, the characterisation of thiol patterns and the fluidic system is described. Initially, thiol pattern characterisation is explained and in the later section, the fluidic system characterisation is discussed. In thiol pattern characterisation, various parameters are considered such as the cleanliness of the PDMS stamp, surface property, the concentration of the thiol compound, and the inking and stamping period of the stamp, etc. ANOVA analysis of the thiol concentration, inking, and stamping is provided to explain the effect of these parameters on the μ CP process. Then the effect of concentration of the compound and pH value on the inking period is provided. The effect of molecular weight on the thiol μ CP process is provided as well. The fluidic system characterisation includes a pump, valve, flow sensor, and flow chamber characterisation. Finally, arsenite contamination testing along with a signal enhancement technique is discussed and results are provided.

5.1 Pattern Characterisation

The thiol patterns were the most important part of the sensor. The quality of the thiol pattern was one of the essential criteria to decide the sensitivity of the sensor. The pattern quality was dependent on many parameters like on the stamp, surface property, the concentration of the thiol compound, the inking and stamping period of the stamp, etc. Hence pattern characterisation was performed to find out all such factors that can affect the pattern quality.

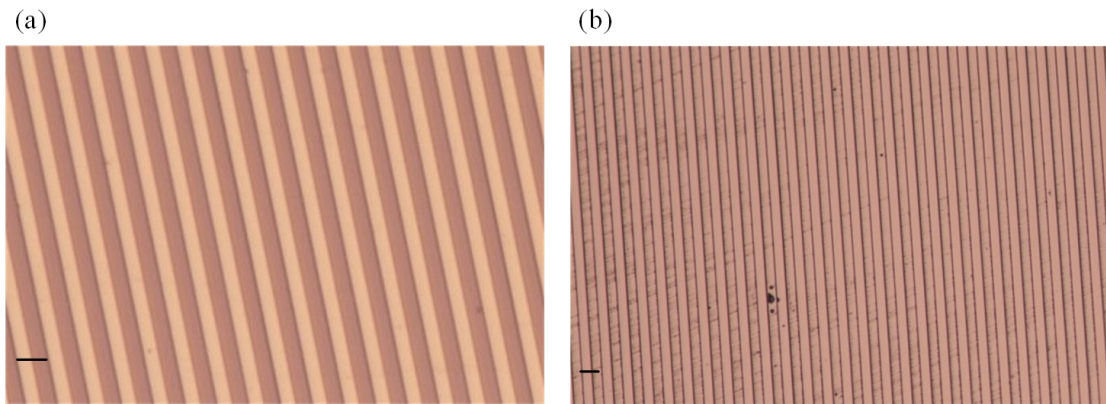


FIGURE 5.1: (a) The patterned side of the stamp is placed opposite the microscope lens. (b) The patterned side of the stamp is placed towards the microscope lens. Scale bar: $10\ \mu\text{m}$.

In this context, the stamp was one of the important factors that can affect the μCP process. To obtain the patterns it was necessary that inking is done on the respite patterned side of the stamp. It is a very tricky part to identify the patterned side of the PDMS stamp. While handling the stamp, it was quite possible to flip the patterned side upside down. Hence, an optical microscope was used to identify the correct side of the stamp. Figure 5.1 explains how to identify the stamp sides in which Fig. 5.1a shows the optical image of the stamp when its patterned side is placed opposite the microscope lens, whereas Fig. 5.1b indicates the image when the patterned side of the stamp is placed towards the microscope lens. Hence, it is possible to identify the patterned side of the PDMS stamp.

Moreover, cleanliness of the stamp was essential to obtain good quality patterns. Initially, the stamp was cleaned with DI water in the ultrasonic cleaner which did not

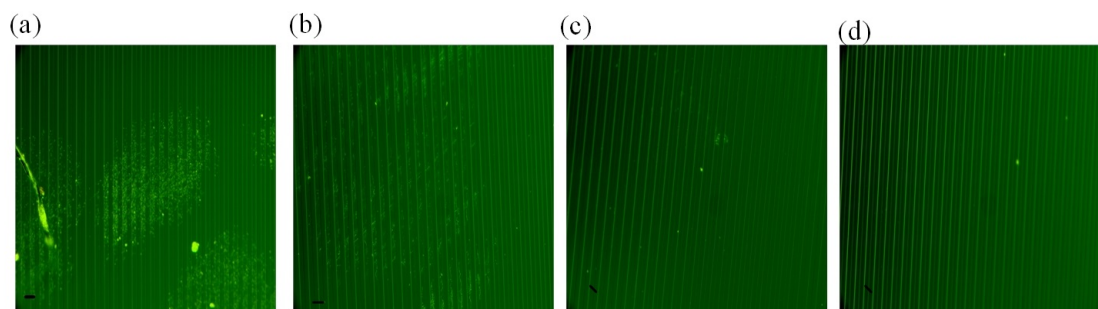


FIGURE 5.2: PDMS stamp (a) Before cleaning, (b) After cleaning with DI water, (c) After cleaning with ethanol, (d) After cleaning with ethanol, followed by acetone. Scale bar: $10\ \mu\text{m}$.

produce the required cleanliness in the stamp. Hence, instead of DI water, ethanol was

used which made the stamp clearer but not very clean. Then the stamp was cleaned in ethanol for 20 min. followed by 10 min cleaning with acetone which made the stamp very clean. Figure 5.2 indicates the stamp before cleaning and after cleaning.

5.1.1 BSA pattern

After obtaining a clean stamp, intense efforts were paid to practising microcontact printing. In order to learn the microcontact printing technique, initially BSA patterns were printed on the compact disk. For this purpose, various concentrations of BSA were pre-

TABLE 5.1: Result of BSA pattern printing on the CD.

Sr. No.	BSA	
	concentration (mg/mL)	Pattern
1	2	No
2	4	Very poor
3	6	Poor
4	8	Good

pared to range from 2 mg/mL to 8 mg/mL. A perfect pattern was obtained at 8 mg/mL. The quality of patterns achieved at different concentrations is indicated in Table 5.1. It indicates that at 2 mg/mL of BSA solution no pattern was achieved on the CD. As the concentration increased from 4 mg/mL onwards, patterns were obtained with poor quality. At 8 mg/mL of BSA, a good pattern was obtained on the CD.

Furthermore, BSA patterns were microcontact printed on the off-shelf gold-coated glass substrate. The experiment included trying different BSA concentrations, periods of ink on stamp and stamp on the gold-coated surface. Table 5.2 indicates the different values of the variables used for the experimental run, whereas Table 5.3 indicates the result of each run.

TABLE 5.2: Variables used in experimental run.

Variable	High value	Low value
Concentration mg/mL	16	8
Ink on stamp min	15	6
Stamp on surface min	15	6

Results in Table 5.3 indicate that the concentration of the ink plays an important role in the microcontact printing of the patterns on the gold substrate. Higher concentrations

TABLE 5.3: Result of experimental run.

Run No	Concentration	Ink on stamp	Stamp on gold surface	Result
1	High	High	High*	Best
2	High	Low	Low	Good
3	High	Low	High	Good
4	High	High	Low*	Best
5	Low	Low	Low	Poor
6	Low	High	Low	Ok
7	Low	High	Low	Ok
8	Low	Low	High	Ok

*"Stamp on gold surface" has negligible effect on the result. However, for a three factor ANOVA, eight results are necessary and for this reason all the results are retained in the table

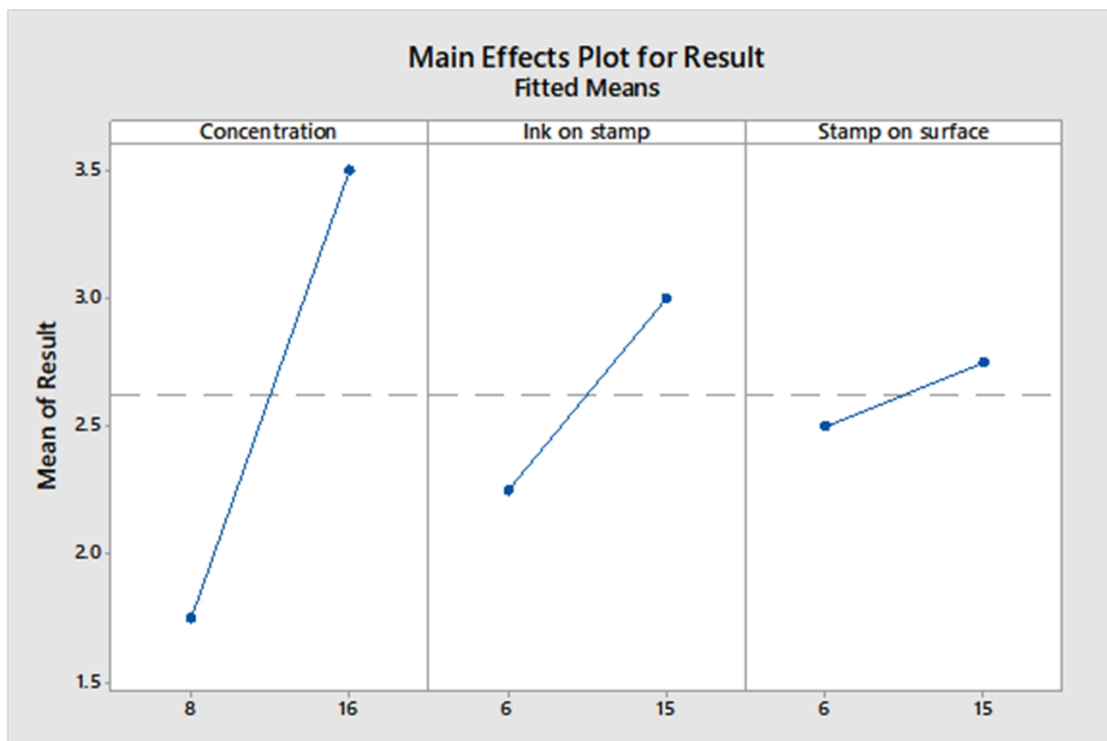


FIGURE 5.3: Main effects plot.

provide good patterns. To determine the significant terms and to predict the best result, minitab is used. AONVA of the result provided the main effects and two-way interaction plots.

Figure 5.3 indicates the changes in the result due to the main effects. Concentration has a significant effect on the pattern quality whereas Stamp on the surface has a negligible effect on the same. All the factors have a positive effect on the result that means when

the values of the factors increase from low to high level, the quality of the pattern improves.

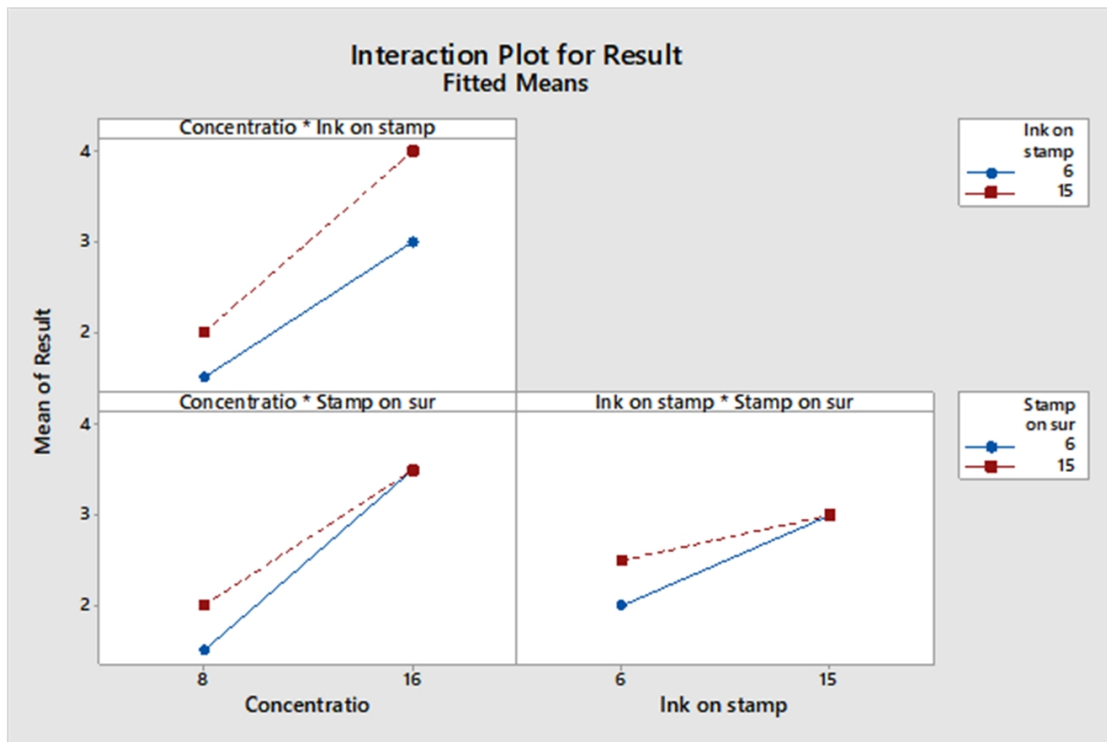


FIGURE 5.4: Two-way interaction plot.

Figure 5.4 indicates the effect of two-way interactions on the result. In the case of Concentration and Inking – there is a significant increase in the result as ink on stamp changes from low to high value when concentration is at 16, whereas result quality improves slightly, as ink on stamp changes from low to high value and concentration is at 8.

In the case of Concentration and Stamping – At concentration 8, there is an improvement in the result as a stamp on gold surface changes from low to high value. On the other hand, when concentration is at 16 there is no change in the resulting quality, even though, the stamp on gold surface timing is increased towards a higher value.

In the case of Inking and Stamping – at lower values of ink on the stamp, there is a change in the quality of the result as a stamp on surface changes from low to high value. However, there is no change in the resulting quality when the ink on a stamp is at high value and stamp on gold surface changes from lower to a higher value.

To summarize, the best pattern can be obtained by keeping concentration and inking at their higher values.

5.1.2 DTT pattern

TABLE 5.4: Result of experimental run using DTT with liquid inking method.

Sr. No.	Concentration gm/mL	Inking (min)	Stamping (min)	Stamp	Gold slide cleaning type	Pattern
1	0.33	15	15	New	B	NO
2	3.56	30	25	Used	A	NO
3	4	38	38	Used	B	NO
4	4.2	30	25	New	B	YES
5	4.2	30	25	Used	B	YES
6	4.26	30	25	New	A and B	NO
7	4.71	30	25	Used	B	YES
8	5.194	30	3	New	C	NO
9	5.194	30	1	New	C	NO
10	5.26	30	30	Used	A	YES
11	5.26	30	30	Used	Not cleaned	Poor
12	5.37	44	30	New	A & B	NO
13	5.37	30	30	New	B	NO
14	5.583	30	25	New	B	YES

The next phase involved printing the patterns using DTT. At first, DTT μ CP was performed on the off-shelf gold-coated glass slides. The required concentration of DTT for obtaining the patterns is not available in the literature, and hence the experiment started with a concentration of 8 mg/mL using DI water to dissolve the DTT. Various concentrations in the range of mg/mL did not work; therefore, higher concentrations in the range of gm/ml were used in the experiment.

As discussed in Chapter 3 (3.1.4), two different methods (liquid inking and inking by immersing PDMS stamp in the ink) were undertaken to obtain the pattern. The result of the random runs with the liquid inking method (as shown in Fig. 5.5) is explained in Table 5.4. Here, the used concentrations were ranging from 0.33 gm/mL to 5.5 gm/mL. Many attempts were made to obtain the pattern in which the inking and stamping periods were altered from 1 to 40 min. During experimental runs, two types of the stamp were used, i.e. new stamp and used stamp. Cleaning methods used for gold slide were – Type A, B and C where Type A – slide dipped in 20 mL ethanol for 10 minutes, Type B – slide cleaning with the help of Kimwipes soaked in ethanol, and Type C – slide cleaned with an ultrasonic cleaner. From the results, it can be considered that

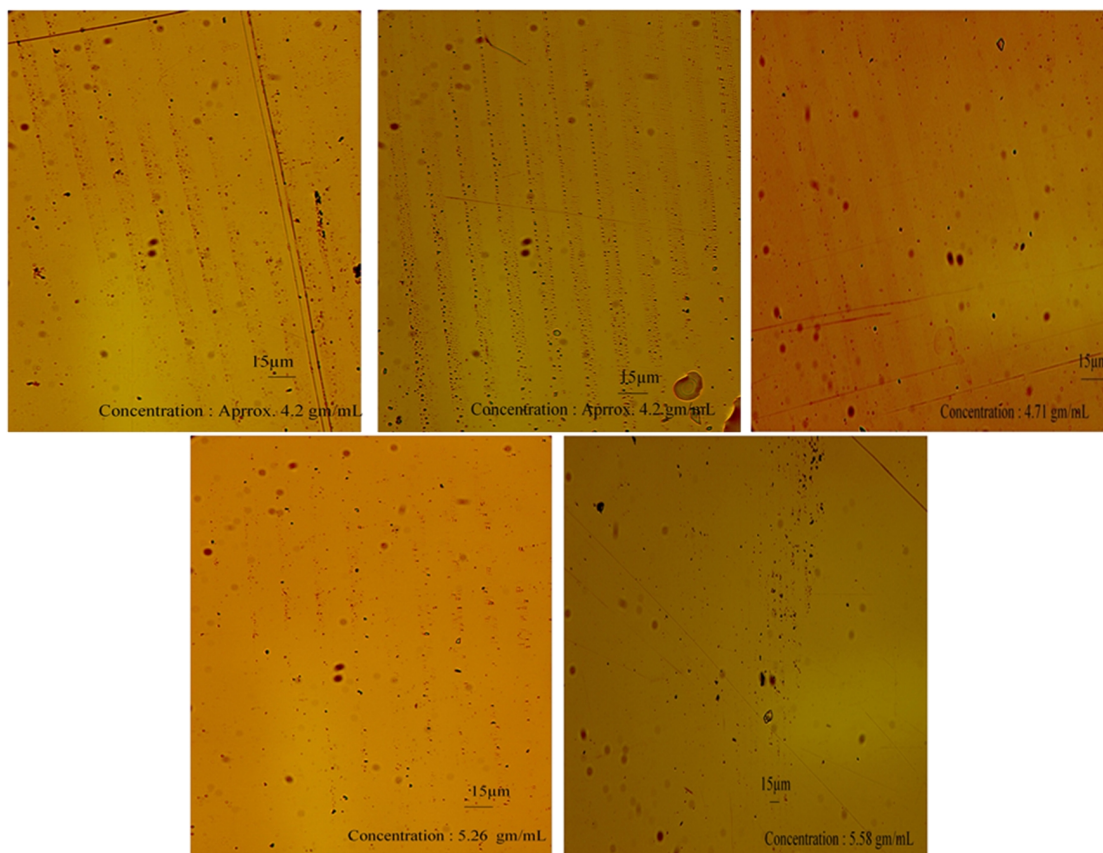


FIGURE 5.5: DTT patterns obtained during experimental runs described in Table 5.4.

an average 30 min inking and 25 min stamping time is essential for obtaining the DTT pattern on the gold-coated slide, whereas the type of stamp does not matter. In addition to this, the Type B cleaning method is useful for obtaining patterns. With this method, the pattern success rate is approximately 35 %. Figure 5.5 shows different DTT patterns obtained as described in Table 5.4.

Table 5.5 indicates the result with inking by immersing the PDMS stamp in the ink (as shown in Fig. 5.6). These experimental runs were performed with the used stamps. Cleaning methods used for the gold-coated slide were Type A and Type B. From the Table it can be considered that an average 12 hrs. Inking period and 20 min. stamping period is required to print the pattern on the gold-coated slide and the B Type cleaning method is useful for obtaining the patterns. With this method, the success rate of obtaining a pattern is approximately 71 %. The patterns resulting from the above experimental runs are displayed in the following Fig. 5.6:

Comparison of the two inking methods shows that the success rate of inking by immersing the PDMS stamp in ink is almost double that of the liquid inking method. In addition to

TABLE 5.5: Result of experimental runs using DTT with inking by immersing PDMS stamp in the ink.

Sr. No.	Concentration gm/mL	Inking (min)	Stamping	Gold slide cleaning type	Pattern
1	less than 0.154	overnight	30	B	YES
2	0.306	overnight	30	A	NO
3	0.33	3.5 hrs	2 sec	B	YES
4	1.27	overnight	60	A & B	YES
5	1.68	overnight	20	B	YES
6	1.68	overnight	20	B	YES
7	2.117	3.5 hrs	35	A	NO

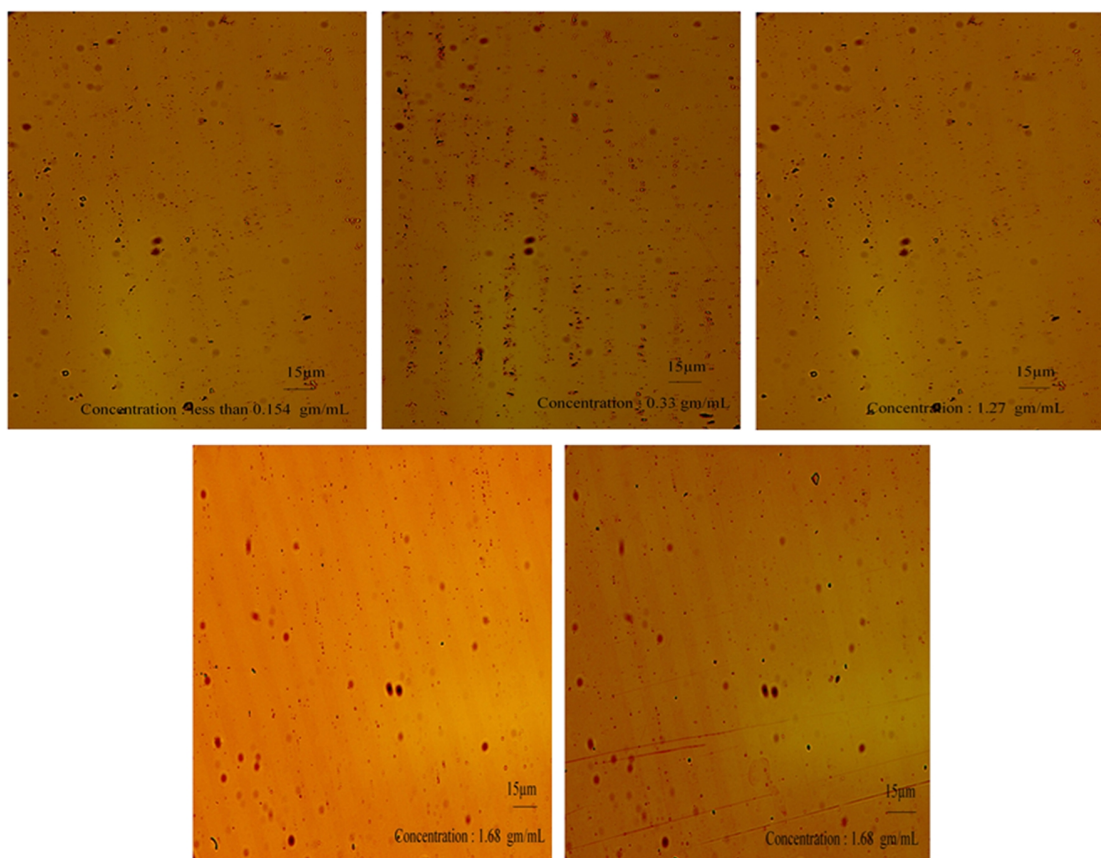


FIGURE 5.6: DTT patterns obtained during experimental runs described in Table 5.5.

this, the required concentration in the case of the reverse method is very much less than that of the normal inking method. However, the volume required for the normal method is much less than for the reverse method. In the case of the liquid inking method, 20 to 25 μL of DTT is required whereas for the other method around 100 μL of DTT is required. After observing the experimental results from Tables 5.4 and 5.5, one can consider that obtaining DTT patterns is a complicated process. Even though the success rate was increased with the help of the reverse method, it was still not 100%. This complexity is due to instability in the strength of the Au – S bonds that have been formed on the

gold surface. As explained earlier, the strength of the Au – S interaction formed on the gold surface depends upon surface properties, pH value, and time duration.

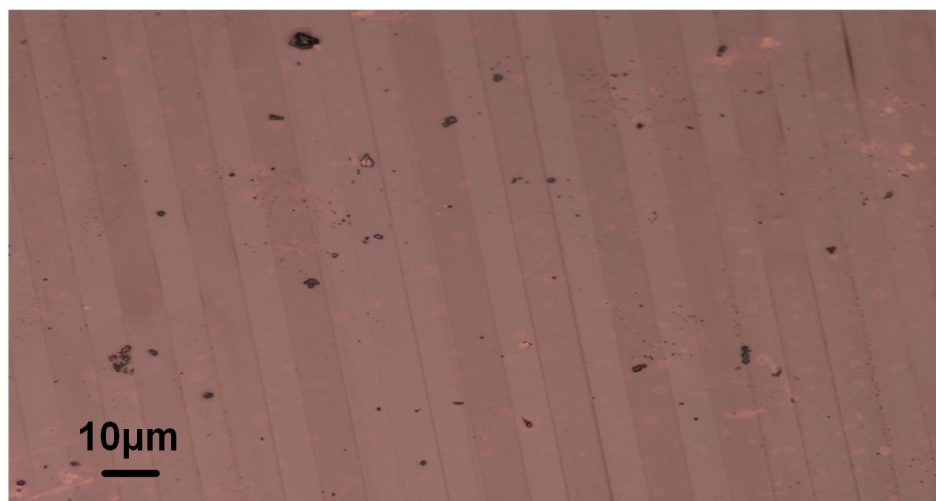


FIGURE 5.7: Optical patterns obtained with DTT

Hence, lab-made gold-coated (gold thickness 50 nm) glass substrates were used to check the effect on the result. The rate of obtaining a pattern was 100% on the freshly prepared lab-made slides where the stamp was immersed in the ink for different time durations. Figure 5.7 shows the optical images of DTT patterns. Furthermore, to enhance the result, different pH value buffers (PBS and pH 10) were used while preparing the DTT solutions instead of DI water. The plot in Fig. 5.8 shows a comparison between the experimental results of the obtained patterns using different pH values.

To observe the effect of concentration on the patterns, different concentrations of DTT (0.002, 0.004, 0.008 and 0.010 gm/mL) solution were prepared. To study the effect of the inking period, the PDMS stamp was immersed in each solution for different time periods (24, 12, 6, 5, 3, 2, 1, and 0.5 hrs.) and then brought into contact with the gold-coated substrate. This was followed by observing the patterns under the optical microscope.

It has been discovered that for concentrations up to 2 mg/mL using PBS as a buffer, the inking period must be at least 24 hours to obtain the pattern. In the case of pH 10 as a buffer, the inking period must be 12 hours. As the DTT concentration rises, there is a consistent reduction in the inking period for both the buffers. However, a minimum of 3 hours is essential to obtain the pattern from 10 mg/mL and above using PBS, whereas a minimum of an hour is adequate using pH 10 as a buffer.

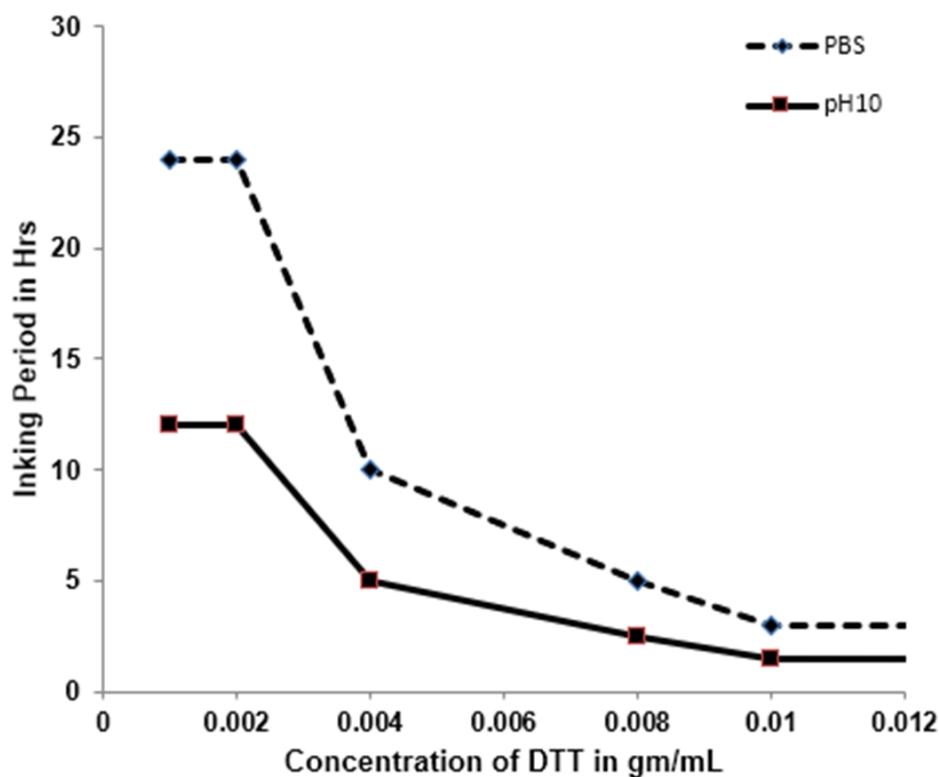


FIGURE 5.8: Effect of concentration and pH value on inking period.

The effect of pH value on producing the micropatterns was verified with the help of two different buffers i.e. pH 7.4 and pH 10. The plot in Fig. 5.8 shows a comparison between the experimental results of obtained micropatterns using different pH values. It is indicated that the required inking period decreases as there is an increase in pH value. It is also observed that the usage of the pH 10 buffer requires almost half the value of inking period than does PBS.

5.1.3 GSH pattern

Different concentrations of GSH (1, 2, 4, 8, 10 and 20 mg/mL) were prepared. The PDMS stamp was immersed in each solution for different time periods (6, 3, 2, 1 hrs.) and brought into contact with the gold-coated substrate, followed by observing the patterns under the optical microscope. Figure 5.9 shows the optical images of DTT patterns.

The experimental results are plotted in Fig. 5.10. Obtaining the self-assembled patterns is potentially dependent on the concentration and the inking period as depicted in the

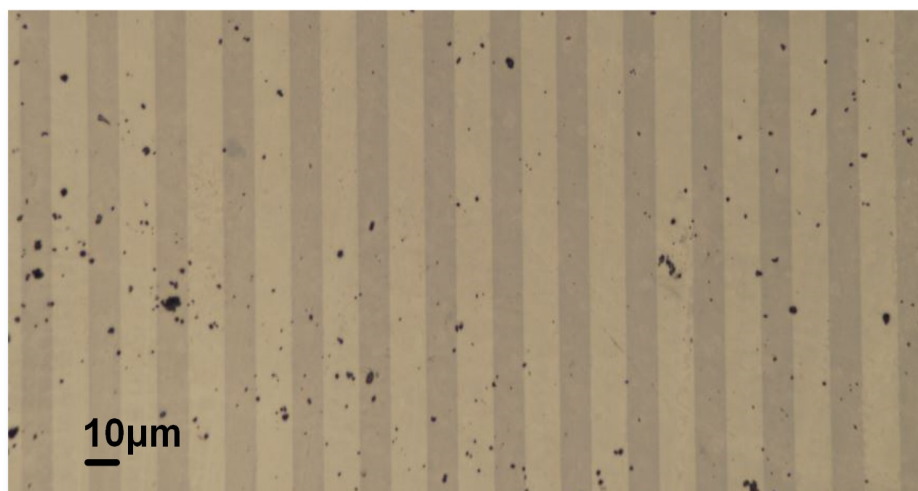


FIGURE 5.9: Optical patterns obtained with GSH

plot. It has been found that to obtain a visible pattern, the minimum concentration of GSH should be at least 1 mg/mL. Further investigations discovered that for the concentrations up to 2 mg/mL using pH 10 as a buffer, the inking period must be at least 6 hours to obtain the pattern. In the case of pH 10 as a buffer, the inking period must be 3 hours. Furthermore, as the GSH concentration increases, there is a decrease in the inking period. However, a minimum of 1 hour is required to obtain the pattern from 10 mg/mL and above. Over and above, it is also observed that a very high concentration (above 1 gm/mL) of GSH is not useful in obtaining the patterns. The graphs in Fig. 5.10 also provides a comparison between the experimental results of obtaining micropatterns using PBS and pH 10. It denotes that the required inking period decreases as there is an increase in pH value. It is observed that the usage of buffer pH 10 requires half the value of the inking period than does PBS.

5.1.4 Effect of molecular weight on thiol microcontact printing

The molecular weight of the thiol compound plays a key role while transferring the thiol ink on the gold substrate. The monothiol GSH molecule is nearly two times heavier than the dithiol DTT molecule. The molecular weight of DTT is 154.253 g/mol whereas GSH is of 307.325 g/mol molecular weight. The experimentation result implies that patterns of GSH molecules take less time to be transferred on the gold-coated substrate when compared with DTT molecules. For example, it took 6 hours to transfer the pattern successfully with 0.002 gm/mL concentration in PBS solution for the GSH molecule. On

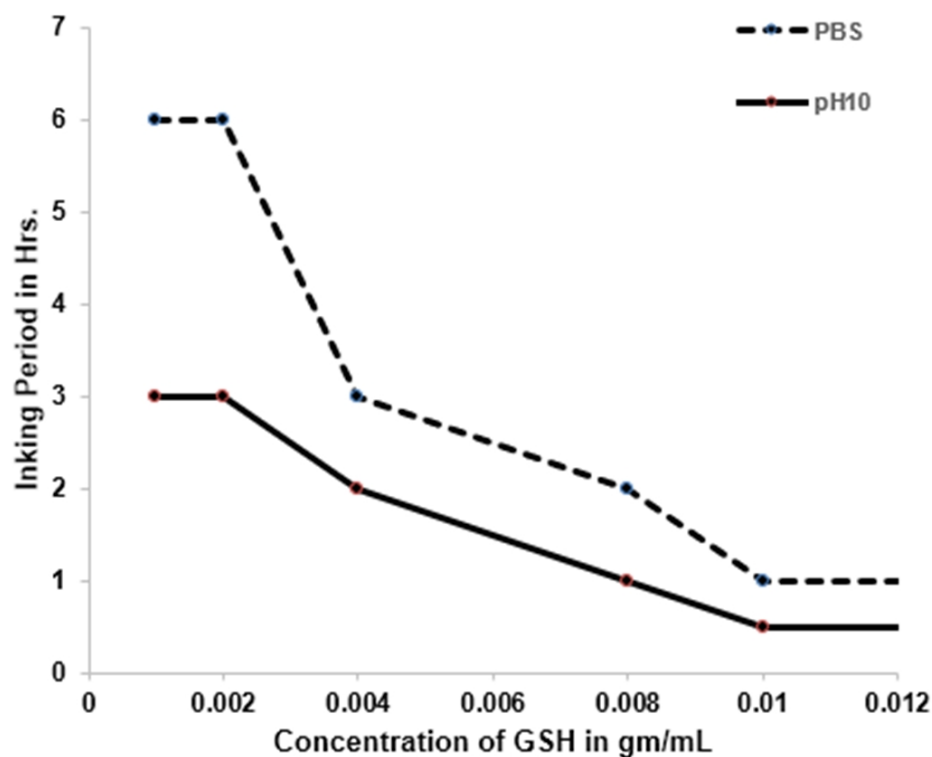


FIGURE 5.10: Effect of concentration and pH value on inking period.

the other hand, for the DTT molecule with the same concentration and buffer, 24 hours were required for the pattern transfer. In conclusion, the higher the molecular weight, the lower the inking period – and lower is the total length of time taken by the μ CP process.

5.1.5 Pattern confirmation

The rate of obtaining thiol patterns improved to 100% with the use of lab-made gold-coated slides and buffer solutions with higher pH values. The next step was to confirm the patterns. The available options for this purpose were SEM imaging and fluorescence imaging. Due to the lean thickness of the thiol patterns, it was difficult to use SEM imaging. Hence fluorescence imaging was performed. Here, bromophenol blue was used as a fluorescent dye as it can bind with DTT and GSH. Its absorption spectrum is between 470 to 570 nm of wavelength. Initially, bromophenol blue (0.001 gm) was diluted in DI water (1 mL). Next, the solution was vigorously and continuously mixed using a vortex mixer at a speed of 1600 rpm for 1 minute. The thiol pattern was then immersed in this prepared solution (100 μ L) for 15 minutes. The fluorescence solution

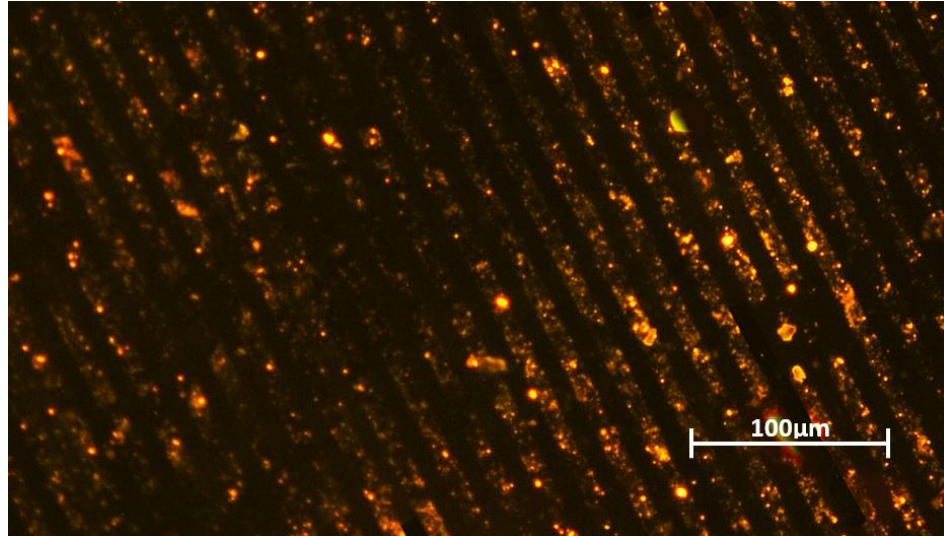


FIGURE 5.11: Confirmation of pattern using fluorescent dye.

was blown away with the help of a moderate nitrogen stream. The pattern was cleaned with DI water and finally, the patterns were observed under the fluorescence microscope. The fluorescence image is displayed in Fig. 5.11.

5.2 Fluidic System Characterisation

The performance of the pump has been characterised using water. Initially, a calibration process was done for the pump. Calibration is intended to verify the correlation between an applied voltage and the resulting flow rate. The input voltage of the pump was varied by changing the PWM of the pump driver IC through a software program.

5.2.1 Dosing peristaltic pump characterisation

The set-up of the calibration process is shown in Fig. 5.12. For flow rate measurement, the volume of water drained from the source was measured while the pump was switched on for 60 sec. Hence, by dividing the volume with time (1 min.), the flow rate was calculated as a function of PWM. The PWM of the pump driver IC was varied from 0 to 255 and the corresponding flow rate was noted down. The experimental results are plotted in Fig. 5.13. As depicted in the graph, there was a nearly linear increase in the flow rate with reference to the increment of PWM. Further investigations discovered that the PWM threshold of the pump, to begin liquid flow, was around 100 PWM with an

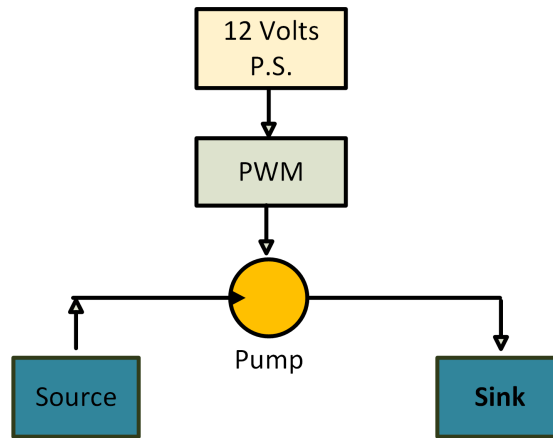


FIGURE 5.12: Dosing peristaltic pump.

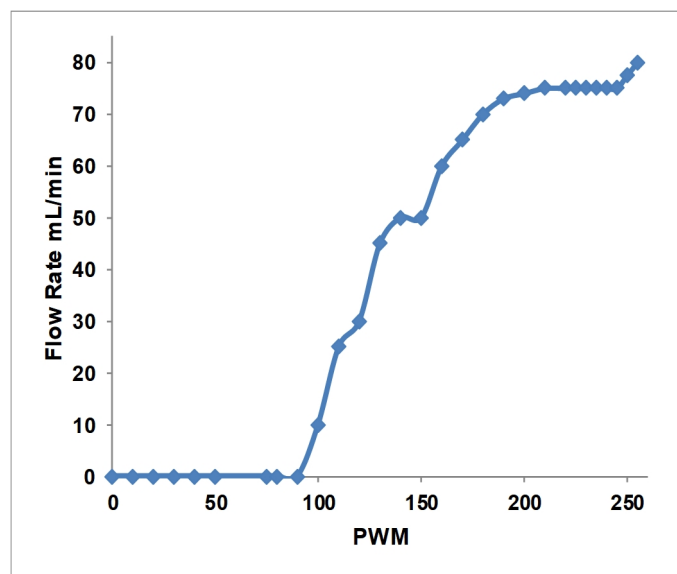


FIGURE 5.13: Measured flow rate vs. pulse width modulation of pump driver.

associated flow rate of 10 mL/min. The maximum flow rate of the pump was 80 mL/min. After the calibration process, the pump performance was characterised by connecting it in the fluidic network. For this characterisation, the volume of water pumped from the source was measured for various time durations by keeping the PWM constant at 255.

Thus, the relationship between the volume of water and the amount of time was verified. Initially, only the pump was connected in the fluidic network and characterisation was performed. Then the pump along with all the control valves was connected in the fluidic network and characterisation was performed. The time duration was varied from 0 to 120 seconds and corresponding volume readings were noted down. A linear relationship between the time (sec) and volume (mL) is shown in Fig. 5.14. The results for the pump in the network and the pump with valves in the network are not significantly

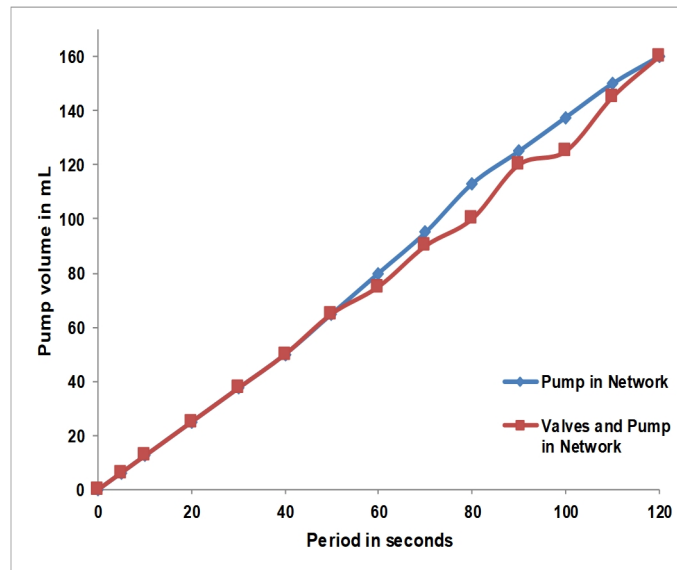


FIGURE 5.14: Measured volumes vs. time duration.

different except for long flow periods. This indicates that the presence of other fluidic components in the network has little effect on the pumping capacity.

5.2.2 Valve characterisation

The valve is rated at 12V/4W and can apply a holding force of 0.5 kg. When the signal is sent, it actuates the solenoid and pinches the tube blocking the flow. The solenoid used in the valve was a commercially available one with a coil resistance of 37.8 . A biomedical grade silicone tube (1.35 mm ID 3.18 mm OD) was used for the tubing material. The average pushing force required to fully close the silicone tubing was determined to be 300 gm. The solenoid provides a holding force of 500 gm. The actuator was assembled with separate parts. Its on/off operation was controlled through the computer. The behaviour of fabricated valves has been characterised at various actuation voltages ranging from 0 volts to 12 volts to find the holding and inrush voltages of the solenoid.

To find the holding voltage, the actuation voltage was increased from 1 volt to 12 volts. At actuation voltage of 6 volts, the valve was completely closed. To find the inrush voltage, actuation voltage was decreased from 12 volts to 0 volts. The minimum voltage to keep the valve in the closed position was 1 volt. Hence, the holding voltage of the valve is 6 volts and the inrush voltage of the valve is 1 volt. It was shown that at the closed position the valve could provide leakage-free operations. Since this valve has two

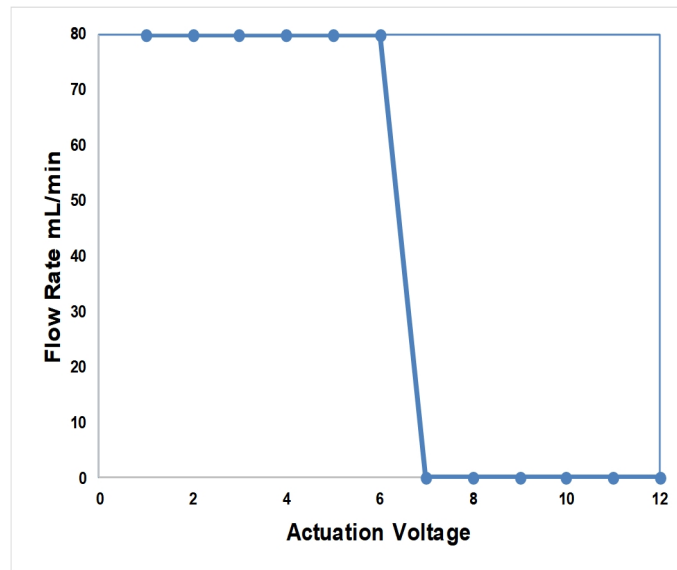


FIGURE 5.15: Characterisation of valve operation

states of operations (open and close), it functions like an on/off switch. One can actuate it using the voltage between 6 to 12 volts to close completely as shown in Fig. 5.15.

5.2.3 Flow sensor characterisation

TABLE 5.6: Sensor Output

Sr.No.	Type of fluid	Sensor o/p (volts)
1	Fluid absent	4
2	DI water	3.1
3	DI water with magnetic particles	3.4

After finalising the white LED, we experimented to find the threshold value for the sensor. The threshold value was the value used to detect the presence of the fluid in the network. The output of the sensor was noted down in the absence of the fluid. Similarly, the output was noted down in the presence of the DI water. After that, the sensor output was noted down in the presence of DI water with magnetic particles (diameter of 0.90 μ m). The results are displayed in Table 5.6. From the results, it has been decided to use 3.5 volts as a threshold value for the sensor. The output of the sensor below 3.5 volts indicates the presence of the fluid, and above 3.5 volts indicates the absence of the fluid.

5.2.4 Flow chamber characterisation

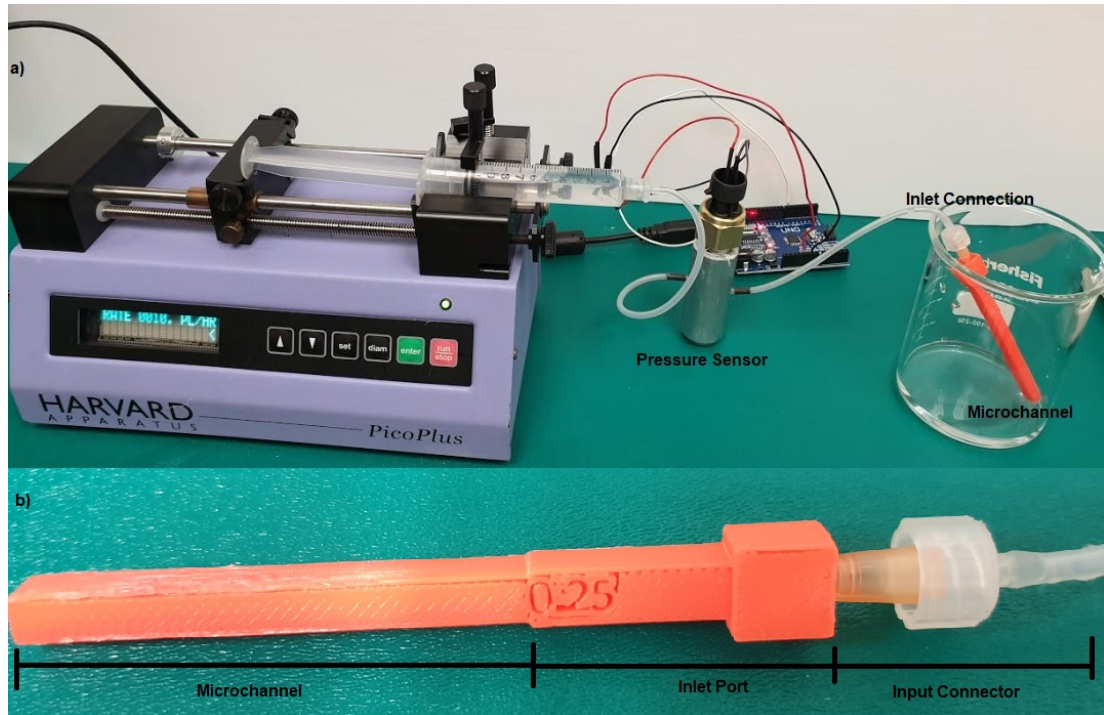


FIGURE 5.16: (a) Experimental set-up, (b) Microchannel printed with FDM method.

To fabricate the flow chamber two technologies (FDM & SLS) have been compared through printing the microchannels. These technologies have been compared in terms of their ability to fabricate the microchannels. The comparison is based on the minimum possible channel size, fluid flow-rate, and leakage in the micro-channel body. The experimental set-up is explained in Fig. 5.16a. Initially, all the printed channels were cleaned with compressed air jets. Water at different flow rates (varying from 0 to 40 $\mu\text{L}/\text{Min}$. in steps of 5) was injected at the input port with the help of the syringe pump. A disposable, 10 mL syringe was actuated on the syringe pump.

A pressure sensor was placed between the syringe pump and the input port of the channel for corresponding pressure measurement. The pressure was obtained as a voltage value which, in turn, was converted into a psi value using the datasheet. The change in flow-rate at the input port resulted in a change in pressure at the input port and leakage was observed in the microchannel.

SLS technology uses nylon powder for laser printing. Consequently, microchannels with a diameter less than 1.5 mm created using this method were filled up with the nylon powder resulting in blocked microchannels. However, microchannels with a diameter

of 1.5 mm and above created using this method did not have any blockages, but the microchannels created using the FDM method having diameters ranging from 0.25 mm to 0.5 mm did not have any blockages (Fig. 5.16b). As a result of these observations, the SLS method was dropped and the FDM method was continued for further experiments. The water was passed through the FDM method-based microchannels to study the effects of various flow rates on the leakage.

The graph (Fig. 5.17) explains the relationships among applied flow rates, the pressure generated at the input port, and the diameter size. As depicted in the graph, there is a proportional relationship between the flow rate and the pressure. Additionally, at a certain flow rate, there is a linear increase in the pressure for a decrease in the diameter size. In the case of microchannels with a diameter of 0.4, 0.45, and 0.5 mm, no leakage is observed. However, in the microchannel with a diameter of 0.35 mm, no leakage has been observed until pressure 0.2 psi; above this pressure, the body of the microchannel started to leak from the top and bottom side near the input port. It has been observed that the microchannels with a diameter of 0.3 mm and less started to leak even at a minimum flow rate. The experimental results showed the correlation of internal feature (microchannel diameter) with the pressure the microfluidic device can handle without any leakages. Further treatment of a microchannel with a void-filling material or chemical can also enhance the overall fluidic pressure in the device. Comparison between the SLS and FDM cannot be presented due to the inability of SLS to print internal features of a microchannel since the cleaning of the internal features at this scale were not successful after numerous attempts. The printed SLS internal features were clear with channel sizes exceeding 1.25 mm which do not fall into the category of microfluidic devices. Finally, FDM was selected to fabricate the flow chamber.

To fabricate the flow chamber, two designs have been simulated using COMSOL Multiphysics software. COMSOL provides an interactive environment for modelling and simulating engineering problems. The main objective of this simulation is to observe the fluid flow pattern in the body of the chamber at various fluid velocities. Coverage of the chamber body with the fluid is very essential in order to ensure coverage of the entire sensor chip.

During the simulation, inflow velocity has been varied to observe the effect of velocity on the fluid flow. Two different inflow velocities used are 0.01 m/sec and 0.1 m/sec. The

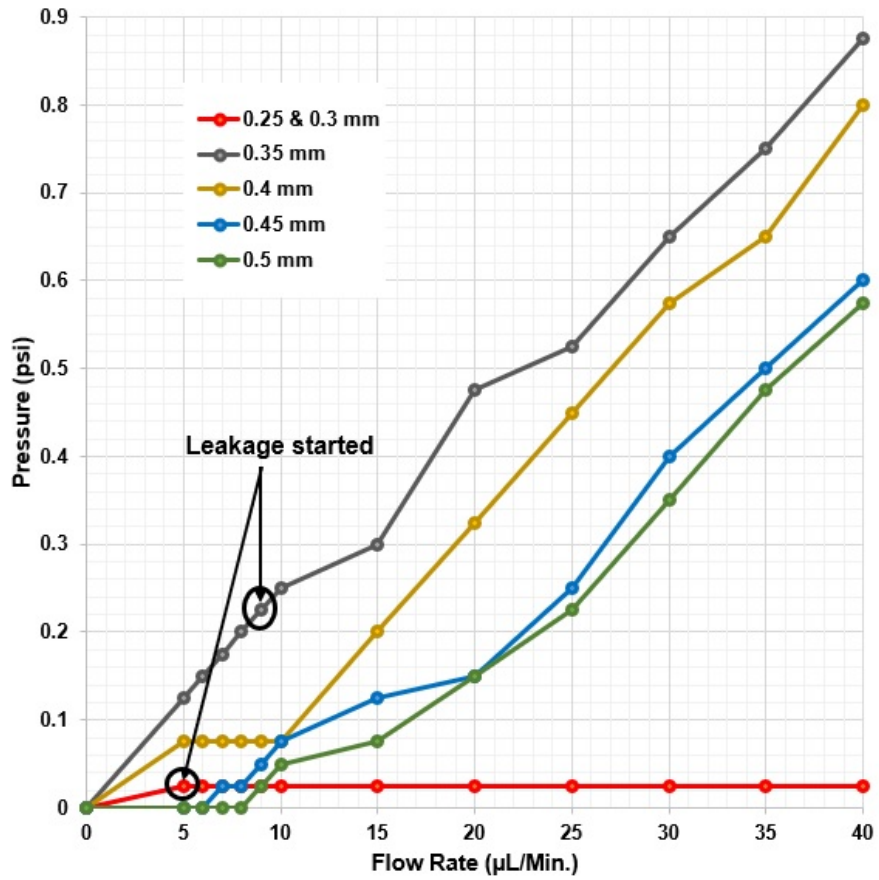


FIGURE 5.17: Change in flow rate vs developed pressure at the input port.

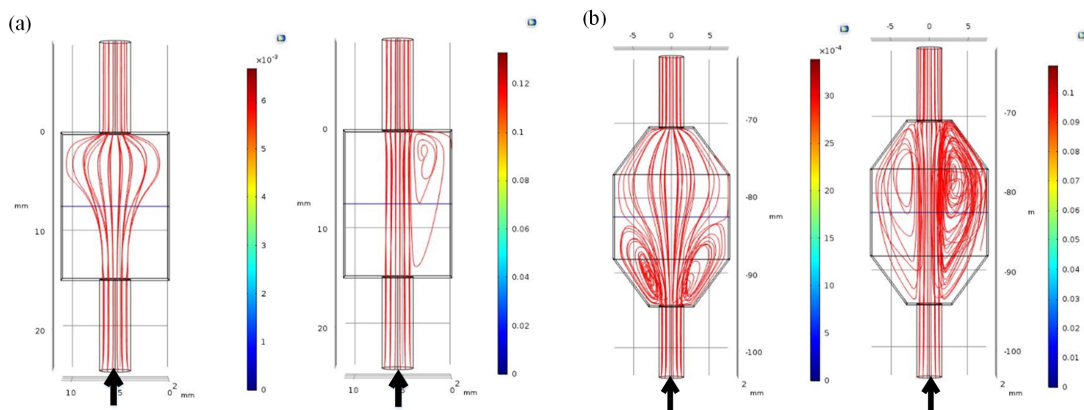


FIGURE 5.18: Design (a) and (b) at inflow velocities of 0.01 m/s & 0.1m/s.

results are displayed in Fig. 5.18 (a) & (b). As per the result, for design(a), as the fluid velocity increases, the coverage area of the chamber body decreases. However, in the case of design(b), there is not much effect on the coverage area even at higher velocities. Hence, design(b) is used during the fabrication.

5.3 Testing and Results

5.3.1 Arsenic detection

For As(III) detection purpose, As(III) stock (1 mg/L) solution was further diluted ((10 $\mu\text{g/L}$, 20 $\mu\text{g/L}$ and 50 $\mu\text{g/L}$)) with the help of DI water. The gold-coated substrates with microcontact printed GSH micropatterns were immersed in the diluted As(III) solutions. Micropatterns (GSH and DTT) are the ligand templates on which arsenic can form optical diffraction gratings. Optical signal detection could be possible due to the interference of coherent light beams reflecting from the bare gold surface and the top of arsenic. However, the thickness of the obtained optical diffraction gratings was not enough to perform the measurement. Hence, signal enhancement by sequential amplification phase was included to make the system measurable. The difference in micropatterns before and after arsenic exposed to As(III) contamination can be seen under the optical microscope (Fig. 5.19).



FIGURE 5.19: Optical micro-graph of GSH patterns (a) Before arsenic exposure, (b) After As(III) (20 $\mu\text{g/L}$) exposure, (c) After As(III) (50 $\mu\text{g/L}$) exposure.

5.3.2 As(III) confirmation with signal enhancement

As(III) contamination was confirmed with the help of aptamer Ars-3. 20 nM biotinylated Ars-3 was received in the dry form. The following steps were performed to achieve

signal enhancement. (All equipment were sterilised before each experiment to make them nuclease-free. This helped in avoiding DNA degradation) -

- Biotinylated Ars-3 resuspension:

1. Initially, the tube containing dry biotinylated Ars-3 was briefly centrifuged at 4000 rpm for 1 min before opening. This ensured that any dried DNA that might be dislodged during shipping was brought down to the bottom of the tube.
2. Next, it was resuspended in TE buffer (10 mM Tris, 0.1 mM EDTA, pH 8.0). In the buffer, Tris acts as a buffer, helping to maintain a constant pH for the solution. EDTA prevents nuclease digestion of the DNA.
3. 200 μL TE buffer was added in dry biotinylated Ars-3 to obtain 100 μM stock solution. The stock solution was stored at 4°C for further use.

- Dilutions of biotinylated Ars-3:

The stock solution of biotinylated Ars-3 was further diluted as required for the experiments. Four different concentrations (0.25, 0.125, 0.05, and 0.0625 μM) were made for arsenic detection. The following formula was used to prepare the concentrations:

$$(V1 * S1) = (V2 * S2)$$

Where, V1 is a volume of the stock solution, S1 is a concentration of the stock solution (100 μM /200 μL i.e. 0.5 $\mu\text{M}/\mu\text{L}$), V2 is the required volume of the dilution, S2 is the required concentration of the dilution,

1. To prepare dilution with the concentration of 0.25 μM , 50 μL biotinylated Ars-3 from the stock solution was dispensed in a nuclease-free microcentrifuge tube. To make a total volume of 100 μL , 50 μL of TE buffer was added in the microcentrifuge tube.
2. The dilution prepared in step 1 was used as a stock solution to prepare 0.125 μM concentration. Hence 50 μL solution from this stock solution was dispensed in a nuclease-free microcentrifuge tube and 50 μL of TE buffer was added to prepare the dilution.

3. Similarly, the dilution prepared in step 2 was used as a stock solution to prepare 0.0625 μM concentration. Therefore, 50 μL solution from this stock solution was dispensed in a nuclease-free microcentrifuge tube and 50 μL of TE buffer was added in it to prepare the dilution.
4. To prepare a dilution with the concentration of 0.05 μM , 10 μL biotinylated Ars-3 from the main stock solution was dispensed in a nuclease-free microcentrifuge tube. To make a total volume of 100 μL , 90 μL of TE buffer was added in the microcentrifuge tube.
5. All the dilutions were mixed carefully and stored at 4°C for further use.

- Streptavidin washing and re-suspension:

BioMag[®] Streptavidin is a nuclease-free suspension of BioMag[®] particles with a size of approximately 1.5 μm . These particles are covalently coated with streptavidin. The received suspension was washed two times as follows:

1. To wash the suspension, the received solution bottle was shaken vigorously so that all the particles were mixed properly.
2. The next step involved – magnetic separation of the BioMag[®] particles and removal of the supernatant using a sterilised micropipette.
3. Further resuspension of the BioMag[®] Streptavidin in 10 mL of PBS and it was mixed vigorously.
4. Steps 2 and 3 were repeated one more time and finally, the particles were resuspended in 20 mL of PBS. The stock solution was stored at 4°C for further use.

- Thiol patterns:

1. PDMS stamps were cleaned in the ultrasonic bath with acetone for 30 min. at 30°C.
2. GSH solution of 10 mg/mL was prepared in PBS and pH 10 buffer and cleaned PDMS stamps were immersed in the solutions for an hour and 30 min. respectively.
3. Similarly, a DTT solution with a concentration of 10 mg/mL was prepared in PBS and pH 10 buffer and cleaned PDMS stamps were immersed in the solutions for 3 and 1 hours respectively.

4. New glass substrates were gold coated in the lab. Thiolated stamps were brought into contact with the gold-coated substrate, applying gentle pressure.
 5. After 3 hours, the stamps were removed carefully from the gold-coated substrate and patterns were observed under the optical microscope.
- Arsenic contamination:
 1. 100 mL As(III) solution with a concentration of 1 mg/L was received. The received As(III) solution was further diluted in DI water to obtain the concentrations of 50, 20, and 10 $\mu\text{g/L}$. These dilutions were stored at 4°C for further use.
 2. The fluidic system displayed in Fig. 4.9 was used during the As(III) detection procedure to circulate the dilutions over the thiol pattern.
 3. 25 mL of each As(III) dilution was dispensed into different glass beakers.
 4. The gold-coated substrates having thiol (GSH and DTT) patterns were kept in the flow-chamber of the fluidic system. The dilution was circulated over the pattern with a speed of 20 mL/min for an hour. Thus, the patterns were incubated in the As(III) solution for an hour at room temperature.
 - Signal enhancement:
 1. 50 μL of BioMag[®] Streptavidin was dispensed from the stock solution into a nuclease-free microcentrifuge tube and further diluted in 450 μL of PBS to make a total volume of 500 μL .
 2. Streptavidin from step 1 was incubated with 20 μL biotinylated oligo Ars-3 for 2 hours at 4°C.
 3. Finally, As(III)-contaminated thiol patterns and thiol patterns without As(III) contamination were immersed in the above solution and allowed to incubate for 1 hour at room temperature.
 4. The results were observed under the optical microscope.

The pictorial illustration of the whole signal enhancement procedure is displayed in Fig. 5.20.

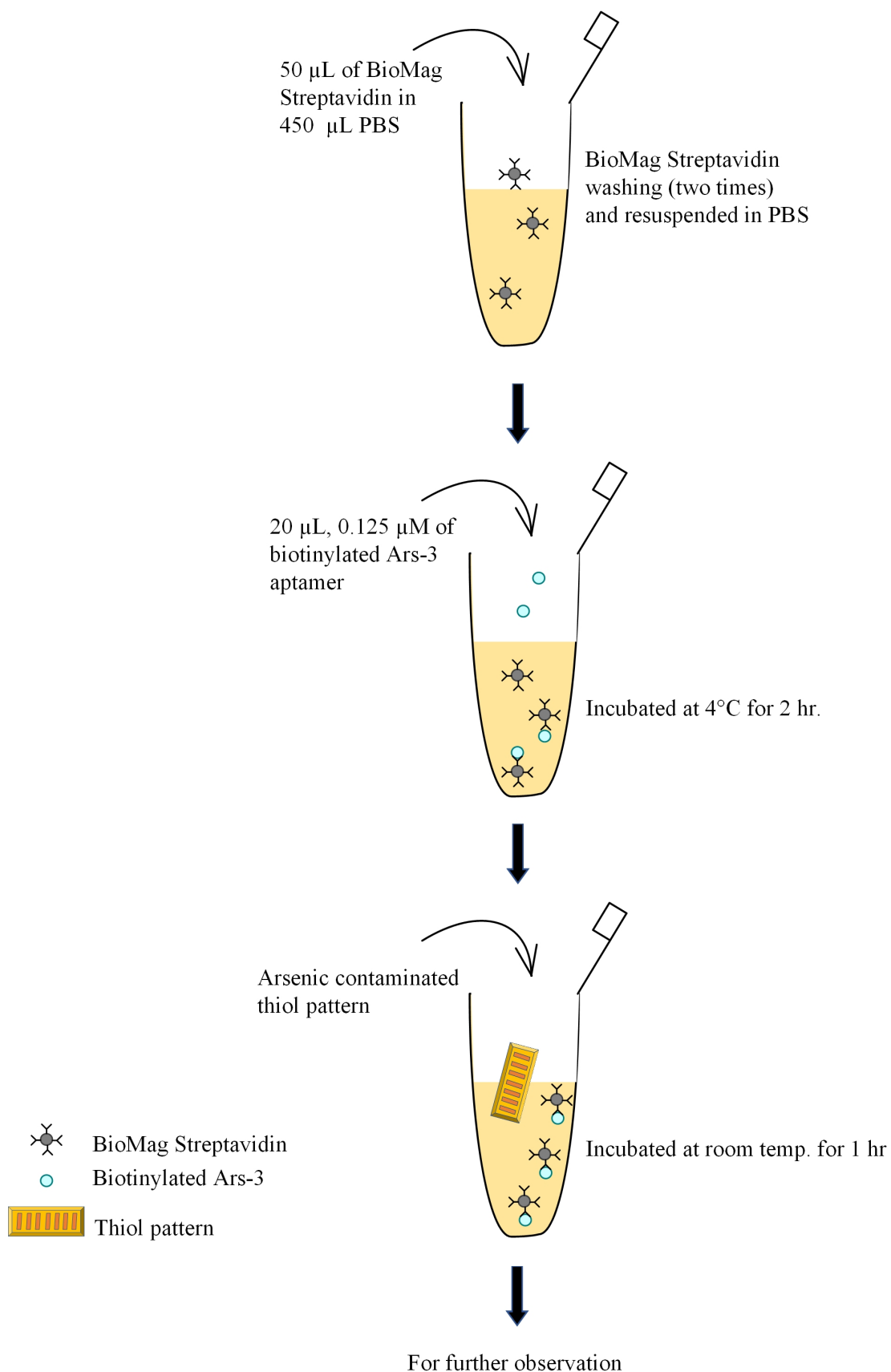


FIGURE 5.20: Illustration of signal enhancement procedure

5.3.3 Results

The signal enhancement is obtained accurately with the GSH solution (prepared in PBS) compared to the DTT solution. Hence the goal to detect As(III) was successfully achieved with the GSH pattern. The limit of detection of the sensor is $20 \mu\text{g/L}$. The results are displayed in Fig. 5.21. GSH patterns are shown in Fig. 5.21a. Figure 5.21b confirms these patterns using a fluorescent dye. It has been observed that the signal enhancement occurred in different ways on these patterns since it was completely dependent on the As(III) concentration. As shown in Fig. 5.21c, d, e and f, an increased number of streptavidin-coated magnetic particles were attracted towards the pattern that was contaminated with 1 mg/L arsenic dilution when compared with the other patterns contaminated with 50 , 20 & $10 \mu\text{g/L}$ As(III) dilutions respectively.

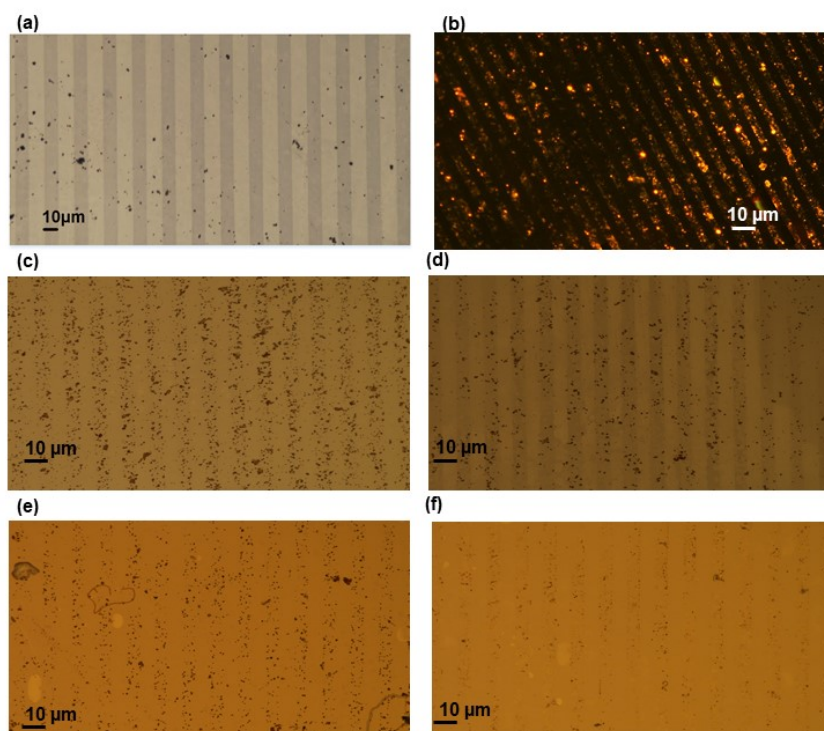


FIGURE 5.21: (a) GSH pattern, (b) Pattern confirmation with fluorescent dye, (c) As(III) contaminated (1 mg/L) pattern after signal enhancement, (d) As(III) contaminated ($50 \mu\text{g/L}$) pattern after signal enhancement, (e) As(III) contaminated ($20 \mu\text{g/L}$) pattern after signal enhancement, (f) As(III) contaminated ($10 \mu\text{g/L}$) pattern after signal enhancement.

Chapter 6

Conclusion and Future Work

6.1 Conclusion

A sensing scheme of a diffraction-based sensor for arsenic detection has been developed. The design, fabrication and testing of the sensor have been successfully conducted in this research. Initially, a literature study on water quality was conducted. Various water pollutants and their sources have been listed in Table 1.1. The consequences of each pollutant on the human body have been listed as well. From the study, arsenic has been identified as the most harmful element. It has been also found that a regular water quality monitoring is a must due to harmful effects of water contaminants on the various functional systems of a human body and a microfluidic-based sensor is the most suitable method for this purpose. Hence, a comprehensive literature review on microfluidic-based water quality based sensors has been conducted. The review includes microfluidic-based electrochemical and optical detection methods for heavy metals, nutrients and pathogen detection in detail along with advantages and disadvantages. The review revealed that an optical diffraction method was yet another sensitive detection method which remained unaddressed in water quality monitoring. This method can produce highly sensitive results and could be incorporated with microfluidic technology. It was noticed that for arsenic detection, many researchers were utilising thiol compounds such as GSH and DTT. Also, a small literature review on the aptamer-based arsenic detection has been conducted. Various detection methods like colorimetric, electrochemical, EIS, SERs etc.

have been included in the aptamer-based detection review. The study provided information about the popular arsenic-specific aptamer Ars-3. Finally, it has been decided to use a thiol based optical diffractometry sensor for arsenic detection.

In the next stage, it has been decided to use μ CP for obtaining optical diffraction patterns as it is a very useful technique in the patterning the SAMs of bio/chemical materials. However, the effectiveness of the technique depends upon various parameters such as type of ink, buffers used to prepare the ink, concentration of the ink, inking period of the PDMS stamp, pH value of the buffer, and molecular weight of the ink material. Hence, experiments were set up to obtain the self-assembled optical diffraction patterns and to find out the effect of the above parameters on the patterns. In experiments, we used two different thiol inks (DTT & GSH) during the process of μ CP due to their popularity in water quality monitoring. The study indicates that the total time taken by the μ CP process to transfer the patterns successfully on the gold-coated substrate is inversely proportional to the concentration of the thiol molecules and pH value of the solvent. When pH value changes from 7.4 to 10, there was a significant reduction in an essential inking period. Lastly, the success of pattern transferring using μ CP is also dependent on a molecular weight of the thiol molecule. Higher is the molecular weight, lower is the inking period and so lower is the total length of time taken by μ CP process.

Simultaneously, the fluidic system was designed with the help of off-the-shelf and/or in-house fabricated components. From the characterization of fluidic components, it has been noted that the peristaltic pump starts pumping at 100 PWM. In the range of 100 to 255 PWM, the flow rate of the pump increases as a function of speed. The maximum flow rate provided by the pump is 80 mL/min. At maximum speed, the volume of the water pumped by the pump increases almost linearly as a function of time. The pumping function is compared by placing the only pump in the network and then connecting the pump along with other fluidic components in the network. The result of the comparison has shown almost similar pump function in both cases. Overall, the fluidic components work reliably in the fluidic network and can be used in sensing application for pumping, mixing and circulation purpose. In the future, it may be possible to miniaturize these components using PDMS and 3D printing technologies. By miniaturizing these components, it is possible to develop a microfluidic system for environmental monitoring applications.

In the third stage, experiments were developed for arsenic detection. It has been reported that the developed self-assembled optical diffraction patterns of GSH can detect dissolved As(III) up to $20 \mu\text{g/L}$. Furthermore for quantitative measurement of dissolved As(III) in water the signal enhancement of the patterns was necessary. Hence, the signal enhancement step was introduced in the experimentation. This step involved the reaction of As(III) with the biotinylated Ars-3 and BioMag[®] Streptavidin.

6.2 Future Work

Currently, the sensor provides qualitative output with the help of an optical microscope, hence it remains a lab-based method and does not give any quantitative output. This issue can be addressed with the help of a suitable detection system. The self-assembled patterns of the sensor can act as an optical diffraction grating. Hence, optical signal detection can be possible by making use of the light beams reflecting from the bare gold surface and the top of signal-enhanced patterns as shown in Fig. 6.1. The detection system will simply consist of a light source such as an LED and a light detector to capture the reflected signal from the pattern. The intensity of the reflected light will vary proportionally to the arsenic concentration variation.

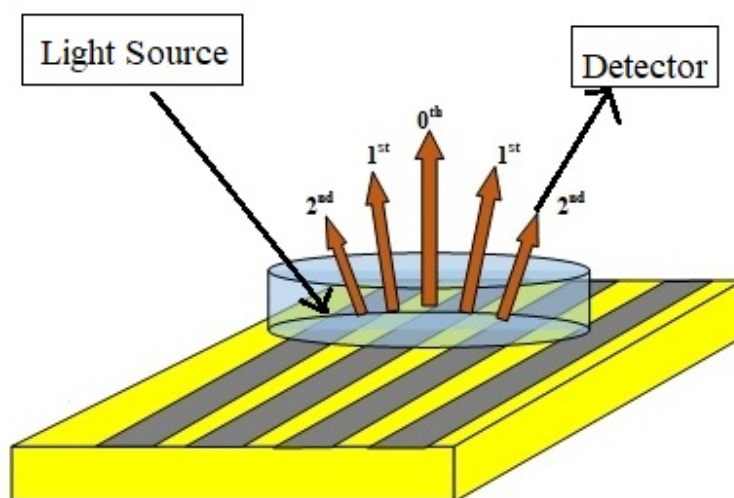


FIGURE 6.1: Illustration of optical signal detection strategy

Future work will also include a study of the matrix effect, as in real sample detection the major challenge will be interference due to the matrix effect. It is equally important to work on improving the sensitivity of the sensor which may include the addition of some

supportive chemical molecules in the GSH solution. Additionally, the same detection scheme can be used for detection of other water contaminants such as nutrients and pathogens with the help of specific chemical ligands.

Furthermore, integration with a suitable fluidic system will provide a high throughput and the simultaneous detection of contaminants. The size of the entire method can be reduced to make it field-effective using microfluidic technology.

Appendix A

List of Publications

1. Jaywant, Swapna A., and Khalid Mahmood Arif. "Study of parameters affecting microcontact printing of thiols on gold-coated substrate." *International Journal of Modern Physics B* (2019): 2040040.
[doi:https://doi.org/10.1142/S0217979220400408](https://doi.org/10.1142/S0217979220400408)
2. Jaywant, Swapna A., and Khalid Mahmood Arif. "A Comprehensive Review of Microfluidic Water Quality Monitoring Sensors." *Sensors* 19.21 (2019): 4781.
[doi:https://doi.org/10.3390/s19214781](https://doi.org/10.3390/s19214781)
3. Jaywant, Swapna A., Potgieter, J., Avci, E., and Khalid Mahmood Arif. "Self-assembled Optical Diffraction Patterns for Applications in Water Quality Monitoring." *Proceedings of 13th International Conference on Sensing Technology, ICST 2019*.
[doi:10.1109/ICST46873.2019.9047737](https://doi.org/10.1109/ICST46873.2019.9047737)
4. Jaywant, Swapna A., Rehmani, A., and Nayak, T., and Khalid Mahmood Arif. "Fabrication and Characterization of 3D Printed Microfluidics." *Proceedings of Mechatronics and Machine Vision in Practice Conference, M2VIP 2019*.
5. Jaywant, Swapna A., Johan Potgieter, and Khalid Arif. "Characterization of Low Cost Fluidic Components for Biosensing Applications." *2018 5th Asia-Pacific World Congress on Computer Science and Engineering (APWC on CSE)*. IEEE, 2018.
[doi:10.1109/APWConCSE.2018.00016](https://doi.org/10.1109/APWConCSE.2018.00016)

6. Jaywant, Swapna A., and Khalid Arif. "Microfluidic System for Water Quality Monitoring." A Poster in The Third National Conference for Innovation in Manufacturing, Design and Entrepreneurship, MaD 2019.
7. Jaywant, Swapna A., and Khalid Arif. "Parameters Affecting Microcontact Printing of Thiol on Gold Substrate." A Poster in Second International Symposium on Advanced Materials, Manufacturing Processes and Devices (MMPD) 2019.
8. Jaywant, Swapna A., Potgieter, J., Avcı, E., and Khalid Mahmood Arif. "Microcontact Printing of Thiol Inks on Gold Substrate." A Poster in NZ Product Accelerator 2018.

International Journal of Modern Physics B
 Vol. 34, Nos. 1-3 (2020) 2040040 (6 pages)
 © World Scientific Publishing Company
 DOI: [10.1142/S0217979220400408](https://doi.org/10.1142/S0217979220400408)



Study of parameters affecting microcontact printing of thiols on gold-coated substrate

Swapna A. Jaywant and Khalid Mahmood Arif*

*School of Food and Advanced Technology,
 Massey University, 909 Dairy Flat Highway,
 Albany, Auckland 0632, New Zealand
 k.arif@massey.ac.nz

Received 30 April 2019
 Accepted 20 August 2019
 Published 12 November 2019

Microcontact printing (μ CP) is a type of soft-lithography technique, which is widely used for patterning self-assembled monolayers (SAMs). It is a convenient method to form SAMs of bio/chemical ink onto different surfaces such as polymers, palladium, silver and gold. A wide range of applications of this technology includes micromachining, patterning proteins, cells or DNA in biosensors. However, the application primarily depends on the type of the ink used. Here, we present an experimental study that provides information about the parameters that affect the μ CP process. Two different thiol inks (dithiothreitol (DTT) and glutathione (GSH)) have been used for obtaining SAMs on gold-coated substrates. Our findings suggest that transferring the alkanethiols over the gold surface is extremely dependent upon the molecular weight of thiol compound, concentration of the thiol solution and pH value of the buffer used. Furthermore, higher the molecular weight, concentration and pH value of the ink, lower is the time required for the process of μ CP.

Keywords: Microcontact printing; self-assembled monolayers; thiol compound.

PACS numbers: 42.82.Cr, 85.40.Hp

1. Introduction

Microcontact printing (μ CP) is gaining popularity in the research areas such as BioMEMS, Lab on a Chip (LoC) devices or cell biology for surface passivation using patterned monolayers with submicron resolution.¹ This technique was introduced by Whitesides and his colleagues in 1993.² It is comparable to the conventional stamping method as it comprises of an ink, a stamp and a substrate. A polymeric stamp with requisite pattern is generally used in μ CP to produce the micro- or

*Corresponding author.

FIGURE A.1: A paper published in International Journal of Modern Physics B



Review

A Comprehensive Review of Microfluidic Water Quality Monitoring Sensors

Swapna A. Jaywant and Khalid Mahmood Arif *

Department of Mechanical and Electrical Engineering, SF&AT, Massey University, Auckland 0632, New Zealand; s.jaywant@massey.ac.nz

* Correspondence: k.arif@massey.ac.nz; Tel.: +64-9-414-0800

Received: 23 September 2019; Accepted: 31 October 2019; Published: 3 November 2019



Abstract: Water crisis is a global issue due to water contamination and extremely restricted sources of fresh water. Water contamination induces severe diseases which put human lives at risk. Hence, water quality monitoring has become a prime activity worldwide. The available monitoring procedures are inadequate as most of them require expensive instrumentation, longer processing time, tedious processes, and skilled lab technicians. Therefore, a portable, sensitive, and selective sensor with in situ and continuous water quality monitoring is the current necessity. In this context, microfluidics is the promising technology to fulfill this need due to its advantages such as faster reaction times, better process control, reduced waste generation, system compactness and parallelization, reduced cost, and disposability. This paper presents a review on the latest enhancements of microfluidic-based electrochemical and optical sensors for water quality monitoring and discusses the relative merits and shortcomings of the methods.

Keywords: microfluidics; water quality monitoring; heavy metals; pathogens; nutrients

1. Introduction

In this century, one of the major challenges that human beings are likely to face is water quality. Due to pollution, the amount of drinkable water is reducing day by day. This water pollution or contamination occurs due to various sources. These sources can be categorized as point sources and nonpoint sources [1,2]. Dumping of organic and inorganic wastes from industrial and domestic discards form the point sources of drinking water contaminants, whereas the nonpoint sources are land runoff, applying chemicals, or leaks from buried solid waste landfills [3]. These sources add dangerous materials such as heavy metals, nutrients, and pathogens to the surface water. Heavy metals (e.g., arsenic (As), lead (Pb), mercury (Hg), etc.) naturally exist in the surroundings, and various anthropogenic actions are also responsible for adding heavy metals to the environment [4]. Most of these heavy metals may cause fatal effects on public health due to their potentially mutagenic or carcinogenic effects on the human body [5–8]. Nutrient contamination is also a concern for water pollution. A key source of nutrients (mostly phosphorus and nitrogen) is land runoff since the nitrate and phosphorus ions are not held by soil particles. Pathogen contamination is another cause for concern [9]. Water polluted with organic waste and human and animal excrement is a potent source of pathogenic bacteria, protozoa, viruses, and parasitic worms. It results in gastrointestinal illness and can be a potential risk to human health. *Escherichia coli* (*E. coli*) is generally considered a faecal indicator bacteria (FIB). Bacterial counts are typically used to evaluate the influence of sewage pollution [10–12]. Higher concentrations of contaminants in water are responsible for fatalities across the world. The complications from water contamination are discussed in detail in the subsequent section.

The harmful outcomes of water pollution are increasing due to two main reasons: first, the level of contaminants in the water is continuously rising and there are no current practical methods to keep

FIGURE A.2: A review paper published in Sensors

Self-assembled Optical Diffraction Patterns for Applications in Water Quality Monitoring

Swapna A. Jaywant, Khalid Mahmood Arif
Department of Mechanical and Electrical engineering
Massey University
 Auckland, New Zealand
 S.Jaywant@massey.ac.nz; K.Arif@massey.ac.nz

Johan Potgieter
School of Food and Advanced Technology
Massey University
 Palmerson North, New Zealand
 J.Potgieter@massey.ac.nz

Ebubekir Avci
Department of Mechanical and Electrical Engineering
Massey University
 Palmerson North, New Zealand
 E.Avci@massey.ac.nz

Abstract—In this paper, we present a novel method with unique surface modification technique to detect dissolved arsenite contamination of water. It features self-assembled patterns of thiol ligand like glutathione (GSH) on the gold-coated glass. Thiol easily binds with gold through Au-S linkage. In addition to this, As(III) has an affinity towards amino acids, amines, peptides and organic micro-molecules due to As-O or As-S linkages. Hence, GSH binds with gold-coated glass and arsenic. The patterns are obtained through a micro-contact printing (μ CP) procedure. When these patterns are exposed to arsenic-contaminated water, the arsenic layer forms on the GSH pattern which produces an optical diffraction grating for the detection system. These self-assembled optical diffraction patterns can detect dissolved arsenite up to 20 μ g/L. Our findings suggest that the proposed method can also be used for detection of a variety of other metallic and pathogenic contaminants like E. coli for water quality monitoring.

Keywords—Microcontact printing; Thiol compound; Metallic contamination; Water quality; Diffraction grating

I. INTRODUCTION

Water is life for every organism on earth; it alone constitutes approximately 60 percent of the human body. Freshwater helps us in living our life - water supports our farming, industries, tourism, and the welfare of communities. According to the United Nations report, currently, 31 countries in the world have water crisis. Additionally, an increase in water contamination continuously decreases the water quality [1]. When water quality deteriorates, it influences society in terms of ecosystem, social, and economic activities. Water pollution is a global issue and causes great damage to human and environmental health. Hence, it is very essential to maintain the water quality by keeping the pollution under check and reduce its ill-effects. The various natural sources such as precipitation, weather, basin physiography, soil erosion and man-made sources like urbanization, industrial and agricultural activities, etc., which pollute the water [2]. Generally, water pollution includes organic, inorganic and bacterial contaminants. Inorganic contamination involves metallic particles such

as arsenic, lead, etc. [3]. Out of these contaminants, arsenic is a major concern worldwide due to its mutagenic and carcinogenic effects on human health [3]–[7].

Arsenic (As) exists in the organic and inorganic form in nature and it has different species like arsenite As(III), arsenate As(V), dimethylarsenic DMA(V), monomethylarsenic MA(V) and various organoarsenic compounds. Among these forms, As(III) and As(V) are the principal species which present in natural water and considered to be more toxic by nature [8], [9]. Several medical studies have endorsed that long-term exposure to inorganic arsenic can lead to affect many different systems within the human body such as cardiovascular, nervous, endocrine, renal, skin, etc. Furthermore, arsenic toxicity causes different types of cancers [10]–[13]. The World Health Organization has recommended maximum contamination limit (MCL) for arsenic in drinking water to be 10 μ g/L [14], [15]. Across the world, countries like Bangladesh, China, Vietnam, India, Chile, USA, and Canada are contaminated with Arsenic [4], [16]–[18]. Arsenic species are also found in New Zealand in 28 geothermal features from Taupo Volcanic Zone and Waikato region [19], [20]. Thus, a rising level of arsenic in drinking water creates the need to periodic monitor its levels in potable water.

Since the last 50 years, several methods have been developed to detect the arsenic species that are present in the drinking water. However, most of these methods include technologies like colorimetric, electrochemical, surface plasmon resonance, spectroscopy, inductively coupled plasma spectrometry or biosensors for detection purpose [21]–[23]. According to Yogarajah, Nevetha and Tsai, Scott S. H. [4], techniques like spectroscopy, inductively plasma coupled methods, chromatography are included under laboratory methods. Whereas, colorimetric kit-based techniques and biosensors are included under portable methods. The most common laboratory arsenic detection methods are expensive and require specific instrumentation due to which they are not considered to be field

FIGURE A.3: A paper published in ICST-2019 Conference proceedings

Fabrication and Characterization of 3D Printed Microfluidics

Swapna A. Jaywant, Muhammad Asif Ali Rehmani, Tanmay Nayak and Khalid Mehmood

Massey University, Department of Mechanical and Electrical engineering, SF&AT,
Auckland-0632, New Zealand
k.Arif@massey.ac.nz

Abstract. Microfluidics is a rapid, high throughput and cost-effective means of processing small quantities of fluids through micro-scale channels. Several techniques are available today for the manufacturing of microfluidic channels such as injection moulding, soft-lithography, and paper microfluidics. Due to the advancements in modern additive manufacturing methods, 3D-printing (3DP) has been shown as a promising platform for the fabrication of microfluidic devices. In this paper, we explore the possibility of using fused deposition modelling (FDM) and selective laser sintering (SLS) technology for internal features of the microfluidic devices. These technologies have been compared in terms of their ability to print internal features to fabricate microfluidic devices. The outcome of the study provides a comparison of the minimum possible diameter size, fluid flowrate, and leakage through the internal features of the microfluidic devices.

Keywords: Microfluidics, 3D Printing, Characterization

1 Introduction

Microfluidics is an integral part of lab-on-chip (LOC) and a micro total analysis system (μ TAS) and sometimes also referred by these names. The field of microfluidics has proven high potential in many applications ranging from environmental assays to clinical analyses. This includes various point-of-care diagnostic tools, therapeutic devices, and water quality monitoring techniques and so on [5, 6, 8, 10, 12, 13, 15]. Several techniques are available today for manufacturing of microfluidic channels such as injection moulding, softlithography and paper microfluidics [1]. Among many methods, softlithography technique using polydimethylsiloxane (PDMS) micro-moulding is a highly popular method [2, 7]. Microfluidics fabrication using PDMS can be easily prototyped with simple procedures [4]. However, this multi-step process requires special equipment, and in many cases access to a cleanroom. Furthermore, it generally manufactures the final product at the second step (casting). The process is manual and cannot be fully automated [2].

FIGURE A.4: A paper published in M2VIP-2019 Conference proceedings

2018 5th Asia-Pacific World Congress on Computer Science and Engineering (APWC on CSE)

Characterization of Low Cost Fluidic Components for Biosensing Applications

1st Swapna A. Jaywant

School of Engineering and Advanced Technology
Massey University
Auckland, New Zealand
S.Jaywant@massey.ac.nz

2nd Johan Potgieter

Massey Agritech Partnership Research Centre
Massey University
Palmerston North, New Zealand
J.Potgieter@massey.ac.nz

3rd Khalid Arif

School of Engineering and Advanced Technology
Massey University
Auckland, New Zealand
K.Arif@massey.ac.nz

Abstract—Here we present, characterizations of generic fluidic components used in biosensing applications. Low-cost fluidic components such as a peristaltic pump, solenoid valve, and flow sensor have been characterized individually in this work. The solenoid valves and an electro-optical flow sensor have been fabricated in-house. An automatic fluidic system has been developed with the help of these custom-made components. Computational data, such as flow rate and volume flow curves, have also been plotted with the experimental results for validation purposes. The peristaltic pump has been used for fluidic processing. The pump performance is evaluated by connecting and disconnecting the solenoid valves in the fluidic network. In both the cases, the pump has shown a linear operation. The observed flow rate was ranging from 0 to 80 mL/min. The solenoid pinch type valves have been fabricated for controlling the fluid flow. These valves have been evaluated on the bases of the electrical parameters. The operating voltage of the valve is 12 volts. The observed holding and inrush voltages are 6 volts and 1 volt respectively. An electro-optical flow sensor has been developed for detecting the presence of fluid in the system. This is achieved by measuring the light scattered by the fluid present in the tubing. The effect of different liquids on the output of the sensor has been investigated. Design strategies are extracted and used to develop a highly sensitive and cost-effective flow sensor.

Index Terms—Biosensing, Flow sensor, Fluidic system, Peristaltic pump, Solenoid valve

I. INTRODUCTION

Biosensing applications or biosensors determine the presence or concentration of biological molecules, biological structures, microorganisms, etc. The term biosensor is used for a compact device that includes the biological sensitive element like antibodies, aptamers, enzymes etc. This element functions as a transducer to measure one or more analytes. Many times, these analytes are human samples such as blood, urine, serum etc. Hence, a microfluidic system is required for sample preparations, processing the throughput, mixing the reagents and controlling the flow conditions for detection purpose [1]. For example, in many diagnostic and therapeutic technologies, microfluidic is essential to perform cell separation and sorting steps [2]. Thus, the processing of fluid plays an

important role in biosensing applications and this processing includes pumping or mixing of sample liquids or circulation of reagents [3]. Components like micropump, microvalve, and flow sensor are considered to be the functional components of any microfluidic system [4]. Since the last decade varieties of micropumps and microvalves have been developed [5]–[13]. Generally, these components are either built-in fabricated or pre-fabricated. Built-in fabricated fluidic components are specifically developed for certain applications which cannot be considered as generic fluidic components. Some explore pre-fabricated fluidic components require pneumatic actuation [14], [15]. Pneumatically actuated fluidic components are not useful in portable applications. In addition to this, most of these microfluidic components possess low throughput [10]. Here, we present an automated system which has been developed using off-the-shelf and/or in-house fabricated components. The general schematic of the system is shown in Fig. 1. This automated system can be used in biosensing scheme where pumping, mixing, and circulation of reagents is necessary. It also provides high throughput. The major components those are used in the system are pump, valves and flow sensor. To obtain the precise control of fluid in the system it is beneficial to operate such complex processes automatically.

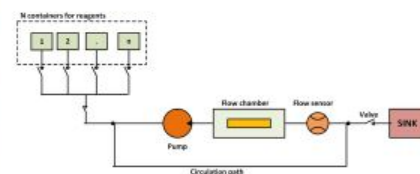


Fig. 1. Schematic layout of a typical fluidic system showing major components and fluid circulation path.



Microcontact Printing of Thiol Inks on Gold Substrate

Swapna A. Jaywant, Dr. Khalid Arif, Prof. Johan Potgieter, Dr. Ebubekir Avci
School of Engineering & Advanced Technology, Massey University, Auckland



MASSEY UNIVERSITY
TE KUNINGA KI PŪREHUOA

We investigate the effect of molecular weight of chemical ink on a pattern during microcontact printing

Introduction

- Microcontact printing (μ CP) is a soft-lithography process which can form self-assembled monolayers of bio/chemical inks.
- It uses respite patterns on PDMS stamps to transfer the bio/chemical ink on the surfaces like gold, silver, etc...
- The applications include patterning proteins/DNA/cells.
- The lateral diffusion due to mobility of the ink can effect the pattern shape.
- The molecular weight of thiol can influence the transfer of alkanethiols over the gold surface.

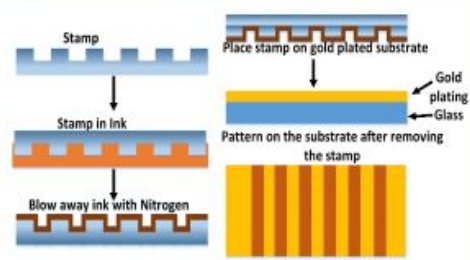


Fig. 1 Pictorial representation of μ CP process.

Methodology

In this research, Dithiol (compound with two $-SH$ molecules) is compared with monothiol (compound with single $-SH$)

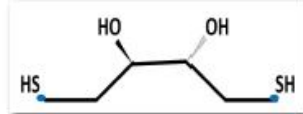


Fig.2 Chemical Structure

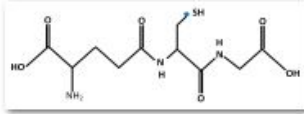


Fig.3 Chemical Structure

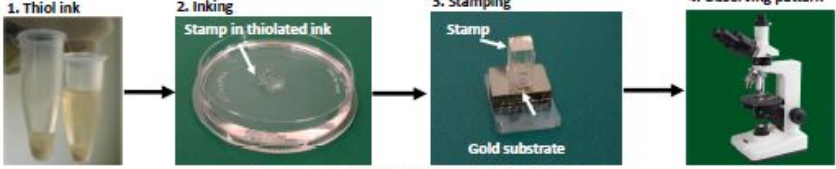


Fig.4 Steps involved in microprinting of thiol ink.

Effect of the molecular weight of the ink on the pattern



Fig.5 DTT Pattern



Fig.6 GSH Pattern

Molecular weight of DTT: 154.253 g/mol
Molecular weight of GSH: 307.325 g/mol

Table 1. DTT Experimentation		Table 2. GSH Experimentation	
Concentration	Inking period	Concentration	Inking period
2 mg/mL	24 hrs	2 mg/mL	6 hrs
1020 mg/mL	0.5 hrs	185 mg/mL	0.5 hrs

Higher the molecular weight, lower the inking period & better the pattern quality.

Sensor and Robotics Lab, School of Engineering and Advanced Technology, 229, Dairy Flat Highway (Off Kell Drive), Massey University, Auckland 0632
Telephone: +64(09) 414 0800 ext. 43580; Email: k.arif@massey.ac.nz

FIGURE A.6: A poster presented at NZ Product Accelerator 2018

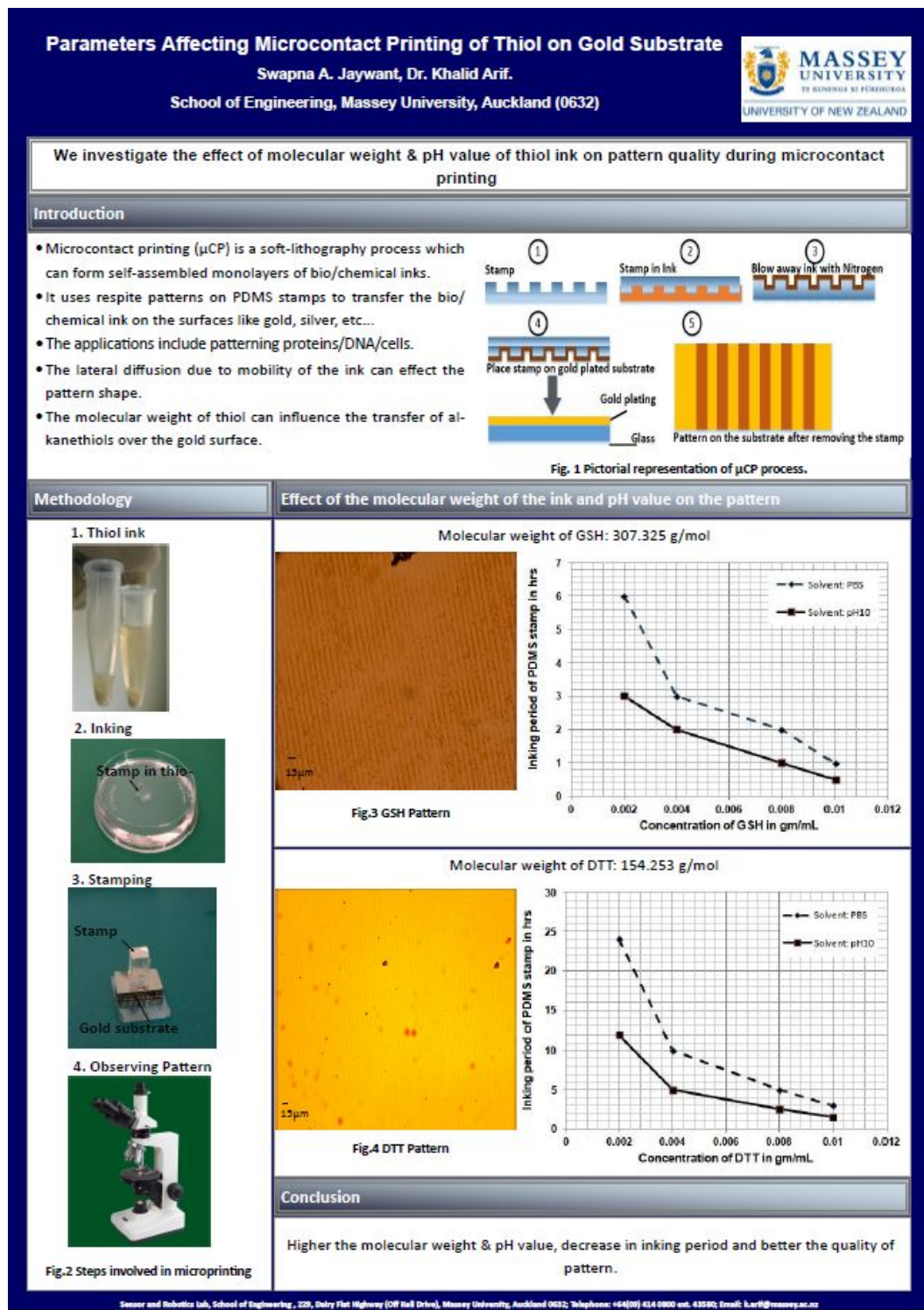


FIGURE A.7: A poster presented at the 2nd International Symposium on Advanced Materials, Manufacturing Processes and Devices (MMPD) 2019



Manufacturing and Design
New Zealand
20th - 21st May 2019, Auckland



MASSEY UNIVERSITY
TE KUNENGA KI PŪREHUROA
UNIVERSITY OF NEW ZEALAND

Microfluidic System For Water Quality Monitoring

Swapna A. Jaywant and Khalid M. Arif
Department of Mechanical and Electrical Engineering, Massey University, Auckland 0632, New Zealand

Motivation

- Water pollution is a global issue and causes a great damage to human and environmental health. There are various natural and manmade sources that pollute water. To prevent ill-effects of pollution, periodic water quality monitoring becomes a necessity.
- Generally, water pollution includes organic, inorganic and bacterial contaminants. Inorganic contamination involves metallic particles such as arsenic, lead, etc. Of these, arsenic is the major concern worldwide due to its mutagenic and carcinogenic effects on human health.
- The most common laboratory arsenic detection methods are expensive due to requirement of specific instrumentation, which limits their use in the field as portable detection systems. Whereas, the colorimetric or similar kits are portable, but are unsafe due to emission of toxic by-products.
- Hence inexpensive, portable arsenic detection system with having high throughput becomes an essential need in the water quality monitoring area.

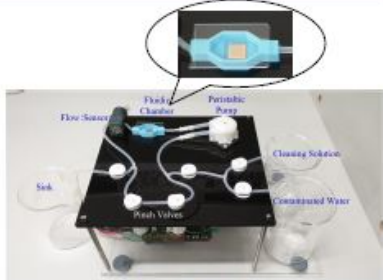


Fig. 4 Automated fluidic system

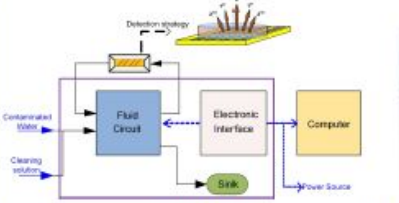


Fig. 1 System layout



Fig. 2 Fluid presence detector

Software

- Graphical user interface is where the user specifies the actions to be performed.
- Fig. 5 shows a sample GUI laid-out in a similar format as the actual system.

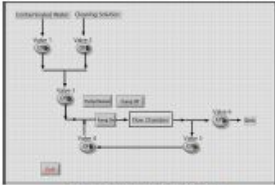


Fig. 5 Graphical user interface

Design

We have developed a fluidic system integrated with a novel sensor and off-the-shelf peristaltic pump, inert tubing, pinch valves, fluidic chamber, flow sensor, and microcontroller. The sensor makes use of unique surface modification technique to detect metallic contamination of water. Fig. 1 depicts a general schematic layout of the fluidic system while fabricated version is shown in Fig. 4. The major features of the system are:

- It automatically executes the fluid handling processes (dispensing and circulating) in a sequence defined by the user through a graphical user interface.
- The system can be programmed, hence it enables the user to execute complicated assays in a convenient fashion. Furthermore, due to its automated nature, it enables the user to precisely control the flow rate.
- The integrated sensor consists of self-assembled patterns of thiol compounds on the gold-coated glass for detection of dissolved arsenic contamination.
- The system can easily be reconfigured for different applications.

Microfluidics

- The fluidic system further can be scaled down in size by using microfluidics.
- The Fig. 6 below, explains the effect of different fluidic chambers.

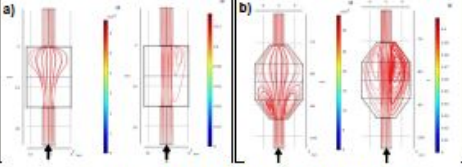


Fig. 6 Design (a) and (b) at inlet velocity of 0.01 m/s & 0.1 m/s

Features

- Fluidic chamber (Fig. 4) to hold the sensor. The sensor includes self-assembled patterns of thiol compounds on the gold coated glass. These patterns are obtained through microcontact printing as illustrated in Fig. 3.
- Expected detection limit of the sensor is 10 µg/L.
- A simple LED and photodiode based optical sensor to detect fluid presence in the tubing as shown in Fig. 2.
- System can handle 1L water.

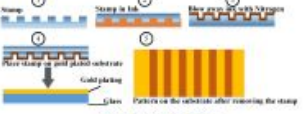


Fig. 3 Sensor designing

Result



Fig. 7 Optical images of pattern (a) Before arsenic exposure (b) After arsenic (20 µg/L) exposure (c) After arsenic (50 µg/L) exposure.

Acknowledgement

We would like to thank Massey University, School of Food and Advanced Technology for providing financial support for this project.

Sensors and Smart Systems Lab, Department of Mechanical and Electrical Engineering, 225, Dairy Flat Highway (Off Kait Drive), Massey University, Auckland 0632
Telephone: +64(0)9 414 0800 ext. 43580; Email: k.arif@massey.ac.nz

FIGURE A.8: A poster presented at Manufacturing and Design (MaD) Conference 2019

Appendix B

Design and Data Files

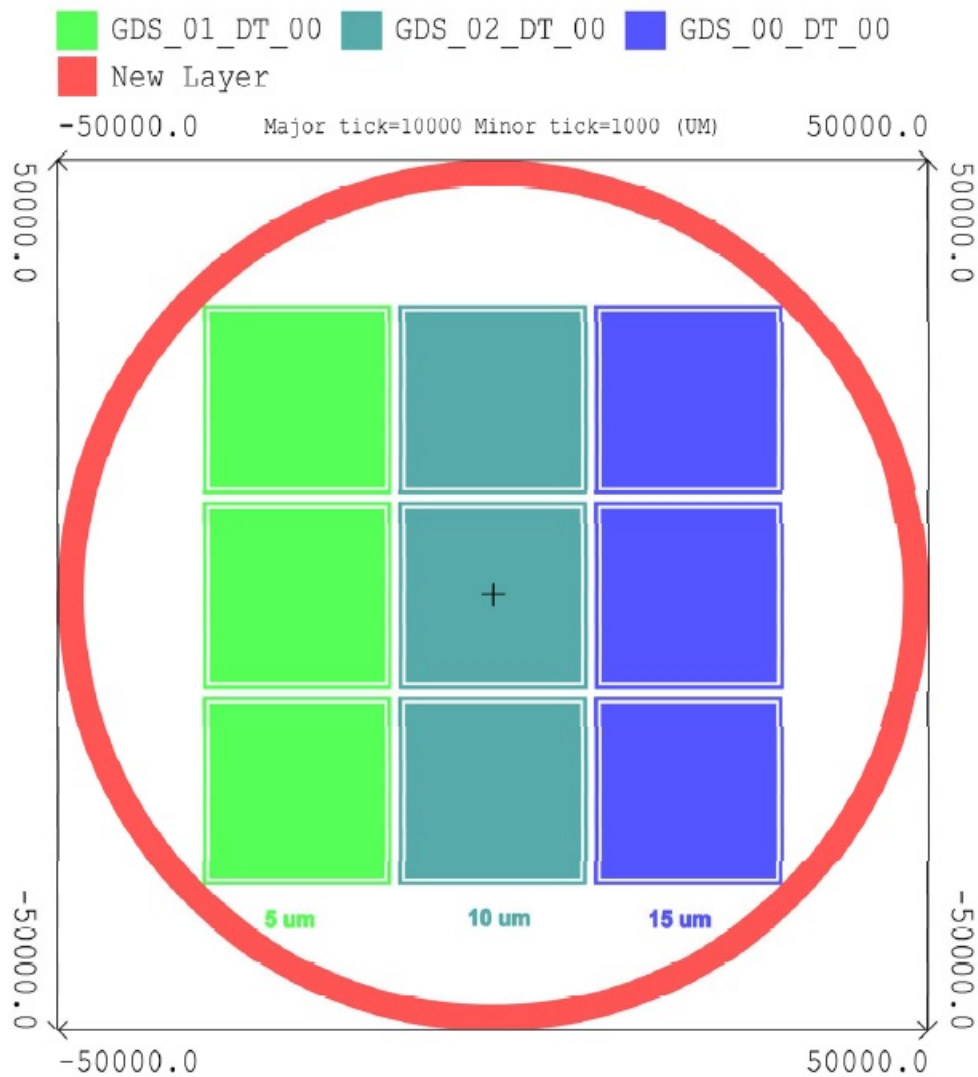


FIGURE B.1: Stamp layout on wafer.

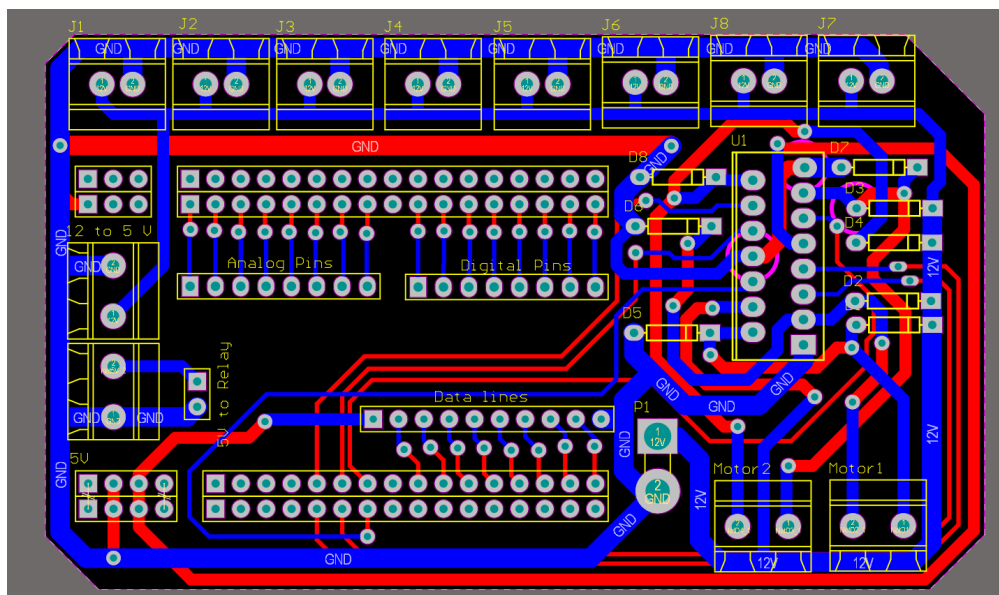


FIGURE B.2: PCB Layout

For life science research only. Not for use in diagnostic procedures.



1,4-Dithiothreitol

Cleland's reagent (threo-1,4-dimercapto-2,3-butanediol)

Cat. No. 10 197 777 001	2 g
Cat. No. 10 708 984 001	10 g
Cat. No. 11 583 786 001	25 g

Version 09

Content version: October 2018

Store at +2 to +8°C

1. What this product does

Contents

Crystalline powder

Storage and Stability

The crystalline powder is stable for at least 12 months at +2 to +8°C when stored in a glass container protected from moisture and light.

A solution of DTT in Hepes buffer (pH 7.75) is stable for one week at +2 to +8°C if the container is tightly sealed and the solution is protected from atmospheric oxygen by argon or nitrogen.

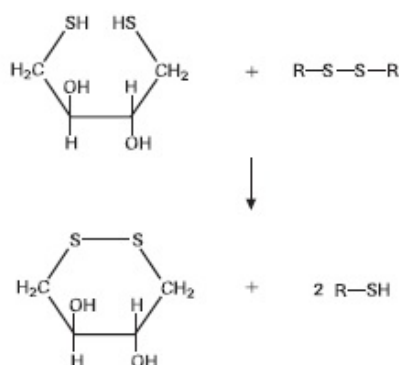
Application

- Isolation and purification of enzymes and proteins
- Measurement of activity of enzymes (reactivation of enzymes) (3, 4)
- Determination of disulfide groups in proteins and enzymes
- Characterization of proteins and enzymes

Product Characteristics

Formular	$C_4H_{10}O_2S_2$
Molecular weight	$M_r = 154.3$
Typical analysis	DTT (with Ellman's reagent) > 97%
Solubility	Gives a clear solution in water (c= 10 mg/ml)

Structure



2. Additional Information on this Product

2.1 Background Information

Dithiothreitol (DTT) is a reducing agent that is primarily used to protect free SH-groups from oxidation during the isolation of proteins or other biochemical procedures. Because of its low redox potential (-0.33 V at pH 7) DTT is able to maintain free SH-groups in the reduced state and to reduce disulfide bridges quantitatively.

DTT is therefore routinely used in all laboratories that work with enzymes or proteins. DTT is extensively used in protein chemistry and in the isolation of enzymes.

DTT is more suitable for the protection of free SH-groups than 2-mercaptoethanol because it forms an intramolecular disulfide bond on oxidation. Generation of this energetically favorable six-membered ring shifts the reaction equilibrium to the side of the oxidized dithiothreitol. As a result, a much smaller excess is needed to protect SH-groups (e.g. in proteins) (1, 2).

Further advantages of DTT are that it:

- produces a clear solution in water,
- is more stable than 2-mercaptoethanol in aqueous solution,
- has a less disagreeable odor,
- has only a slight tendency to oxidize in air.

References

- 1 Cleland, W.W. (1964) *Biochemistry* **3**, 480
- 2 Stevens, R. Stevens, L. & Price, N.C. (1983) *Biochem. Education* **11** (2), 70.
- 3 Stolle, D. & Rick, W. (1976) *J. Clin. Chem. Clin. Biochem.* **14**, 239
- 4 Nealon, A.N. & Henderson, R. (1977) *Clin. Chem.* **23** (5), 816
- 5 Rintamäki, E. *et al.*, (2000) *PNAS* **97**, 11644-11649
- 6 Baillat, D. *et al.*, (2002) *J. Biol. Chem.* **277**, 29386-29398.

SIGMA-ALDRICH®

sigma-aldrich.com

3050 Spruce Street, Saint Louis, MO 63103, USA

Website: www.sigmaaldrich.com

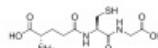
Email USA: techserv@sial.com

Outside USA: eurtechserv@sial.com

Product Specification

Product Name:
L-Glutathione reduced - $\geq 98.0\%$

Product Number: G4251
CAS Number: 70-18-8
MDL: MFCD00065939
Formula: C₁₀H₁₇N₃O₆S
Formula Weight: 307.32 g/mol
Storage Temperature: 2 - 8 °C



TEST	Specification
Appearance (Color)	White
Appearance (Form)	Powder
Solubility (Color)	Colorless
Solubility (Turbidity)	Clear
50 mg/mL, H ₂ O	
¹ H NMR Spectrum	Conforms to Structure
Purity (HPLC)	$\geq 98.0\%$
Titration with Iodine	$\geq 99\%$
Recommended Retest Period	-----
5 years	

Specification: PRD.2.ZQ5.10000014977



SPECIFICATION SHEET

www.idtdna.com

10-Jul-2019

Order No. **8746155**Ref. No. **102158000****Sequence - Ars-3**

20 nmole Ultramer® DNA Oligo, 100 bases

5'- /5Biosg/GGT AAT ACG ACT CAC TAT AGG GAG ATA CCA GCT TAT TCA ATT TTA CAG AAC AAC CAA
CGT CGC TCC GGG TAC TTC TTC ATC GAG ATA GTA AGT GCA ATC T -3'

Properties**Amount Of Oligo**T_m (50mM NaCl)*: 69.9 °C

20nmol

GC Content: 42.0%

Molecular Weight: 31,160.4

nmoles/OD260: 1.0

ug/OD260: 31.8

Ext. Coefficient: 981,200 L/(mole·cm)

Secondary Structure Calculations

Lowest folding free energy (kcal/mole): -2.18 at 25 °C

Strongest Folding T_m: 33.3 °C**Oligo Base Types**

Quantity

DNA Bases

100

Modifications and Services

Quantity

Standard Desalting

1

5' Biotin

1

Mfg. ID301279531 Labels - Peel here

**I N S T R U C T I O N S**

*Lyophilized contents may appear as either a translucent film or a white powder. This variance does not affect the quality of the oligo.

*Please centrifuge tubes prior to opening. Some of the product may have been dislodged during shipping.

*The T_m shown takes no account of Mg²⁺ and dNTP concentrations. Use the OligoAnalyzer® Program at www.idtdna.com/scitools to calculate accurate T_m for your reaction conditions.

M

Appendix C

DRC 16 V-3 Forms



DRC 16

STATEMENT OF CONTRIBUTION DOCTORATE WITH PUBLICATIONS/MANUSCRIPTS

We, the candidate and the candidate's Primary Supervisor, certify that all co-authors have consented to their work being included in the thesis and they have accepted the candidate's contribution as indicated below in the *Statement of Originality*.

Name of candidate:	Swapna Ashwin Jaywant	
Name/title of Primary Supervisor:	Dr. Khalid Arif	
Name of Research Output and full reference:		
<small>Jaywant, Swapna A., and Khalid Mahmood Arif "Study of parameters affecting microcontact printing of fibrils on gold-coated substrate." International Journal of Modern Physics B (2019): 2040040. https://doi.org/10.1142/S021797220400408</small>		
In which Chapter is the Manuscript /Published work:	3 & 5	
Please indicate:		
<ul style="list-style-type: none"> The percentage of the manuscript/Published Work that was contributed by the candidate: 	80%	
and		
<ul style="list-style-type: none"> Describe the contribution that the candidate has made to the Manuscript/Published Work: 	As the first author, Swapna has made major contribution of this published work. Swapna developed the theory, performed the experiments, analysed the results and wrote the manuscript under the supervision of Dr. Khalid Arif.	
For manuscripts intended for publication please indicate target journal:		
Candidate's Signature:	Swapna A. Jaywant	<small>Digitally signed by Swapna A. Jaywant Date: 2020.01.22 21:06:09 +13'00'</small>
Date:	22-01-2020	
Primary Supervisor's Signature:	Khalid Arif, Senior Lecturer	<small>Digitally signed by Khalid Arif, Senior Lecturer Date: 2020.01.23 11:23:48 +13'00'</small>
Date:	23/01/2020	

(This form should appear at the end of each thesis chapter/section/appendix submitted as a manuscript/ publication or collected as an appendix at the end of the thesis)



DRC 16

STATEMENT OF CONTRIBUTION DOCTORATE WITH PUBLICATIONS/MANUSCRIPTS

We, the candidate and the candidate's Primary Supervisor, certify that all co-authors have consented to their work being included in the thesis and they have accepted the candidate's contribution as indicated below in the *Statement of Originality*.

Name of candidate:	Swapna Ashwin Jaywant	
Name/title of Primary Supervisor:	Dr. Khalid Arif	
Name of Research Output and full reference:		
Jaywant, Swapna A., and Khalid Mahmood Arif. "A Comprehensive Review of Microfluidic Water Quality Monitoring Sensors." <i>Sensors</i> 19.21 (2019): 4781. https://doi.org/10.3390/s19214781		
In which Chapter is the Manuscript /Published work:	1 & 2	
Please indicate:		
<ul style="list-style-type: none"> The percentage of the manuscript/Published Work that was contributed by the candidate: 	80 %	
and		
<ul style="list-style-type: none"> Describe the contribution that the candidate has made to the Manuscript/Published Work: 		
As the first author, Swapna has made major contribution of this published work. Swapna read the papers, based on the comparison made the review, and wrote the manuscript under the supervision of Dr. Khalid Arif.		
For manuscripts intended for publication please indicate target journal:		
Candidate's Signature:	Swapna A. Jaywant	Digitally signed by Swapna A. Jaywant Date: 2020.01.22 21:06:09 +13'00'
Date:	22-1-2020	
Primary Supervisor's Signature:	Khalid Arif, Senior Lecturer	Digitally signed by Khalid Arif, Senior Lecturer Date: 2020.01.23 11:24:00 +13'00'
Date:	23/01/2020	

(This form should appear at the end of each thesis chapter/section/appendix submitted as a manuscript/ publication or collected as an appendix at the end of the thesis)



DRC 16

STATEMENT OF CONTRIBUTION DOCTORATE WITH PUBLICATIONS/MANUSCRIPTS

We, the candidate and the candidate's Primary Supervisor, certify that all co-authors have consented to their work being included in the thesis and they have accepted the candidate's contribution as indicated below in the *Statement of Originality*.

Name of candidate:	Swapna Ashwin Jaywant	
Name/title of Primary Supervisor:	Dr. Khalid Arif	
Name of Research Output and full reference:		
<small>Jaywant, Swapna A., Potgieter, J., Avci, E., and Khalid Mahmood Arif "Self-assembled Optical Diffraction Patterns for Applications in Water Quality Monitoring" Proceedings of 19th International Conference on Sensing Technology, ICST 2019.</small>		
In which Chapter is the Manuscript /Published work:	3 & 5	
Please indicate:		
<ul style="list-style-type: none"> The percentage of the manuscript/Published Work that was contributed by the candidate: 	70%	
and		
<ul style="list-style-type: none"> Describe the contribution that the candidate has made to the Manuscript/Published Work: 	As the first author, Swapna has made major contribution of this published work. Swapna developed the theory, performed the experiments, analysed the results and wrote the manuscript under the supervision of Dr. Khalid Arif.	
For manuscripts intended for publication please indicate target journal:		
Candidate's Signature:	Swapna A. Jaywant	<small>Digitally signed by Swapna A. Jaywant Date: 2020.01.22 21:06:09 +13'00'</small>
Date:	22-01-2020	
Primary Supervisor's Signature:	Khalid Arif, Senior Lecturer	<small>Digitally signed by Khalid Arif, Senior Lecturer Date: 2020.01.23 11:24:17 +13'00'</small>
Date:	23/01/2020	

(This form should appear at the end of each thesis chapter/section/appendix submitted as a manuscript/ publication or collected as an appendix at the end of the thesis)



DRC 16

STATEMENT OF CONTRIBUTION DOCTORATE WITH PUBLICATIONS/MANUSCRIPTS

We, the candidate and the candidate's Primary Supervisor, certify that all co-authors have consented to their work being included in the thesis and they have accepted the candidate's contribution as indicated below in the *Statement of Originality*.

Name of candidate:	Swapna Ashwin Jaywant	
Name/title of Primary Supervisor:	Dr. Khalid Arif	
Name of Research Output and full reference:		
Jaywant, Swapna A., Rehmani, A., and Nayak, T., and Khalid Mahmood Arif. "Fabrication and Characterization of 3D Printed Microfluidics." Proceedings of Mechatronics and Machine Vision in Practice Conference, MQVIP 2019.		
In which Chapter is the Manuscript /Published work:	4 & 5	
Please indicate:		
<ul style="list-style-type: none"> • The percentage of the manuscript/Published Work that was contributed by the candidate: 	70%	
and		
<ul style="list-style-type: none"> • Describe the contribution that the candidate has made to the Manuscript/Published Work: 		
<p>As the first author, Swapna has made major contribution of this published work. Swapna developed the theory, performed the experiments, analysed the results and wrote the manuscript under the supervision of Dr. Khalid Arif.</p>		
For manuscripts intended for publication please indicate target journal:		
Candidate's Signature:	Swapna A. Jaywant	Digitally signed by Swapna A. Jaywant Date: 2020.01.22 21:06:09 +13'00'
Date:	22-01-2020	
Primary Supervisor's Signature:	Khalid Arif, Senior Lecturer	Digitally signed by Khalid Arif, Senior Lecturer Date: 2020.01.23 11:24:38 +13'00'
Date:	23/01/2020	

(This form should appear at the end of each thesis chapter/section/appendix submitted as a manuscript/ publication or collected as an appendix at the end of the thesis)



DRC 16

STATEMENT OF CONTRIBUTION DOCTORATE WITH PUBLICATIONS/MANUSCRIPTS

We, the candidate and the candidate's Primary Supervisor, certify that all co-authors have consented to their work being included in the thesis and they have accepted the candidate's contribution as indicated below in the *Statement of Originality*.

Name of candidate:	Swapna Ashwin Jaywant	
Name/title of Primary Supervisor:	Dr. Khalid Arif	
Name of Research Output and full reference:		
Jaywant, Swapna A., Johan Poljater, and Khalid Arif. "Characterization of Low Cost Fluidic Components for Blowing Applications." 2018 5th Asia-Pacific World Congress on Computer Science and Engineering (APWC on CSE). IEEE, 2018. 10.1109/		
In which Chapter is the Manuscript /Published work:	4 & 5	
Please indicate:		
<ul style="list-style-type: none"> The percentage of the manuscript/Published Work that was contributed by the candidate: 	80%	
and		
<ul style="list-style-type: none"> Describe the contribution that the candidate has made to the Manuscript/Published Work: 		
As the first author, Swapna has made major contribution of this published work. Swapna developed the theory, performed the experiments, analysed the results and wrote the manuscript under the supervision of Dr. Khalid Arif.		
For manuscripts intended for publication please indicate target journal:		
Candidate's Signature:	Swapna A. Jaywant	Digitally signed by Swapna A. Jaywant Date: 2020.01.22 21:06:09 +13'00'
Date:	22-01-2020	
Primary Supervisor's Signature:	Khalid Arif, Senior Lecturer	Digitally signed by Khalid Arif, Senior Lecturer Date: 2020.01.23 11:23:04 +13'00'
Date:	23/01/2020	

(This form should appear at the end of each thesis chapter/section/appendix submitted as a manuscript/ publication or collected as an appendix at the end of the thesis)

References

- [1] Chaogui Chen, Jichao Zhang, Yan Du, Xiurong Yang, and Erkang Wang. Micro-fabricated on-chip integrated au–ag–au three-electrode system for in situ mercury ion determination. *Analyst*, 135(5):1010–1014, 2010.
- [2] Wooseok Jung, Am Jang, Paul L Bishop, and Chong H Ahn. A polymer lab chip sensor with microfabricated planar silver electrode for continuous and on-site heavy metal measurement. *Sensors and Actuators B: Chemical*, 155(1):145–153, 2011.
- [3] Unyoung Kim, Jessica VanderGiessen, Benjamin Demaree, Mary Reynolds, and Kyle Perricone. Development of low-cost plastic microfluidic sensors toward rapid and point-of-use detection of arsenic in drinking water for global health. In *2013 IEEE Biomedical Circuits and Systems Conference (BioCAS)*, pages 113–117. IEEE, 2013.
- [4] Kwi Nam Han, Cheng Ai Li, Minh-Phuong Ngoc Bui, Xuan-Hung Pham, Bum Sung Kim, Yong Ho Choa, Eun Kyu Lee, and Gi Hun Seong. On-chip electrochemical detection of bio/chemical molecule by nanostructures fabricated in a microfluidic channel. *Sensors and Actuators B: Chemical*, 177:472–477, 2013.
- [5] Jianjun Shi, Fan Tang, Honglong Xing, Huxiang Zheng, Bi Lianhua, and Wang Wei. Electrochemical detection of pb and cd in paper-based microfluidic devices. *Journal of the Brazilian Chemical Society*, 23(6):1124–1130, 2012.
- [6] Fernando Cortés-Salazar, Siham Beggah, Jan Roelof van der Meer, and Hubert H Girault. Electrochemical as (iii) whole-cell based biochip sensor. *Biosensors and Bioelectronics*, 47:237–242, 2013.

- [7] Manas Ranjan Gartia, Björn Braunschweig, Te-Wei Chang, Parya Moinzadeh, Barbara S Minsker, Gul Agha, Andrzej Wieckowski, Laura L Keefer, and Gang Logan Liu. The microelectronic wireless nitrate sensor network for environmental water monitoring. *Journal of Environmental Monitoring*, 14(12):3068–3075, 2012.
- [8] Antonio Calvo-López, Eva Arasa-Puig, Mar Puyol, Joan Manel Casalta, and Julián Alonso-Chamarro. Biparametric potentiometric analytical microsystem for nitrate and potassium monitoring in water recycling processes for manned space missions. *Analytica chimica acta*, 804:190–196, 2013.
- [9] Xinhao Wang, Manas Ranjan Gartia, Jing Jiang, Te-Wei Chang, Junle Qian, Yong Liu, Xiangrong Liu, and Gang Logan Liu. Audio jack based miniaturized mobile phone electrochemical sensing platform. *Sensors and Actuators B: Chemical*, 209: 677–685, 2015.
- [10] Md Azahar Ali, Yueyi Jiao, Shawana Tabassum, Yifei Wang, Huawei Jiang, and Liang Dong. Electrochemical detection of nitrate ions in soil water using graphene foam modified by tio 2 nanofibers and enzyme molecules. In *2017 19th International Conference on Solid-State Sensors, Actuators and Microsystems (TRANSDUCERS)*, pages 238–241. IEEE, 2017.
- [11] Unyoung Kim, Sarah Ghanbari, Anusha Ravikumar, John Seubert, and Silvia Figueira. Rapid, affordable, and point-of-care water monitoring via a microfluidic dna sensor and a mobile interface for global health. *IEEE journal of translational engineering in health and medicine*, 1:3700207–3700207, 2013.
- [12] Zeynep Altintas, Mete Akgun, Guzin Kokturk, and Yildiz Uludag. A fully automated microfluidic-based electrochemical sensor for real-time bacteria detection. *Biosensors and Bioelectronics*, 100:541–548, 2018.
- [13] Mallory M Mentele, Josephine Cunningham, Kirsten Koehler, John Volckens, and Charles S Henry. Microfluidic paper-based analytical device for particulate metals. *Analytical chemistry*, 84(10):4474–4480, 2012.
- [14] Hu Wang, Ya-jie Li, Jun-feng Wei, Ji-run Xu, Yun-hua Wang, and Guo-xia Zheng. based three-dimensional microfluidic device for monitoring of heavy metals with a camera cell phone. *Analytical and bioanalytical chemistry*, 406(12):2799–2807, 2014.

- [15] Peuli Nath, Ravi Kumar Arun, and Nripen Chanda. A paper based microfluidic device for the detection of arsenic using a gold nanosensor. *RSC Advances*, 4(103):59558–59561, 2014.
- [16] Mosfera Chowdury, Noosheen Walji, Md Mahmud, and Brendan MacDonald. based microfluidic device with a gold nanosensor to detect arsenic contamination of groundwater in bangladesh. *Micromachines*, 8(3):71, 2017.
- [17] Chunhui Fan, Shijiang He, Gang Liu, Lianhui Wang, and Shiping Song. A portable and power-free microfluidic device for rapid and sensitive lead (pb2+) detection. *Sensors*, 12(7):9467–9475, 2012.
- [18] Ji Qi, Bowei Li, Xinran Wang, Zhong Zhang, Zhuo Wang, Jinglong Han, and Lingxin Chen. Three-dimensional paper-based microfluidic chip device for multiplexed fluorescence detection of cu2+ and hg2+ ions based on ion imprinting technology. *Sensors and Actuators B: Chemical*, 251:224–233, 2017.
- [19] J Theytaz, Thomas Braschler, Harald Van Lintel, Philippe Renaud, E Diesel, D Merulla, and J Van der Meer. Biochip with e. coli bacteria for detection of arsenic in drinking water. *Procedia Chemistry*, 1(1):1003–1006, 2009.
- [20] Frederic Truffer, Nina Buffi, Davide Merulla, Siham Beggah, Harald Van Lintel, Philippe Renaud, Jan Roelof van der Meer, and Martial Geiser. Compact portable biosensor for arsenic detection in aqueous samples with escherichia coli bioreporter cells. *Review of Scientific Instruments*, 85(1):015120, 2014.
- [21] B Manori Jayawardane, Shen Wei, Ian D McKelvie, and Spas D Kolev. Microfluidic paper-based analytical device for the determination of nitrite and nitrate. *Analytical chemistry*, 86(15):7274–7279, 2014.
- [22] Deirdre Cogan, Cormac Fay, David Boyle, Conor Osborne, Nigel Kent, John Cleary, and Dermot Diamond. Development of a low cost microfluidic sensor for the direct determination of nitrate using chromotropic acid in natural waters. *Analytical Methods*, 7(13):5396–5405, 2015.
- [23] Yan Xiong, Cheng-Jie Wang, Tao Tao, Ming Duan, Shen-Wen Fang, and Min Zheng. A miniaturized fiber-optic colorimetric sensor for nitrite determination by coupling with a microfluidic capillary waveguide. *Analytical and bioanalytical chemistry*, 408(13):3413–3423, 2016.

- [24] Tu San Park and Jeong-Yeol Yoon. Smartphone detection of escherichia coli from field water samples on paper microfluidics. *IEEE Sensors Journal*, 15(3):1902–1907, 2014.
- [25] Onur Tokel, Umit Hakan Yildiz, Fatih Inci, Naside Gozde Durmus, Okan Oner Ekiz, Burak Turker, Can Cetin, Shruthi Rao, Kaushik Sridhar, Nalini Natarajan, et al. Portable microfluidic integrated plasmonic platform for pathogen detection. *Scientific reports*, 5:9152, 2015.
- [26] Mina Kim, Hyun-Ju Um, SunBaek Bang, Sang-Hee Lee, Suk-Jung Oh, Ji-Hye Han, Kyoung-Woong Kim, Jiho Min, and Yang-Hoon Kim. Arsenic removal from vietnamese groundwater using the arsenic-binding dna aptamer. *Environmental science & technology*, 43(24):9335–9340, 2009.
- [27] M. I. Kilani, Y. S. Haik, S. Y. Jaw, and C. J. Chen. Numerical simulation of flow in a screw-type blood pump. *Journal of Visualization*, 8(1):33–40, 2005. ISSN 1875-8975. doi: 10.1007/BF03181600. URL <https://doi.org/10.1007/BF03181600>.
- [28] Mohammad Haji Gholizadeh, Assefa M. Melesse, and Lakshmi Reddi. Water quality assessment and apportionment of pollution sources using apcs-mlr and pmf receptor modeling techniques in three major rivers of south florida. *The Science of the Total Environment*, page 1552, 2016. ISSN 0048-9697.
- [29] Nancy Diersing. *Water Quality: Frequently Asked Questions*. Florida Brooks National Marine Sanctuary, Key West, FL, 2009.
- [30] Arif Jan, Mudsser Azam, Kehkashan Siddiqui, Arif Ali, Inho Choi, and Qazi Haq. Heavy metals and human health: mechanistic insight into toxicity and counter defense system of antioxidants. *International journal of molecular sciences*, 16(12):29592–29630, 2015.
- [31] Hong Yao, Xin Qian, Hong Yin, Hailong Gao, and Yulei Wang. Regional risk assessment for point source pollution based on a water quality model of the taiapu river, china. *Risk Analysis: An International Journal*, 35(2):265–277, 2015. ISSN 02724332.
- [32] R. L. Calderon. The epidemiology of chemical contaminants of drinking water. *Food and Chemical Toxicology*.

- [33] Shao-You Lu, Hui-Min Zhang, Samuel O. Sojinu, Gui-Hua Liu, Jian-Qing Zhang, and Hong-Gang Ni. Trace elements contamination and human health risk assessment in drinking water from shenzhen, china. *Environmental Monitoring And Assessment*, 187(1):4220–4220, 2015. ISSN 1573-2959.
- [34] Memet Varol. Assessment of heavy metal contamination in sediments of the tigris river (turkey) using pollution indices and multivariate statistical techniques. *Journal of Hazardous Materials*, 195:355–364, 2011.
- [35] Md Saiful Islam, Md Kawser Ahmed, Mohammad Raknuzzaman, Md Habibullah-Al-Mamun, and Muhammad Kamrul Islam. Heavy metal pollution in surface water and sediment: a preliminary assessment of an urban river in a developing country. *Ecological indicators*, 48:282–291, 2015.
- [36] Hyun Soo Kim, Yeo Jin Kim, and Young Rok Seo. An overview of carcinogenic heavy metal: molecular toxicity mechanism and prevention. *Journal of cancer prevention*, 20(4):232, 2015.
- [37] Jin-Yong Chung, Seung-Do Yu, and Young-Seoub Hong. Environmental source of arsenic exposure. *Journal of preventive medicine and public health*, 47(5):253, 2014.
- [38] Zhong-Gang Liu and Xing-Jiu Huang. Voltammetric determination of inorganic arsenic. *TrAC Trends in Analytical Chemistry*, 60:25–35, 2014. ISSN 01659936.
- [39] Kevin A Francesconi and Doris Kuehnelt. Determination of arsenic species: a critical review of methods and applications, 20002003. *Analyst*, 129(5):373–395, 2004.
- [40] Orhan Gunduz, Celalettin Simsek, and Altug Hasozbek. Arsenic pollution in the groundwater of simav plain, turkey: its impact on water quality and human health. *Water, air, and soil pollution*, 205(1-4):43, 2010.
- [41] P Bhattacharya, AC Samal, J Majumdar, and SC Santra. Arsenic contamination in rice, wheat, pulses, and vegetables: a study in an arsenic affected area of west bengal, india. *Water, Air, & Soil Pollution*, 213(1-4):3–13, 2010.

- [42] Kongkea Phan, Suthipong Sthiannopkao, Kyoung-Woong Kim, Ming Hung Wong, Vibol Sao, Jamal Hisham Hashim, Mohamed Salleh Mohamed Yasin, and Syed Mohamed Aljunid. Health risk assessment of inorganic arsenic intake of cambodia residents through groundwater drinking pathway. *Water Research*, 44(19):5777–5788, 2010.
- [43] Michael F Hughes. Arsenic toxicity and potential mechanisms of action. *Toxicology letters*, 133(1):1–16, 2002. ISSN 0378-4274.
- [44] Paul B Tchounwou, Jose A Centeno, and Anita K Patlolla. Arsenic toxicity, mutagenesis, and carcinogenesis a health risk assessment and management approach. *Molecular and cellular biochemistry*, 255(1-2):47–55, 2004. ISSN 0300-8177.
- [45] Ning-Xin Wang, Yue-Yue Liu, Zhong-Bo Wei, Liu-Yan Yang, and Ai-Jun Miao. Waterborne and dietborne toxicity of inorganic arsenic to the freshwater zooplankton daphnia magna. *Environmental science and technology*, 52(15):8912–8919, 2018. ISSN 0013-936X.
- [46] Yaguang Fan, Yong Jiang, Ping Hu, Runsheng Chang, Shuxiang Yao, Bin Wang, Xuebing Li, Qinghua Zhou, and Youlin Qiao. Modification of association between prior lung disease and lung cancer by inhaled arsenic: A prospective occupational-based cohort study in yunnan, china. *Journal of Exposure Science and Environmental Epidemiology*, 26(5):464, 2016.
- [47] Robin A Bernhoft. Cadmium toxicity and treatment. *The Scientific World Journal*, 2013, 2013.
- [48] Monisha Jaishankar, Tenzin Tseten, Naresh Anbalagan, Blessy B Mathew, and Krishnamurthy N Beeregowda. Toxicity, mechanism and health effects of some heavy metals. *Interdisciplinary toxicology*, 7(2):60–72, 2014.
- [49] Jean-Marc Moulis and Frank Thévenod. New perspectives in cadmium toxicity: an introduction, 2010.
- [50] ANGSHUMAN Sarkar, GEETHANJALI Ravindran, and VISHNUVARDHAN Krishnamurthy. A brief review on the effect of cadmium toxicity: from cellular to organ level. *Int J Biotechnol Res*, 3(1):17–36, 2013.

- [51] Monalisa Mohanty and Hemanta Kumar Patra. Attenuation of chromium toxicity by bioremediation technology. In *Reviews of Environmental Contamination and Toxicology Volume 210*, pages 1–34. Springer, 2011.
- [52] Shakhawat Chowdhury, M. A. Jafar Mazumder, Omar Al-Attas, and Tahir Husain. Heavy metals in drinking water: Occurrences, implications, and future needs in developing countries. *Science of the Total Environment*, 569:476–488, 2016. ISSN 00489697.
- [53] ML Dotaniya, JK Thakur, VD Meena, DK Jajoria, and Gopal Rathor. Chromium pollution: a threat to environment-a review. *Agricultural Reviews*, 35(2), 2014.
- [54] Ab Latif Wani, Anjum Ara, and Jawed Ahmad Usmani. Lead toxicity: a review. *Interdisciplinary toxicology*, 8(2):55–64, 2015.
- [55] Bruce S Gillis, Zarema Arbieva, and Igor M Gavin. Analysis of lead toxicity in human cells. *BMC genomics*, 13(1):344, 2012.
- [56] Alessia Carocci, Nicola Rovito, Maria Stefania Sinicropi, and Giuseppe Genchi. Mercury toxicity and neurodegenerative effects. In *Reviews of environmental contamination and toxicology*, pages 1–18. Springer, 2014.
- [57] Mark C Houston. Role of mercury toxicity in hypertension, cardiovascular disease, and stroke. *The Journal of Clinical Hypertension*, 13(8):621–627, 2011.
- [58] Lygia Therese Budnik and Ludwine Casteleyn. Mercury pollution in modern times and its socio-medical consequences. *Science of The Total Environment*, 654:720–734, 2019.
- [59] Md Eshrat E Alahi and Subhas Chandra Mukhopadhyay. Detection methods of nitrate in water: a review. *Sensors and Actuators A: Physical*, 2018.
- [60] Helen Bridle, Brian Miller, and Marc PY Desmulliez. Application of microfluidics in waterborne pathogen monitoring: A review. *water research*, 55:256–271, 2014.
- [61] Anju Agrawal, Ravi S Pandey, and Bechan Sharma. Water pollution with special reference to pesticide contamination in india. *Journal of Water Resource and Protection*, 2(05):432, 2010.

- [62] Daniel J Sobota, Jana E Compton, Michelle L McCrackin, and Shweta Singh. Cost of reactive nitrogen release from human activities to the environment in the united states. *Environmental Research Letters*, 10(2):025006, 2015.
- [63] Larry J Puckett. Identifying the major sources of nutrient water pollution. *Environmental Science & Technology*, 29(9):408A–414A, 1995.
- [64] Katia Fajerweg, Vaiata Ynam, Bruno Chaudret, Véronique Garçon, Danièle Thouron, and Maurice Comtat. An original nitrate sensor based on silver nanoparticles electrodeposited on a gold electrode. *Electrochemistry Communications*, 12(10):1439–1441, 2010.
- [65] Hasan Bagheri, Ali Hajian, Mosayeb Rezaei, and Ali Shirzadmehr. Composite of cu metal nanoparticles-multiwall carbon nanotubes-reduced graphene oxide as a novel and high performance platform of the electrochemical sensor for simultaneous determination of nitrite and nitrate. *Journal of hazardous materials*, 324:762–772, 2017.
- [66] Micaela Badea, Aziz Amine, Giuseppe Palleschi, Danila Moscone, Giulia Volpe, and Antonella Curulli. New electrochemical sensors for detection of nitrites and nitrates. *Journal of Electroanalytical Chemistry*, 509(1):66–72, 2001.
- [67] Jie Chen, Hao Wu, Hui Qian, and Yanyan Gao. Assessing nitrate and fluoride contaminants in drinking water and their health risk of rural residents living in a semiarid region of northwest china. *Exposure and Health*, 9(3):183–195, 2017.
- [68] Briseis A Kilfoy, Yawei Zhang, Yikyung Park, Theodore R Holford, Arthur Schatzkin, Albert Hollenbeck, and Mary H Ward. Dietary nitrate and nitrite and the risk of thyroid cancer in the nih-aarp diet and health study. *International journal of cancer*, 129(1):160–172, 2011.
- [69] Pramod K Pandey, Philip H Kass, Michelle L Soupir, Sagor Biswas, and Vijay P Singh. Contamination of water resources by pathogenic bacteria. *Amb Express*, 4(1):51, 2014.
- [70] Pierre Payment and Annie Locas. Pathogens in water: value and limits of correlation with microbial indicators. *Groundwater*, 49(1):4–11, 2011.

- [71] Nicholas J Ashbolt. Microbial contamination of drinking water and human health from community water systems. *Current environmental health reports*, 2(1):95–106, 2015.
- [72] Erin K Lipp, Samuel A Farrah, and Joan B Rose. Assessment and impact of microbial fecal pollution and human enteric pathogens in a coastal community. *Marine pollution bulletin*, 42(4):286–293, 2001.
- [73] João PS Cabral. Water microbiology. bacterial pathogens and water. *International journal of environmental research and public health*, 7(10):3657–3703, 2010.
- [74] René P Schwarzenbach, Thomas Egli, Thomas B Hofstetter, Urs Von Gunten, and Bernhard Wehrli. Global water pollution and human health. *Annual Review of Environment and Resources*, 35:109–136, 2010.
- [75] Satoshi Ishii and Michael J Sadowsky. Escherichia coli in the environment: implications for water quality and human health. *Microbes and Environments*, 23(2):101–108, 2008. ISSN 1342-6311.
- [76] M^a Figueras and Juan J Borrego. New perspectives in monitoring drinking water microbial quality. *International journal of environmental research and public health*, 7(12):4179–4202, 2010.
- [77] Paul B Tchounwou, Clement G Yedjou, Anita K Patlolla, and Dwayne J Sutton. Heavy metal toxicity and the environment. In *Molecular, clinical and environmental toxicology*, pages 133–164. Springer, 2012.
- [78] Manoj Kumar and Avinash Puri. A review of permissible limits of drinking water. *Indian Journal of Occupational and Environmental Medicine*, 16(1):40–44, 2012. ISSN 0973-2284 1998-3670.
- [79] Stephen M Testa, J Guertin, JA Jacobs, and CP Avakian. *Sources of chromium contamination in soil and groundwater*. CRC Press: Boca Raton, FL, pp143-164, 2004.
- [80] M Cempel and G Nikel. Nickel: A review of its sources and environmental toxicology. *Polish Journal of Environmental Studies*, 15(3), 2006.
- [81] Frederick A Armah, Samuel Obiri, David O Yawson, Edward E Onumah, Genesis T Yengoh, Ernest KA Afrifa, and Justice O Odoi. Anthropogenic sources

- and environmentally relevant concentrations of heavy metals in surface water of a mining district in Ghana: a multivariate statistical approach. *Journal of Environmental Science and Health Part A*, 45(13):1804–1813, 2010.
- [82] Kamala Kanta Borah, Bhabajit Bhuyan, and Hari Prasad Sarma. Lead, arsenic, fluoride, and iron contamination of drinking water in the tea garden belt of Darrang district, Assam, India. *Environmental Monitoring and Assessment*, 169(1-4):347–352, 2010.
- [83] Ting Yang, Xiao-Xiao Zhang, Jian-Yu Yang, Yi-Ting Wang, and Ming-Li Chen. Screening arsenic (III)-binding peptide for colorimetric detection of arsenic (III) based on the peptide induced aggregation of gold nanoparticles. *Talanta*, 177: 212–216, 2018.
- [84] Nguyen Le Thao Nguyen, Chan Yeong Park, Jong Pil Park, Suresh Kumar Kailasa, and Tae Jung Park. Synergistic molecular assembly of an aptamer and surfactant on gold nanoparticles for the colorimetric detection of trace levels of As^{3+} ions in real samples. *New Journal of Chemistry*, 42(14):11530–11538, 2018.
- [85] Koji Matsunaga, Yu Okuyama, Reiko Hirano, Satoshi Okabe, Masahiro Takahashi, and Hisashi Satoh. Development of a simple analytical method to determine arsenite using a DNA aptamer and gold nanoparticles. *Chemosphere*, 224:538–543, 2019.
- [86] Ali A Ensafi, N Kazemifard, and B Rezaei. A simple and sensitive fluorimetric aptasensor for the ultrasensitive detection of arsenic (III) based on cysteamine stabilized CdTe/ZnS quantum dots aggregation. *Biosensors and Bioelectronics*, 77: 499–504, 2016.
- [87] K Sekabira, H Oryem Origa, TA Basamba, G Mutumba, and E Kakudidi. Assessment of heavy metal pollution in the urban stream sediments and its tributaries. *International journal of environmental science & technology*, 7(3):435–446, 2010.
- [88] Am Jang, Zhiwei Zou, Kang Kug Lee, Chong H Ahn, and Paul L Bishop. State-of-the-art lab chip sensors for environmental water monitoring. *Measurement Science and Technology*, 22(3):032001, 2011.
- [89] Michael Weller. Immunoassays and biosensors for the detection of cyanobacterial toxins in water. *Sensors*, 13(11):15085–15112, 2013.

- [90] Warish Ahmed, Bridie Hughes, and Valerie Harwood. Current status of marker genes of bacteroides and related taxa for identifying sewage pollution in environmental waters. *Water*, 8(6):231, 2016.
- [91] David Kuczynski. Occurrence of pathogenic bacteria in surface water of an urban river in argentina (reconquista river, buenos aires). *Int. J. Aquat. Science*, 7(1):30–38, 2016.
- [92] Christiane Schreiber, Andrea Rechenburg, Esther Rind, and Thomas Kistemann. The impact of land use on microbial surface water pollution. *International journal of hygiene and environmental health*, 218(2):181–187, 2015.
- [93] Junjie Ma, Fansheng Meng, Yuexi Zhou, Yeyao Wang, and Ping Shi. Distributed water pollution source localization with mobile uv-visible spectrometer probes in wireless sensor networks. *Sensors*, 18(2):606, 2018.
- [94] Fourth Edition. Guidelines for drinking-water quality. *WHO chronicle*, 38(4):104–8, 2011.
- [95] Ke Yang, Hagit Peretz-Soroka, Yong Liu, and Francis Lin. Novel developments in mobile sensing based on the integration of microfluidic devices and smartphones. *Lab on a Chip*, 16(6):943–958, 2016.
- [96] George M Whitesides. The origins and the future of microfluidics. *Nature*, 442(7101):368, 2006.
- [97] Josiane P Lafleur, Alexander Joensson, Silja Senkbeil, and Joerg P Kutter. Recent advances in lab-on-a-chip for biosensing applications. *Biosensors and Bioelectronics*, 76:213–233, 2016.
- [98] Songzi Kou, Danhui Cheng, Fei Sun, and I-Ming Hsing. Microfluidics and microbial engineering. *Lab on a Chip*, 16(3):432–446, 2016.
- [99] Zerong Liao, Jianfeng Wang, Pengjie Zhang, Yang Zhang, Yunfei Miao, Shimeng Gao, Yulin Deng, and Lina Geng. Recent advances in microfluidic chip integrated electronic biosensors for multiplexed detection. *Biosensors and Bioelectronics*, 2018.
- [100] Sabo Wada Dutse and Nor Azah Yusof. Microfluidics-based lab-on-chip systems in dna-based biosensing: an overview. *Sensors*, 11(6):5754–5768, 2011.

- [101] Jun Zhang, Sheng Yan, Dan Yuan, Gursel Alici, Nam-Trung Nguyen, Majid Ebrahimi Warkiani, and Weihua Li. Fundamentals and applications of inertial microfluidics: a review. *Lab on a Chip*, 16(1):10–34, 2016.
- [102] Ehsan Samiei, Maryam Tabrizian, and Mina Hoorfar. A review of digital microfluidics as portable platforms for lab-on a-chip applications. *Lab on a Chip*, 16(13):2376–2396, 2016.
- [103] FAN Yi-Qiang, WANG Hong-Liang, GAO Ke-Xin, LIU Jing-Ji, CHAI Dong-Ping, and Ya-Jun ZHANG. Applications of modular microfluidics technology. *Chinese Journal of Analytical Chemistry*, 46(12):1863–1871, 2018.
- [104] Helene Andersson and Albert Van den Berg. Microfluidic devices for cellomics: a review. *Sensors and actuators B: Chemical*, 92(3):315–325, 2003.
- [105] Guansheng Du, Qun Fang, and Jaap MJ den Toonder. Microfluidics for cell-based high throughput screening platforms a review. *Analytica chimica acta*, 903:36–50, 2016.
- [106] Laia Reverté, Beatriz Prieto-Simón, and Mònica Campàs. New advances in electrochemical biosensors for the detection of toxins: Nanomaterials, magnetic beads and microfluidics systems. a review. *Analytica chimica acta*, 908:8–21, 2016.
- [107] Samaneh Mashaghi, Alireza Abbaspourrad, David A Weitz, and Antoine M van Oijen. Droplet microfluidics: A tool for biology, chemistry and nanotechnology. *TrAC Trends in Analytical Chemistry*, 82:118–125, 2016.
- [108] Gina S Fiorini and Daniel T Chiu. Disposable microfluidic devices: fabrication, function, and application. *BioTechniques*, 38(3):429–446, 2005.
- [109] Kangning Ren, Jianhua Zhou, and Hongkai Wu. Materials for microfluidic chip fabrication. *Accounts of chemical research*, 46(11):2396–2406, 2013.
- [110] Nirveek Bhattacharjee, Arturo Urrios, Shawn Kang, and Albert Folch. The upcoming 3d-printing revolution in microfluidics. *Lab on a Chip*, 16(10):1720–1742, 2016.
- [111] Kyoung G Lee, Kyun Joo Park, Seunghwan Seok, Sujeong Shin, Jung Youn Park, Yun Seok Heo, Seok Jae Lee, Tae Jae Lee, et al. 3d printed modules for integrated microfluidic devices. *Rsc Advances*, 4(62):32876–32880, 2014.

- [112] Yuangen Wu, Le Liu, Shenshan Zhan, Faze Wang, and Pei Zhou. Ultrasensitive aptamer biosensor for arsenic (iii) detection in aqueous solution based on surfactant-induced aggregation of gold nanoparticles. *Analyst*, 137(18):4171–4178, 2012.
- [113] Alireza Ahmadian Yazdi, Adam Popma, William Wong, Tammy Nguyen, Yayue Pan, and Jie Xu. 3d printing: an emerging tool for novel microfluidics and lab-on-a-chip applications. *Microfluidics and Nanofluidics*, 20(3):50, 2016.
- [114] Sidra Waheed, Joan M Cabot, Niall P Macdonald, Trevor Lewis, Rosanne M Guijt, Brett Paull, and Michael C Breadmore. 3d printed microfluidic devices: enablers and barriers. *Lab on a Chip*, 16(11):1993–2013, 2016.
- [115] Rahul Antony, MS Giri Nandagopal, Nidhin Sreekumar, and N Selvaraju. Detection principles and development of microfluidic sensors in the last decade. *Microsystem Technologies*, 20(6):1051–1061, 2014.
- [116] Hai-Fang Li and Jin-Ming Lin. Applications of microfluidic systems in environmental analysis. *Analytical and bioanalytical chemistry*, 393(2):555–567, 2009.
- [117] Jana C Jokerst, Jason M Emory, and Charles S Henry. Advances in microfluidics for environmental analysis. *Analyst*, 137(1):24–34, 2012.
- [118] Roberto Pol, Francisco Céspedes, David Gabriel, and Mireia Baeza. Microfluidic lab-on-a-chip platforms for environmental monitoring. *TrAC Trends in Analytical Chemistry*, 95:62–68, 2017.
- [119] Kevin Ward and Z Hugh Fan. Mixing in microfluidic devices and enhancement methods. *Journal of Micromechanics and Microengineering*, 25(9):094001, 2015.
- [120] N Scott Lynn Jr, José-Israel Martínez-López, Markéta Bocková, Pavel Adam, Victor Coello, Héctor R Siller, and Jiří Homola. Biosensing enhancement using passive mixing structures for microarray-based sensors. *Biosensors and Bioelectronics*, 54: 506–514, 2014.
- [121] J Martínez-López, Mauricio Mojica, Ciro Rodríguez, and Héctor Siller. Xurography as a rapid fabrication alternative for point-of-care devices: Assessment of passive micromixers. *Sensors*, 16(5):705, 2016.

- [122] Ming Li, Honglei Gou, Israa Al-Ogaidi, and Nianqiang Wu. Nanostructured sensors for detection of heavy metals: a review, 2013.
- [123] Aizat Azmi, Ahmad Amsyar Azman, Sallehuddin Ibrahim, and Mohd Amri Md Yunus. Techniques in advancing the capabilities of various nitrate detection methods: A review. *International Journal on Smart Sensing & Intelligent Systems*, 10(2), 2017.
- [124] Jürgen Mairhofer, Kriemhilt Roppert, and Peter Ertl. Microfluidic systems for pathogen sensing: a review. *Sensors*, 9(6):4804–4823, 2009.
- [125] Behzad Nasserri, Neda Soleimani, Navid Rabiee, Alireza Kalbasi, Mahdi Karimi, and Michael R Hamblin. Point-of-care microfluidic devices for pathogen detection. *Biosensors and Bioelectronics*, 117:112–128, 2018.
- [126] Nathan A Lacher, Kenneth E Garrison, R Scott Martin, and Susan M Lunte. Microchip capillary electrophoresis/electrochemistry. *Electrophoresis*, 22(12):2526–2536, 2001.
- [127] Jiri Kudr, Ondrej Zitka, Martin Klimanek, Radimir Vrba, and Vojtech Adam. Microfluidic electrochemical devices for pollution analysis—a review. *Sensors and Actuators B: Chemical*, 246:578–590, 2017.
- [128] Sai Guruva Reddy Avuthu, Jared Thomas Wabeke, Binu Baby Narakathu, Dinesh Maddipatla, Jaliya Samarakoon Arachchilage, Sherine O Obare, and Massood Z Atashbar. A screen printed phenanthroline-based flexible electrochemical sensor for selective detection of toxic heavy metal ions. *IEEE Sensors Journal*, 16(24):8678–8684, 2016.
- [129] Yang Lin, Dmitry Gritsenko, Shaolong Feng, Yi Chen Teh, Xiaonan Lu, and Jie Xu. Detection of heavy metal by paper-based microfluidics. *Biosensors and Bioelectronics*, 83:256–266, 2016.
- [130] Lori Busa, Saeed Mohammadi, Masatoshi Maeki, Akihiko Ishida, Hirofumi Tani, and Manabu Tokeshi. Advances in microfluidic paper-based analytical devices for food and water analysis. *Micromachines*, 7(5):86, 2016.

- [131] Piotr Lisowski and Paweł K Zarzycki. Microfluidic paper-based analytical devices (μ pads) and micro total analysis systems (μ tas): development, applications and future trends. *Chromatographia*, 76(19-20):1201–1214, 2013.
- [132] Lung-Ming Fu and Yao-Nan Wang. Detection methods and applications of microfluidic paper-based analytical devices. *TrAC Trends in Analytical Chemistry*, 2018.
- [133] Cody Carrell, Alyssa Kava, Michael Nguyen, Ruth Menger, Zarina Munshi, Zachary Call, Mark Nussbaum, and Charles Henry. Beyond the lateral flow assay: A review of paper-based microfluidics. *Microelectronic Engineering*, 206:45–54, 2019.
- [134] Tugce Akyazi, Lourdes Basabe-Desmots, and Fernando Benito-Lopez. Review on microfluidic paper-based analytical devices towards commercialisation. *Analytica chimica acta*, 1001:1–17, 2018.
- [135] Maria Cuartero, Gaston A Crespo, and Eric Bakker. Tandem electrochemical desalination–potentiometric nitrate sensing for seawater analysis. *Analytical chemistry*, 87(16):8084–8089, 2015.
- [136] Xiang Li, Karen Scida, and Richard M Crooks. Detection of hepatitis b virus dna with a paper electrochemical sensor. *Analytical chemistry*, 87(17):9009–9015, 2015.
- [137] Myounggon Kim, Taekeon Jung, Youngjin Kim, Changgeun Lee, Kyungchul Woo, Jae Hun Seol, and Sung Yang. A microfluidic device for label-free detection of escherichia coli in drinking water using positive dielectrophoretic focusing, capturing, and impedance measurement. *Biosensors and Bioelectronics*, 74:1011–1015, 2015.
- [138] Jing Jiang, Xinhao Wang, Ran Chao, Yukun Ren, Chengpeng Hu, Zhida Xu, and Gang Logan Liu. Smartphone based portable bacteria pre-concentrating microfluidic sensor and impedance sensing system. *Sensors and Actuators B: Chemical*, 193:653–659, 2014.
- [139] Casper Clausen, Maria Dimaki, Christian Bertelsen, Gustav Skands, Romen Rodriguez-Trujillo, Joachim Thomsen, and Winnie Svendsen. Bacteria detection and differentiation using impedance flow cytometry. *Sensors*, 18(10):3496, 2018.

- [140] MM Maw, JS Wang, KZ Yu, YJ Wang, BW Dai, XD Wu, and XX Pan. An examination of the validity of mrps method for the detection of label-free e. coli and enterococci in ships ballast water. In *IOP Conference Series: Earth and Environmental Science*, volume 171, page 012032. IOP Publishing, 2018.
- [141] Shibajyoti Ghosh Dastider, Syed Barizuddin, Nuh S Yuksek, Majed Dweik, and Mahmoud F Almasri. Efficient and rapid detection of salmonella using microfluidic impedance based sensing. *Journal of Sensors*, 2015, 2015.
- [142] Bio nano consulting product page, . Available online: <http://www.bio-nano-consulting.com/product-developmentdrinksafe> (accessed on Oct 22, 2019).
- [143] Palmsense compact electrochemical interfaces italsens is-c page, . Available online: <https://www.palmsens.com/product/italsens-is-c/> (accessed on Oct 22, 2019).
- [144] gtq silicon technologies for sensing services and product page, . Available online: <http://gtq.imb-cnm.csic.es/en/services-and-products/technology-offer/fv00620231869> (accessed on Oct 22, 2019).
- [145] Mediray+ ion selective electrodes page, . Available online: <https://www.mediray.co.nz/laboratory/shop/the-hanna-range/ion-selective-electrodes-ises/ion-selective-electrodes/nitrate-combination-ion-selective-electrode-hi4113/> (accessed on Oct 22, 2019).
- [146] xylem let's solve water product page, . Available online: <https://www.xylemanalytics.com/en/general-product/id-151/ISE-combination-sensor-for-ammonium-and-nitrate---WTW> (accessed on Oct 22, 2019).
- [147] Vernier nitrate ion-selective electrode page, . Available online: <https://www.vernier.com/products/sensors/ion-selective-electrodes/labquest-ise/no3-bta/> (accessed on Oct 22, 2019).
- [148] Hanna instruments nitrate combination ion selective electrode page, . Available online: <https://hannainst.com/>

- [hi4113-nitrate-combination-ion-selective-electrode.html](#) (accessed on Oct 22, 2019).
- [149] Hosein Khoshsafar, Hasan Bagheri, Mosayeb Rezaei, Ali Shirzadmehr, Ali Hajian, and Zahra Sepehri. Magnetic carbon paste electrode modified with a high performance composite based on molecularly imprinted carbon nanotubes for sensitive determination of levofloxacin. *Journal of The Electrochemical Society*, 163(8):B422–B427, 2016.
- [150] Edward P Randviir and Craig E Banks. Electrochemical impedance spectroscopy: an overview of bioanalytical applications. *Analytical Methods*, 5(5):1098–1115, 2013.
- [151] Douglas A Boehm, Philip A Gottlieb, and Susan Z Hua. On-chip microfluidic biosensor for bacterial detection and identification. *Sensors and Actuators B: Chemical*, 126(2):508–514, 2007.
- [152] Tao Sun and Hywel Morgan. Single-cell microfluidic impedance cytometry: a review. *Microfluidics and Nanofluidics*, 8(4):423–443, 2010.
- [153] George Luka, Ali Ahmadi, Homayoun Najjaran, Evangelyn Alocilja, Maria DeRosa, Kirsten Wolthers, Ahmed Malki, Hassan Aziz, Asmaa Althani, and Mina Hoorfar. Microfluidics integrated biosensors: A leading technology towards lab-on-a-chip and sensing applications. *Sensors*, 15(12):30011–30031, 2015.
- [154] Weiwei Chen, Xueen Fang, Hua Li, Hongmei Cao, and Jilie Kong. A simple paper-based colorimetric device for rapid mercury (ii) assay. *Scientific reports*, 6:31948, 2016.
- [155] Attila Bonyar, Péter Nagy, Viktor Mayer, András Vitéz, András Gerecs, Hunor Sántha, and Gábor Harsányi. A colorimetry based, semi-automated portable sensor device for the detection of arsenic in drinking water. *Sensors and Actuators B: Chemical*, 251:1042–1049, 2017.
- [156] Nan Qi, Bowei Li, Huiyan You, Wei Zhang, Longwen Fu, Yunqing Wang, and Lingxin Chen. Surface-enhanced raman scattering on a zigzag microfluidic chip: towards high-sensitivity detection of as (iii) ions. *Analytical Methods*, 6(12):4077–4082, 2014.

- [157] Waraporn Som-Aum, Haifang Li, Jiangjiang Liu, and Jin-Ming Lin. Determination of arsenate by sorption pre-concentration on polystyrene beads packed in a microfluidic device with chemiluminescence detection. *Analyst*, 133(9):1169–1175, 2008.
- [158] Mohammad Khanfar, Wisam Al-Faqheri, Alaaldeen Al-Halhouli, et al. Low cost lab on chip for the colorimetric detection of nitrate in mineral water products. *Sensors*, 17(10):2345, 2017.
- [159] Alexander D Beaton, Christopher L Cardwell, Rupert S Thomas, Vincent J Sieben, François-Eric Legiret, Edward M Waugh, Peter J Statham, Matthew C Mowlem, and Hywel Morgan. Lab-on-chip measurement of nitrate and nitrite for in situ analysis of natural waters. *Environmental science & technology*, 46(17):9548–9556, 2012.
- [160] Alexander G Vincent, Robin W Pascal, Alexander D Beaton, John Walk, Joanne E Hopkins, E Malcolm S Woodward, Matthew Mowlem, and Maeve C Lohan. Nitrate drawdown during a shelf sea spring bloom revealed using a novel microfluidic in situ chemical sensor deployed within an autonomous underwater glider. *Marine Chemistry*, 205:29–36, 2018.
- [161] Udara Dharmasiri, Małgorzata A Witek, Andre A Adams, John K Osiri, Mateusz L Hupert, Thomas S Bianchi, Daniel L Roelke, and Steven A Soper. Enrichment and detection of escherichia coli o157: H7 from water samples using an antibody modified microfluidic chip. *Analytical chemistry*, 82(7):2844–2849, 2010.
- [162] Alexander Golberg, Gregory Linshiz, Ilia Kravets, Nina Stawski, Nathan J Hillson, Martin L Yarmush, Robert S Marks, and Tania Konry. Cloud-enabled microscopy and droplet microfluidic platform for specific detection of escherichia coli in water. *PloS one*, 9(1):e86341, 2014.
- [163] Yuyuan Li, Chunsun Zhang, and Da Xing. Integrated microfluidic reverse transcription-polymerase chain reaction for rapid detection of food-or waterborne pathogenic rotavirus. *Analytical biochemistry*, 415(2):87–96, 2011.
- [164] Katherine E Boehle, Jake Gilliland, Christopher R Wheeldon, Amethyst Holder, Jaelyn A Adkins, Brian J Geiss, Elizabeth P Ryan, and Charles S Henry. Utilizing

- paper-based devices for antimicrobial-resistant bacteria detection. *Angewandte Chemie International Edition*, 56(24):6886–6890, 2017.
- [165] Anna Malec, Georgios Kokkinis, Christoph Haiden, and Ioanna Giouroudi. Biosensing system for concentration quantification of magnetically labeled e. coli in water samples. *Sensors*, 18(7):2250, 2018.
- [166] Fondriest environmental products hach arsenic test kit page, . Available online: <https://www.fondriest.com/hach-arsenic-test-kit.htm> (accessed on Oct 22, 2019).
- [167] Lulu Song, Kang Mao, Xiaodong Zhou, and Jiming Hu. A novel biosensor based on au@ ag core-shell nanoparticles for sers detection of arsenic (iii). *Talanta*, 146: 285–290, 2016.
- [168] Palintest water analysis technology arsenator digital arsenic test page, . Available online: <https://www.palintest.com/products/arsenator/> (accessed on).
- [169] P s analytical ”applying the power of atomic fluorescence” arsenic page, . Available online: <http://psanalytical.com/information/asarsenic.html> (accessed on Oct 22, 2019).
- [170] Chemsee heavy metal detectors page, . Available online: <https://www.chemsee.com/residential/heavy-metal-detector-products/> (accessed on Oct 22, 2019).
- [171] Hanna instruments nitrate-nitrogen portable photometer page, . Available online: <https://hannainst.com/hi96728-nitrate-portable-photometer.html> (accessed on Oct 22, 2019).
- [172] Hydrometrics home page, . Available online: <http://www.hydrometrics.co.nz/> (accessed on Oct 22, 2019).
- [173] Ott hydromet product page, . Available online: <https://www.ott.com/products/water-quality-2/ott-econ-2439/> (accessed on Oct 22, 2019).
- [174] Biovision incorporated pcr detection kits page, . Available online: <https://www.biovision.com/pcr-campylobacter-detection-kit.html> (accessed on Oct 22, 2019).

- [175] Xu Li, David R Ballerini, and Wei Shen. A perspective on paper-based microfluidics: Current status and future trends. *Biomicrofluidics*, 6(1):011301, 2012.
- [176] Pham Thi Kim Trang, Michael Berg, Pham Hung Viet, Nguyen Van Mui, and Jan Roelof van der Meer. Bacterial bioassay for rapid and accurate analysis of arsenic in highly variable groundwater samples. *Environmental science & technology*, 39(19):7625–7630, 2005.
- [177] Nina Buffi, Davide Merulla, Julien Beutier, Fanny Barbaud, Siham Beggah, Harald Van Lintel, Philippe Renaud, and Jan Roelof van der Meer. Development of a microfluidics biosensor for agarose-bead immobilized escherichia coli bioreporter cells for arsenite detection in aqueous samples. *Lab on a Chip*, 11(14):2369–2377, 2011.
- [178] Jodi Dutt and James Davis. Current strategies in nitrite detection and their application to field analysis. *Journal of Environmental Monitoring*, 4(3):465–471, 2002.
- [179] Jingyun Wang, Maria Rowena N Monton, Xi Zhang, Carlos DM Filipe, Robert Pelton, and John D Brennan. Hydrophobic sol–gel channel patterning strategies for paper-based microfluidics. *Lab on a Chip*, 14(4):691–695, 2014.
- [180] Juewen Liu, Zehui Cao, and Yi Lu. Functional nucleic acid sensors. *Chemical reviews*, 109(5):1948–1998, 2009.
- [181] Yu Xiang, Aijun Tong, and Yi Lu. Abasic site-containing dnzyme and aptamer for label-free fluorescent detection of pb²⁺ and adenosine with high sensitivity, selectivity, and tunable dynamic range. *Journal of the American Chemical Society*, 131(42):15352–15357, 2009.
- [182] Juewen Liu, Andrea K Brown, Xiangli Meng, Donald M Cropek, Jonathan D Istok, David B Watson, and Yi Lu. A catalytic beacon sensor for uranium with parts-per-trillion sensitivity and millionfold selectivity. *Proceedings of the National Academy of Sciences*, 104(7):2056–2061, 2007.
- [183] Yuangen Wu, Shenshan Zhan, Faze Wang, Lan He, Wenting Zhi, and Pei Zhou. Cationic polymers and aptamers mediated aggregation of gold nanoparticles for the colorimetric detection of arsenic (iii) in aqueous solution. *Chemical communications*, 48(37):4459–4461, 2012.

- [184] Yuangen Wu, Faze Wang, Shenshan Zhan, Le Liu, Yanfang Luo, and Pei Zhou. Regulation of hemin peroxidase catalytic activity by arsenic-binding aptamers for the colorimetric detection of arsenic (iii). *Rsc Advances*, 3(48):25614–25619, 2013.
- [185] Sheng Lin, Wanhe Wang, Chong Hu, Guanjun Yang, Chung-Nga Ko, Kangning Ren, Chung-Hang Leung, and Dik-Lung Ma. The application of a g-quadruplex based assay with an iridium (iii) complex to arsenic ion detection and its utilization in a microfluidic chip. *Journal of Materials Chemistry B*, 5(3):479–484, 2017.
- [186] Mar Oroval, Carmen Coll, Andrea Bernardos, María D Marcos, Ramón Martínez-Máñez, Dmitry G Shchukin, and Felix Sancenon. Selective fluorogenic sensing of as (iii) using aptamer-capped nanomaterials. *ACS applied materials & interfaces*, 9(13):11332–11336, 2017.
- [187] Jiafeng Pan, Qiong Li, Danhua Zhou, and Junhua Chen. Ultrasensitive aptamer biosensor for arsenic (iii) detection based on label-free triple-helix molecular switch and fluorescence sensing platform. *Talanta*, 189:370–376, 2018.
- [188] Karlene Vega-Figueroa, Jaime Santillan, Valerie Ortiz-Gomez, Edwin O Ortiz-Quiles, Beatriz A Quinones-Colon, David A Castilla-Casadiago, Jorge Almodovar, Marvin J Bayro, Jose A Rodríguez-Martínez, and Eduardo Nicolau. Aptamer-based impedimetric assay of arsenite in water: Interfacial properties and performance. *ACS omega*, 3(2):1437–1444, 2018.
- [189] Lin Cui, Jie Wu, and Huangxian Ju. Label-free signal-on aptasensor for sensitive electrochemical detection of arsenite. *Biosensors and Bioelectronics*, 79:861–865, 2016.
- [190] Sorour Salehi Baghbaderani and Abdollah Noorbakhsh. Novel chitosan-nafion composite for fabrication of highly sensitive impedimetric and colorimetric as (iii) aptasensor. *Biosensors and Bioelectronics*, 131:1–8, 2019.
- [191] Talifhani Mushiana, Nonhlangabezo Mabuba, Azeez O Idris, Gbenga M Peleyeju, Benjamin O Orimolade, Duduzile Nkosi, Rachel F Ajayi, and Omotayo A Arotiba. An aptasensor for arsenic on a carbon-gold bi-nanoparticle platform. *Sensing and Bio-Sensing Research*, 24:100280, 2019.

- [192] Yuangen Wu, Shenshan Zhan, Haibo Xing, Lan He, Lurong Xu, and Pei Zhou. Nanoparticles assembled by aptamers and crystal violet for arsenic (iii) detection in aqueous solution based on a resonance rayleigh scattering spectral assay. *Nanoscale*, 4(21):6841–6849, 2012.
- [193] Meiling Tang, Guiqing Wen, Aihui Liang, and Zhiliang Jiang. A simple and sensitive resonance rayleigh scattering method for determination of as (iii) using aptamer-modified nanogold as a probe. *Luminescence*, 29(6):603–608, 2014.
- [194] Ru-Ping Liang, Lu-Dan Yu, Yuan-Jun Tong, Shao-Hua Wen, Shu-Ping Cao, and Jian-Ding Qiu. An ultratrace assay of arsenite based on the synergistic quenching effect of ru (bpy) $3\ 2+$ and arsenite on the electrochemiluminescence of au-gc 3 n 4 nanosheets. *Chemical communications*, 54(99):14001–14004, 2018.
- [195] Ji Hyun An and Jyongsik Jang. A highly sensitive fet-type aptasensor using flower-like mos 2 nanospheres for real-time detection of arsenic (iii). *Nanoscale*, 9(22):7483–7492, 2017.
- [196] HUN-SOO KIM, YOUNG-MIN BAE, YOUNG-KEE KIM, BYUNG-KEUN OH, and JEONG-WOO CHOI. Antibody layer fabrication for protein chip to detect e. coli o157: H7, using microcontact printing technique. *Journal of microbiology and biotechnology*, 16(1):141–144, 2006. ISSN 1017-7825.
- [197] Tobias Kaufmann and Bart Jan Ravoo. Stamps, inks and substrates: polymers in microcontact printing. *Polymer Chemistry*, 1(4):371–387, 2010.
- [198] CY Hui, A Jagota, Yu-Yun Lin, and EJ Kramer. Constraints on microcontact printing imposed by stamp deformation. *Langmuir*, 18(4):1394–1407, 2002.
- [199] Andrs Perl, David N Reinhoudt, and Jurriaan Huskens. Microcontact printing: limitations and achievements. *Advanced Materials*, 21(22):2257–2268, 2009. ISSN 0935-9648.
- [200] Franois Bessueille, Mateu Pla-Roca, Christopher A Mills, Elena Martinez, Josep Samitier, and Abdelhamid Errachid. Submerged microcontact printing (scp): An unconventional printing technique of thiols using high aspect ratio, elastomeric stamps. *Langmuir*, 21(26):12060–12063, 2005. ISSN 0743-7463.

- [201] Yurui Xue, Xun Li, Hongbin Li, and Wenke Zhang. Quantifying thiolgold interactions towards the efficient strength control. *Nature communications*, 5:4348, 2014. ISSN 2041-1723.
- [202] Xingyu Jiang, Wenfu Zheng, Shuichi Takayama, Robert G Chapman, Ravi S Kane, and George M Whitesides. *Micro-scale patterning of cells and their environment*, pages 359–384. Elsevier, 2014.
- [203] Ashutosh Agarwal, Josue Adrian Goss, Alexander Cho, Megan Laura McCain, and Kevin Kit Parker. Microfluidic heart on a chip for higher throughput pharmacological studies. *Lab on a Chip*, 13(18):3599–3608, 2013.
- [204] Ashutosh Agarwal, Josue Adrian Goss, Alexander Cho, Megan Laura McCain, and Kevin Kit Parker. Microfluidic heart on a chip for higher throughput pharmacological studies. *Lab on a Chip*, 13(18):3599–3608, 2013.
- [205] Laurent Libioulle, Alexander Bietsch, Heinz Schmid, Bruno Michel, and Emmanuel Delamarche. Contact-inking stamps for microcontact printing of alkanethiols on gold. *Langmuir*, 15(2):300–304, 1999. ISSN 0743-7463.
- [206] Younan Xia, Xiao-Mei Zhao, and George M Whitesides. Pattern transfer: Self-assembled monolayers as ultrathin resists. *Microelectronic Engineering*, 32(1-4):255–268, 1996. ISSN 0167-9317.
- [207] J Christopher Love, Lara A Estroff, Jennah K Kriebel, Ralph G Nuzzo, and George M Whitesides. Self-assembled monolayers of thiolates on metals as a form of nanotechnology. *Chemical reviews*, 105(4):1103–1170, 2005. ISSN 0009-2665.
- [208] Colin D Bain, Joe Evall, and George M Whitesides. Formation of monolayers by the coadsorption of thiols on gold: variation in the head group, tail group, and solvent. *Journal of the American Chemical Society*, 111(18):7155–7164, 1989. ISSN 0002-7863.
- [209] Yurui Xue, Xun Li, Hongbin Li, and Wenke Zhang. Quantifying thiolgold interactions towards the efficient strength control. *Nature communications*, 5:4348, 2014. ISSN 2041-1723.
- [210] Sami Alom Ruiz and Christopher S Chen. Microcontact printing: A tool to pattern. *Soft Matter*, 3(2):168–177, 2007. ISSN 1744-6848.

- [211] AR MacDairmid, MC Gallagher, and JT Banks. Structure of dithiothreitol monolayers on au (111). *The Journal of Physical Chemistry B*, 107(36):9789–9792, 2003. ISSN 1520-6106.
- [212] Chengbei Li, Aydan Eli Baaran, and Julian F Tyson. Determination of inorganic arsenic in water by a quartz crystal microbalance. *Analytical Methods*, 5(22):6286–6291, 2013.
- [213] Hannu Hkkinen. The gold-sulfur interface at the nanoscale. *Nature chemistry*, 4(6):443–455, 2012. ISSN 1755-4330.
- [214] Maurcia B FritzenGarcia, Vincius C Zoldan, Ins Rosane WZ Oliveira, Valdir Soldi, Andr A Pasa, and Tnia B CreczynskiPasa. Peroxidase immobilized on phospholipid bilayers supported on au (111) by dtt selfassembled monolayers: Application to dopamine determination. *Biotechnology and bioengineering*, 110(2):374–382, 2013. ISSN 1097-0290.
- [215] Yurui Xue, Xun Li, Hongbin Li, and Wenke Zhang. Quantifying thiol-gold interactions towards the efficient strength control. *Nature communications*, 5:4348, 2014. ISSN 2041-1723.
- [216] Jhansi Rani Kalluri, Tahir Arbnesi, Sadia Afrin Khan, Adria Neely, Perry Candice, Birsan Varisli, Marla Washington, Sharda McAfee, Britinia Robinson, and Santanu Banerjee. Use of gold nanoparticles in a simple colorimetric and ultrasensitive dynamic light scattering assay: selective detection of arsenic in groundwater. *Angewandte Chemie*, 121(51):9848–9851, 2009. ISSN 1521-3757.
- [217] De-Hao Tsai, Tae Joon Cho, Frank W DelRio, Justin M Gorham, Jiwen Zheng, Jiaojie Tan, Michael R Zachariah, and Vincent A Hackley. Controlled formation and characterization of dithiothreitol-conjugated gold nanoparticle clusters. *Langmuir*, 30(12):3397–3405, 2014. ISSN 0743-7463.
- [218] De-Hao Tsai, Melanie P Shelton, Frank W DelRio, Sherrie Elzey, Suvajyoti Guha, Michael R Zachariah, and Vincent A Hackley. Quantifying dithiothreitol displacement of functional ligands from gold nanoparticles. *Analytical and bioanalytical chemistry*, 404(10):3015–3023, 2012. ISSN 1618-2642.
- [219] Lingxin Chen, Na Zhou, Jinhua Li, Zhaopeng Chen, Chunyang Liao, and Jiannong Chen. Synergy of glutathione, dithiothreitol and n-acetyl-l-cysteine self-assembled

- monolayers for electrochemical assay: sensitive determination of arsenic (iii) in environmental and drinking water. *Analyst*, 136(21):4526–4532, 2011.
- [220] Brian D Iverson and Suresh V Garimella. Recent advances in microscale pumping technologies: a review and evaluation. *Microfluidics and Nanofluidics*, 5(2):145–174, 2008. ISSN 1613-4982.
- [221] Majid Ebrahimi Warkiani, Lidan Wu, Andy Kah Ping Tay, and Jongyoon Han. Large-volume microfluidic cell sorting for biomedical applications. *Annual review of biomedical engineering*, 17, 2015.
- [222] Robert Gorkin, Jiwoon Park, Jonathan Siegrist, Mary Amasia, Beom Seok Lee, Jong-Myeon Park, Jintae Kim, Hanshin Kim, Marc Madou, and Yoon-Kyoung Cho. Centrifugal microfluidics for biomedical applications. *Lab on a Chip*, 10(14):1758–1773, 2010.
- [223] Nam-Trung Nguyen and Xiaoyang Huang. Miniature valveless pumps based on printed circuit board technique. *Sensors and Actuators A: Physical*, 88(2):104–111, 2001. ISSN 0924-4247.
- [224] K-P Kamper, J Dopfer, W Ehrfeld, and S Oberbeck. A self-filling low-cost membrane micropump. In *Micro Electro Mechanical Systems, 1998. MEMS 98. Proceedings., The Eleventh Annual International Workshop on*, pages 432–437. IEEE. ISBN 078034412X.
- [225] Khalid Mahmood Arif, Johan Potgieter, and Olaf Diegel. Simulation of nanoparticle enhanced diffraction grating biosensor using dda. In *Photonics (ICP), 2013 IEEE 4th International Conference on*, pages 265–267. IEEE. ISBN 1467360759.
- [226] Jin-Woo Choi, Kwang W Oh, Arum Han, C Ajith Wijayawardhana, Chad Lannes, Shekhar Bhansali, Kevin T Schlueter, William R Heineman, H Brian Halsall, and Joseph H Nevin. Development and characterization of microfluidic devices and systems for magnetic bead-based biochemical detection. *Biomedical microdevices*, 3(3):191–200, 2001. ISSN 1387-2176.
- [227] Ccero R de Lima, Sandro L Vatanabe, Andres Choi, Paulo Henrique Nakasone, Rogrio Felipe Pires, and Emlio Carlos Nelli Silva. A biomimetic piezoelectric pump: Computational and experimental characterization. *Sensors and Actuators A: Physical*, 152(1):110–118, 2009. ISSN 0924-4247.

- [228] Jin-Woo Choi, Kwang W Oh, Arum Han, C Ajith Wijayawardhana, Chad Lannes, Shekhar Bhansali, Kevin T Schlueter, William R Heineman, H Brian Halsall, and Joseph H Nevin. Development and characterization of microfluidic devices and systems for magnetic bead-based biochemical detection. *Biomedical microdevices*, 3(3):191–200, 2001. ISSN 1387-2176.
- [229] Kwang W Oh, Rong Rong, and Chong H Ahn. Miniaturization of pinch-type valves and pumps for practical micro total analysis system integration. *Journal of Micromechanics and Microengineering*, 15(12):2449, 2005. ISSN 0960-1317.
- [230] Adel Pourmand, Seyed Ali Mousavi Shaegh, Habib Badri Ghavifekr, Esmail Najafi Aghdam, Mehmet Remzi Dokmeci, Ali Khademhosseini, and Yu Shrike Zhang. Fabrication of whole-thermoplastic normally closed microvalve, micro check valve, and micropump. *Sensors and Actuators B: Chemical*, 262:625–636, 2018. ISSN 0925-4005.
- [231] Mohammad Mahdi Aeinehvand, Fatimah Ibrahim, Wisam Al-Faqheri, Karunan Joseph, and Marc J Madou. Recent advances in the development of micropumps, microvalves and micromixers and the integration of carbon electrodes on centrifugal microfluidic platforms. *International Journal of Nanotechnology*, 15(1-3): 53–68, 2018. ISSN 1475-7435.
- [232] Burak Derkus. Applying the miniaturization technologies for biosensor design. *Biosensors and Bioelectronics*, 79:901–913, 2016. ISSN 0956-5663.
- [233] Pan Gu, Ke Liu, Hong Chen, Toshikazu Nishida, and Z Hugh Fan. Chemical-assisted bonding of thermoplastics/elastomer for fabricating microfluidic valves. *Analytical chemistry*, 83(1):446–452, 2010. ISSN 0003-2700.
- [234] Seyed Ali Mousavi Shaegh, Zhenfeng Wang, Sum Huan Ng, Ruige Wu, Huu Tuan Nguyen, Leon Cong Zhi Chan, Alicia Guek Geok Toh, and Zhiping Wang. Plug-and-play microvalve and micropump for rapid integration with microfluidic chips. *Microfluidics and Nanofluidics*, 19(3):557–564, 2015. ISSN 1613-4982.
- [235] Farid Amirouche, Yu Zhou, and Tom Johnson. Current micropump technologies and their biomedical applications. *Microsystem technologies*, 15(5):647–666, 2009. ISSN 0946-7076.

- [236] Pan Zheng, Yousef Haik, Mohammad Kilani, and Ching-Jen Chen. Force and torque characteristics for magnetically driven blood pump. *Journal of Magnetism and Magnetic Materials*, 241(2):292–302, 2002. ISSN 0304-8853.
- [237] Kwang W Oh and Chong H Ahn. A review of microvalves. *Journal of micromechanics and microengineering*, 16(5):R13, 2006. ISSN 0960-1317.
- [238] Nima Arjmandi, Chengxun Liu, Willem Van Roy, Liesbet Lagae, and Gustaaf Borghs. Method for flow measurement in microfluidic channels based on electrical impedance spectroscopy. *Microfluidics and nanofluidics*, 12(1-4):17–23, 2012. ISSN 1613-4982.
- [239] Yong Duk Han, Hyeong Jin Chun, and Hyun C Yoon. The transformation of common office supplies into a low-cost optical biosensing platform. *Biosensors and Bioelectronics*, 59:259–268, 2014. ISSN 0956-5663.
- [240] Chengpeng Chen, Benjamin T Mehl, Akash S Munshi, Alexandra D Townsend, Dana M Spence, and R Scott Martin. 3d-printed microfluidic devices: fabrication, advantages and limitationsa mini review. *Analytical Methods*, 8(31):6005–6012, 2016.
- [241] Sidra Waheed, Joan M Cabot, Niall P Macdonald, Trevor Lewis, Rosanne M Guijt, Brett Paull, and Michael C Breadmore. 3d printed microfluidic devices: enablers and barriers. *Lab on a Chip*, 16(11):1993–2013, 2016.
- [242] Lucas P Bressan, Jessica Robles-Najar, Cristina B Adamo, Reverson F Quero, Brenda MC Costa, Dosil P de Jesus, and José AF da Silva. 3d-printed microfluidic device for the synthesis of silver and gold nanoparticles. *Microchemical Journal*, 146:1083–1089, 2019.